This is the Author Accepted Manuscript (postprint) of the following paper:

Yoon, Hyungsub, Matteini, Paolo, Hwang, Byungil, **"Review on three-dimensional ceramic filler networking composites for thermal conductive applications"**, JOURNAL OF NON-CRYSTALLINE SOLIDS, vol. 576, 2022, https://dx.doi.org/10.1016/j.jnoncrysol.2021.121272

Review on Three-dimensional Ceramic Filler Networking Composites for Thermal Conductive Applications

Hyungsub Yoon[a], Paolo Matteini[b] and Byungil Hwang[a,*]

[a]*School of Integrative Engineering, Chung-Ang University, Seoul 06974, Republic of Korea*

[b]*Institute of Applied Physics "Nello Carrara," National Research Council, Via Madonna del Piano 10, Sesto Fiorentino, 50019, Italy*

Corresponding author Email: **bihwang@cau.ac.kr*

Abstract

Three-dimensional (3D) ceramic filler networking composites feature isotropic heat dissipation properties owing to the spatial distribution of their fillers, which form continuous thermal conduction paths that ensure a high thermal conductivity. Therefore, this type of filler networking is considered ideal in thermally conductive ceramic-filler-based composites. This review discusses the research advances achieved thus far for improving the heat dissipation properties of thermally conductive ceramic filler networking composites, with a special focus on structural engineering applications. The most popular methods for fabricating composites with 3D filler networking are also examined. Finally, existing issues and future perspectives associated with the use of these composites are considered.

Keywords: Thermally conductive composites, Ceramic-based composites, Polymer-matrix composites, Manufacturing/Processing.

Contents

Abbreviations			
3D	Three-dimensional	MGO	Modified graphene oxide
3D-C	3D carbon nanorod-based foam	MWCNT	Multiwalled carbon nanotube
3D-NS-BN	3D boron nitride nanosheets-based foam	NaCl	Sodium chloride
3D-R-BN	3D boron nitride nanorod-based foam	NFC	Nanofibrillated cellulose
Al	Aluminum	NH_4HCO_3	Ammonium bicarbonate
Al_2O_3	Aluminum oxide	PAA	Poly(amic acid)
AlN	Aluminum nitride	PBN	Polyethylene glycol/ BN without a framework
AlN-H	Aluminum nitride honeycomb	PBNF	Polyethylene glycol/ BN framework
APTES	3-Aminopropyltriethoxysilane	PDA	Polydopamine
BN	Boron nitride	PDMS	Polydimethylsiloxane
BNF	Boron nitride foam	PEI	Polyethyleneimine
BNMB	Boron nitride microbead	PF	Polypropylene fiber
BNNS	Boron nitride nanosheet	PI	Polyimide
BNNP	Boron nitride nanoplatelet	PMIA	Poly(m-phenylene isophthalamide)
CNF	Cellulose nanofiber	PMMA	Poly(methyl methacrylate)
Cu	Copper	PP	Polypropylene
CuNW	Copper nanowire	PPS	Poly(phenylene sulfide)
CVD	Chemical vapor deposition	PU	Polyurethane
EDX	Energy dispersive X-ray spectroscopy	PVA	Poly(vinyl alcohol)
EP	Epoxy	PVDF	Poly(vinylidene fluoride)
EVA	Ethylene–vinyl acetate	rGO	Reduced graphene

	copolymer		oxide
f-Al_2O_3	Functionalized aluminum oxide	SCA	Silane coupling agent
FBN	Functionalized boron nitride	SDS	Sodium dodecyl sulfate
Fe_3O_4	Iron(II,III) oxide	SEM	Scanning electron microscopy
f-SiC	Functionalized silicon carbide	SiC	Silicon carbide
GO	Graphene oxide	SiO_2	Silicon dioxide
GPTMS	3-Glycidoxypropyltrimethoxy silane	SPI	Soy protein isolate
h-BN	Hexagonal boron nitride	TA	Tannic acid
h-BNNS	Hexagonal boron nitride nanosheet	TBA	Tert-butyl alcohol
LAO	Lauramide propyl amine oxide	TEM	Transmission electron microscopy
LED	Light-emitting diode	TIM	Thermal interface material
MF	Melamine foam	VTES	Vinyl triethoxysilane

1. Introduction

With the continuing miniaturization and high integration density of electronic devices, there are increasing demands for thermally conductive composites to dissipate the thermal energy generated by the increased power density of these devices. Given that the thermal energy isolated in these devices degrades their reliability and lifespans and may even cause devices to explode, using efficient heat dissipation materials is crucial not only in existing applications but also for the development of next-generation electronic devices [1-7]. For example, a temperature increase of 10–15 °C can degrade the device lifetime by a factor of two [8, 9].

Practical applications of thermally conductive composites include light-emitting diodes

(LEDs) [10-15], three-dimensional (3D) packaging of memory devices [16-21], printed circuit boards for 5G communications technology [22-25], electric vehicles [6, 26-30], separators for batteries or electrochemical capacitors [31-36], and heat dissipation films in thermoelectric generators [37-40]. For example, mini- and micro-LED displays employ a vast amount of increasingly small LEDs in a single panel, but the considerable thermal energy that they produce can cause color shifts and reduce the light output and lifetime of the LEDs, which are serious quality issues [14, 41]. Thus, appropriate thermal conduction materials are required to manage this heat, thereby stabilizing such LED displays. In 3D packaging systems, highly miniaturized and integrated circuits generate a great deal of thermal energy in devices; thus, thermally conductive composites are positioned between dies and heat sinks to dissipate this thermal energy [42]. In addition, thermally conductive composites are used as underfill materials in such packaging, which fill the gaps between solder bumps to help remove the thermal energy from the devices [43-45]. In the case of 5G communications technology, ultrahigh-speed signals of millimeter waves cause the loss of microwave radiation, thereby producing heat. For this application, the thermally conductive composite must have a low dielectric constant and dielectric loss to avoid a signal delay or loss [25, 46-48]. In electric vehicles, the thermal safety of existing batteries is problematic [26, 49]. When the batteries are charged and discharged, the heat energy that they generate can overheat the battery, which can result in a fire. Furthermore, the uneven temperature distribution in the battery can deteriorate its performance and reduce its lifetime. Therefore, thermal management is essential to the batteries of electric vehicles; thus, thermally conductive composites have been used in the gap between the battery and cooling system [50]. Furthermore, thermally conductive composites with high ionic conductivity have been used as the separator and all-solid-state polymer electrolyte in batteries to reduce the temperature

gradients while dissipating the heat produced during battery operation [31, 34, 51, 52]. Capacitors also require thermally conductive composites as repeated charge–discharge cycles generate heat energy that degrades their electrical performance and stability [36, 53, 54]. Thermally conductive composites are also attractive in energy harvesting applications such as a thermoelectric generators, where they are used to enhance performance by maximizing the heat conduction between the heat sink and source [39, 55]. These composites can also increase the energy harvesting efficiency by enhancing the heat energy absorption and dissipation on the hot and cold sides of thermoelectric generators [56, 57].

For heat dissipation in electronic devices, thermal interface materials (TIMs) are the most essential components [58-60]. From a thermal management point of view, electronic devices can be categorized as heat sources or heat sinks, wherein heat sources are the operating components that generate heat, and heat sinks are the corresponding components that dissipate heat to cool down the heat source. As shown in Fig. 1, TIMs are located between the heat source and sink, thereby enabling the heat to flow from the source to the sink to efficiently cool the devices. Without the TIM, the contacts between the heat source and sink are imperfect owing to the irregular surfaces of the components. In this situation, a large part of the heat flows through air, which has a low thermal conductivity of 0.024 W/mK, thereby significantly limiting the cooling performance of the device. In turn, the heat isolated in the components degrades the performance of the entire device. However, by adopting TIMs, the air gap is replaced with highly thermally conductive materials that increase the heat dissipation. Correspondingly, the cooling performance of the device largely depends on the TIM properties.

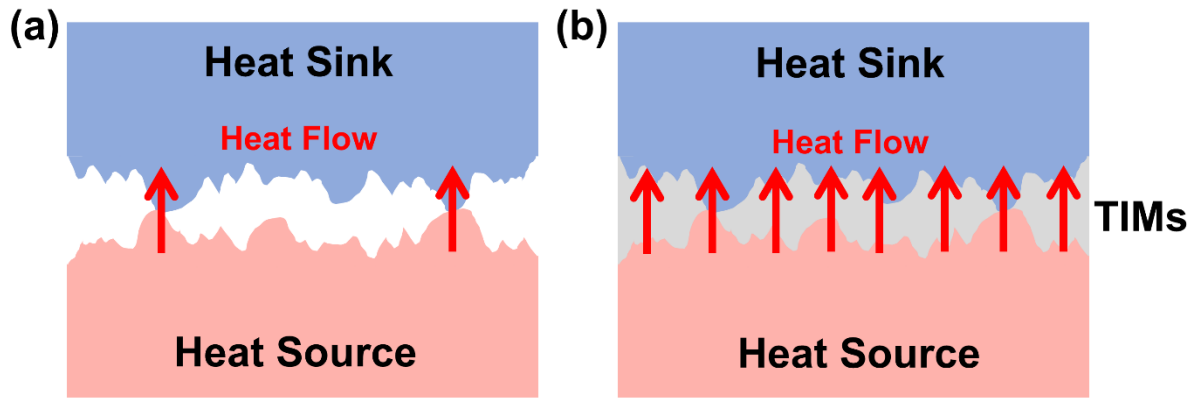

Fig. 1. Schematic diagrams of heat flow in devices (a) without and (b) with TIMs.

The most extensively used TIMs are thermally conductive composites formed by distributing conductive fillers in a polymeric matrix. Polymers are appropriate as the TIM matrix owing to their excellent flexibility, processability, electrically insulating property, chemical reliability, low cost, and light weight. However, because of their intrinsically low thermal conductivity, thermally conductive fillers should be mixed into the polymer matrix to render them thermally conductive [61-64]. Given that most of the heat flows through these conductive fillers, the thermal management property of the composites is mostly determined by the thermal conduction performance of the fillers. There are three main categories for the thermally conductive fillers: i) metals (such as copper, silver, and aluminum), ii) carbon-based materials (such as carbon nanotubes, carbon fibers, and graphene), and iii) ceramics (such as aluminum oxide (Al_2O_3), aluminum nitride (AIN), and boron nitride (BN)). Metal- or carbon-based materials are common fillers in these thermally conductive composites because of their excellent thermal conductivity [65-76]. However, their high electrical conductivity limits their utility in applications requiring electrical insulation properties, such as underfill composites for electronic packaging [42, 77, 78], prepreg materials in printed

circuit boards for 5G communication technology [25, 79, 80], components of energy storage systems such as batteries and capacitors [7, 31, 34, 51-54], energy harvesting systems such as thermoelectric generators [4, 40, 57, 81], and personal thermal regulation [82, 83]. In contrast with metal- or carbon-based fillers, ceramic-based fillers are electrically insulating but thermally conductive, which makes them promising alternatives. However, their thermal conductivities are lower than those of metal- or carbon-based fillers, so ceramic-filled composites generally exhibit a lower ability to dissipate heat than metal- and carbon-filled composites [2, 58].

The development of thermally conductive composites began with the observation of ceramic fillers randomly distributed in polymeric matrices [84, 85]. Owing to the high crystallinity of ceramic fillers, their thermal conductivity is higher than that of the polymeric matrix; thus, the heat dissipation properties of these composites is governed mostly by the loading of ceramic fillers, i.e., increasing the filler loading increases the overall thermal conductivity. The parallel thermal conductivity can be predicted using the rule of mixtures. This rule can be expressed as $K_c = V_f K_f + (1-V_f)K_m$, where K_c, K_f, and K_m are the thermal conductivities of the composites, fillers, and matrix, respectively, and V_f is the volume fractions of the fillers [2, 86]. Realistically, however, the total thermal conductivity of the composite is lower than that calculated using the rule of mixtures [87-90]. There are two reasons for the difference in the total thermal conductivity values between the calculated and experimentally confirmed values: i) interfacial thermal resistance and ii) the agglomeration of fillers in the composites. The interfacial thermal resistance is a property of filler–filler or filler–polymer matrix interfaces, which act as a barrier to heat transfer [91-95]. As this resistance increases, the phonon scattering increases, which hinders thermal energy transfer, thereby decreasing the total thermal conductivity of the composites. Therefore, engineering the materials to reduce

the interfacial thermal resistance at filler–polymer or filler–filler contacts can achieve a composite with a high thermal conductivity close to the theoretical value. In addition, the thermal resistance at filler–polymer matrix interfaces is higher than that at filler–filler interfaces. This difference can be attributed to the larger phonon scattering from the polymeric matrix owing to its amorphous structure, whereas the thermal conduction at filler–filler interfaces mostly occurs by atomic vibration, which minimizes phonon scattering [96]. Thus, the other way to enhance the thermal conductivity is to construct composite structures with continuous filler–filler interfaces and fewer filler–polymer matrix interfaces. Second, the aggregation of the fillers reduces thermal conduction in these composites [97-100]. Given that heat is conducted more efficiently through the ceramic fillers than through the polymeric matrix, decreasing the gaps between individual fillers should enhance the heat transfer. However, when fillers aggregate, they leave behind localized areas in the polymer matrix with no fillers, which decreases the number of effective thermal conduction paths, thereby decreasing the total thermal conductivity of the composite. A simple solution to the issues caused by interfacial thermal resistance and aggregation is to increase the amounts of fillers in the composites [1, 101, 102]. A high loading of ceramic fillers not only forms more effective thermal conduction paths that pass through more filler–filler interfaces but also offsets the degradation of the thermal conduction caused by filler agglomeration. However, a high filler loading can also degrade the physical properties imparted by the polymer matrix, including stretchability, strength, and optical transmittance; thus, there is trade-off between these properties and the thermal conductivity, which limits the ceramic filler loading in the composite.

To solve the limitations of typical thermally conductive composites with randomly distributed ceramic fillers, researchers have developed a technology for aligning the fillers in the

polymeric matrix [103-107]. The continuous anisotropic thermal conduction paths formed by the aligned ceramic fillers allow efficient thermal conduction through the filler–filler interfaces and decrease the aggregation of the fillers. Thus, composites with aligned ceramic fillers are much more thermally conductive than those with randomly distributed ceramic fillers, even with equal amounts of fillers [108-114]. For example, Chen et al. [113] introduced a doctor blade method that used shear forces to align BN nanosheet (BNNS) fillers in a cellulose nanofiber (CNF) composite. The maximum thermal conductivity of the shear-oriented composites was three times higher (24.66 W/mK) than that of the composites with randomly distributed fillers (8.61 W/mK). Similarly, Kim et al. [114] aligned BN nanoplatelets (BNNPs) in epoxy (EP) resin, thereby enhancing the thermal conductivity from ~0.47 to 1.07 W/mK. Section 3 provides further examples of this strategy and discusses the associated thermal conductivity enhancement in detail. Although these composites with aligned fillers exhibited enhanced thermal conductivity, the anisotropy of this conductivity limits their use in applications that require isotropic heat dissipation properties [42, 115-117].

Recently, 3D filler networking composites were developed to simultaneously resolve the low thermal conductivity of composites with the randomly distributed ceramic fillers and the anisotropy observed in composites with aligned ceramic fillers [118-123]. Such 3D filler networking composites are categorized into three different classes depending on the method used to form their 3D-structured ceramic frames: 1) fabrication of 3D-structured ceramic frames through freeze- casting/drying or foaming agents, 2) deposition of a thin ceramic layer on an existing metal or polymer-based 3D structure, and 3) in situ fabrication of 3D-structured composites by heating and compressing ceramic-filler-covered polymer spheres. As shown in Fig. 2, these 3D filler networking composites have shown high thermal conductivity because their continuous thermal conduction paths can minimize the thermal

resistance at the filler interfaces. Fabricating 3D interconnected ceramic fillers not only prevents the ceramic fillers from aggregating but also provides isotropic thermal conduction that can maximize heat dissipation through the composites thanks to their 3D structure. Therefore, 3D filler networking composites have attracted considerable attention, especially for TIMs applied in next-generation electronic devices with ultrahigh integration and power densities. However, although there are many reviews on traditional thermally conductive composites with randomly distributed or anisotropically aligned ceramic fillers in the literature, the number of reviews on the 3D filler networking composites is limited.

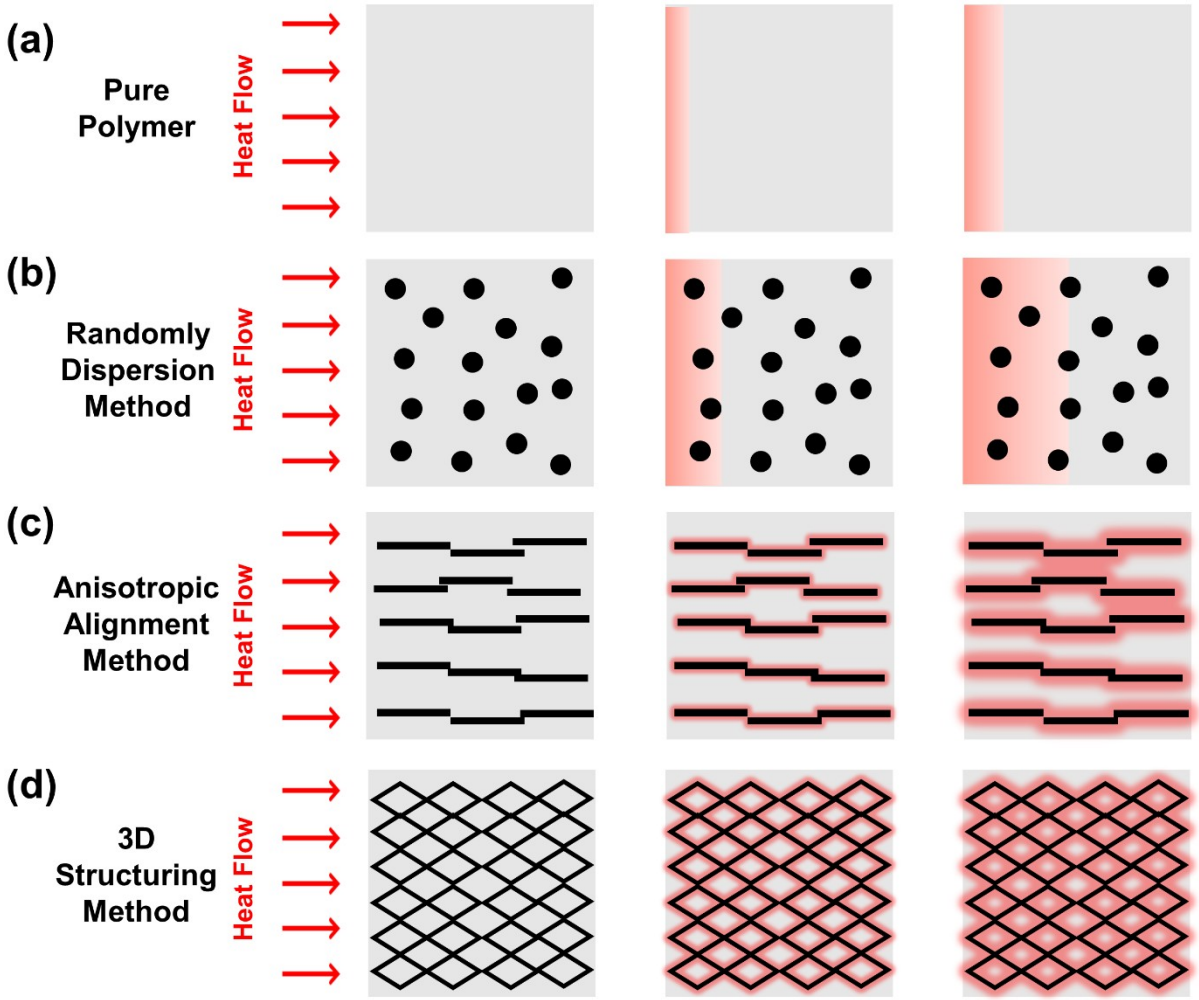

Fig. 2. Schematic diagrams of heat flow in (a) a pure polymer and thermally conductive composites with (b) randomly dispersed fillers, (c) anisotropically aligned fillers, and (d) 3D networking fillers.

Fig. 3 briefly summarizes the current state of the art in thermally conductive composites. This review discusses technological trends in these composites, particularly the current status of 3D ceramic filler networking composites. First, methods for fabricating conventional thermally conductive composites with the randomly distributed and anisotropically aligned ceramic fillers are briefly introduced; however, most of this review focuses on technologies used to form 3D filler networking composites, which combine the advantages of good electrical insulation and isotropic thermal conductivity. Thus, this review aims to give readers a broad understanding of the latest technology in TIMs as well as insights into the solutions for future electronic devices, which will face considerable thermal management challenges.

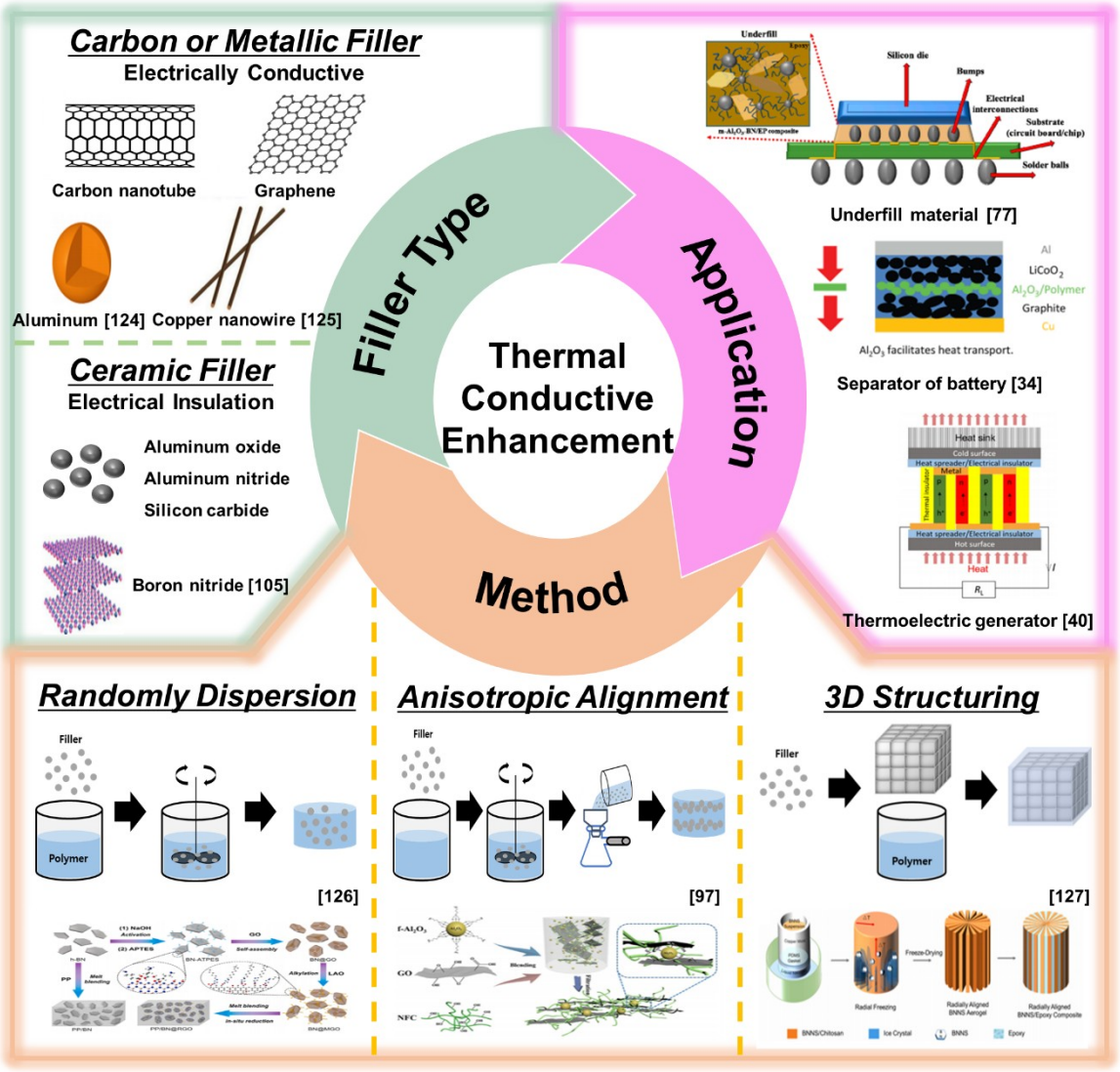

Fig. 3. Overview of thermally conductive composites [34, 40, 77, 97, 105, 124-127]. Reprinted with permission from [34]; copyright 2016 Elsevier. Reprinted with permission from [40]; copyright 2018 Elsevier. Reprinted with permission from [77]; copyright 2021 MDPI. Reprinted with permission from [97]; copyright 2019 Elsevier. Reprinted with permission from [105]; copyright 2020 Elsevier. Reprinted with permission from [124]; copyright 2019 Elsevier. Reprinted with permission from [125]; copyright 2018 Elsevier. Reprinted with permission from [126]; copyright 2021 Elsevier. Reprinted with permission from [127]; copyright 2020 Elsevier.

2. Various filler types used in typical thermally conductive composites

2.1. Ceramic fillers

Ceramic fillers have high thermal conductivity; however, their electrical conductivity is low enough to be used for applications requiring electrical insulation. Table 1 presents the thermal conductivity and insulation properties of thermally conductive fillers. Al_2O_3, silicon carbide (SiC), AlN, or BN, are all ceramic fillers, but each of these compounds have advantages and disadvantages. For example, Al_2O_3 is extensively used in industry because of its excellent chemical stability, abrasion resistance, and cost-efficiency [128-131]. However, its intrinsic thermal conductivity of ~30 W/mK is lower than that of other ceramic fillers, and thus, the thermal conductivity of the corresponding Al_2O_3 composites is relatively low. In the work by Yan et al. [132], the thermal conductivity of the unmodified Al_2O_3 composites was only 1.37 W/mK at an Al_2O_3 loading of 80 wt%. Meanwhile, SiC has a higher thermal conductivity of approximately 90 W/mK, as well as high thermal stability, low thermal expansion coefficient, good mechanical properties, and excellent chemical stability [133-137]. However, its high dielectric constant (40 at 1 MHz) limits its use in highly integrated electronic packaging applications that require rapid signal transport [96]. Yang et al. [137] prepared an EP nanocomposite filled with SiC nanoparticles, which showed only a conductivity of ~0.8 W/mK at a loading of 20 vol%. AlN exhibits excellent thermal conductivity in the range of 200–320 W/mK with a low dielectric constant of 8.8 at 1 MHz and a thermal expansion coefficient of 4×10^{-6} K^{-1} [138-141]. Although Wu et al. [141] developed AlN-filled composites with a relatively high thermal conductivity of ~1.21 W/mK at a filler loading of 57.4 vol%, AlN filers have poor moisture resistance; thus, an additional surface treatment is required for AlN [142-146]. This treatment not only increases the processing cost but also limits the diversity of solvents that can be used with AlN. BN is an emerging ceramic filler for thermally conductive composites owing to its excellent in-plane thermal conductivity of

~600 W/mK, low density of 2.1 g/cm³, low dielectric constant of 4 at 1 MHz, and high chemical stability [96, 147-149]. Lin et al. [43] fabricated composites with unmodified BNNSs. At a loading of only 5 wt% BNNSs, the resulting thermal conductivity was ~113% higher than that of pure EP (0.15 W/mK). However, BN is expensive; thus, a breakthrough is required in methods for the synthesizing BN at a large scale to lower its cost. Nonetheless, BN has recently been intensively studied for thermally conductive composites owing to its excellent performance. Thus, the largest proportion of studies reviewed in this paper used BN or its allotropes as ceramic fillers.

Table 1. Thermal and electrical conductivities and other properties of various fillers.

	Filler	Thermal conductivity (W/mK)	Advantage	Disadvantage
Metallic	Gold (Au)	315	· High thermal conductivity	· High electrical conductivity · High density · High cost
	Silver (Ag)	427	· High thermal conductivity	· High electrical conductivity · High density · High cost
	Aluminum (Al)	234	· High thermal conductivity · Low cost	· High electrical conductivity · High density · Oxidation
	Copper (Cu)	386	· High thermal conductivity · Low cost	· High electrical conductivity · High density · Oxidation
Carbon-based	Carbon nanotube	1000-4000	· High thermal conductivity · Low density	· High electrical conductivity · High cost
	Carbon fiber	300-1000	· High thermal conductivity · Low cost · Low density	· High electrical conductivity
	Graphene	2000-6000	· High thermal conductivity	· High electrical conductivity

			· Low density	· High cost
	Graphite	100-400	· High thermal conductivity · Low cost · Low density	· High electrical conductivity
Ceramic	Aluminum oxide (Al_2O_3)	~30	· Electrical insulation · Low cost	· Low thermal conductivity
	Silicon dioxide (SiO_2)	1	· Electrical insulation · Easy to synthesize · Low cost	· Low thermal conductivity
	Zinc oxide (ZnO)	29-60	· Electrical insulation · Low cost	-
	Boron nitride (BN)	29-600	· High thermal conductivity · Electrical insulation · Low density	· High cost
	Aluminum nitride (AIN)	200-320	· High thermal conductivity · Electrical insulation · Low cost	· Poor resistance to moisture
	Silicon carbide (SiC)	90~390	· High thermal conductivity · Electrical insulation · Low cost	-

2.2. Hybrid-type composites

Hybrid-type composites contain multiple types of fillers with different features, thereby exploiting the different advantages of each filler to enhance the performance of the composites. In hybrid composites, fillers of different sizes and shapes can be used to increase their packing densities because small fillers can fill in the voids formed between larger fillers. As the packing density of fillers increases, the thermal conductivity is also enhanced owing to the increased thermal conduction paths. For example, Duan et al. [150] prepared a poly(m-phenylene isophthalamide) (PMIA)-based composite with different sizes of h-boron nitride (h-BN) fillers, and they fixed the ratio of the micro-sized (1 μm) and nano-sized (150 nm) fillers at 7:3. With a total filler content of 30 wt%, the thermal conductivity of the composite was 0.94 W/mK with different sizes of fillers, but it was 0.86 W/mK with single-size fillers. The enhanced thermal conductivity was attributed to the additional conduction paths formed by the nano-sized fillers, which bridged the larger fillers. Leung et al. [151] enhanced the thermal conductivity of a composite with different shapes of BN fillers (Fig. 4). Specifically, spherical BN (PTX60) and BN platelets (PT100) were mixed into a poly(phenylene sulfide) (PPS) matrix. The thermal conductivity of the composite filled with 33.3 vol% fillers with a spherical/platelet BN ratio of 3:1 was 2.04 W/mK, which was higher than those of the corresponding composites with only spherical BN (1.77 W/mK) or BN platelets (1.55 W/mK), as shown in Fig. 4a.

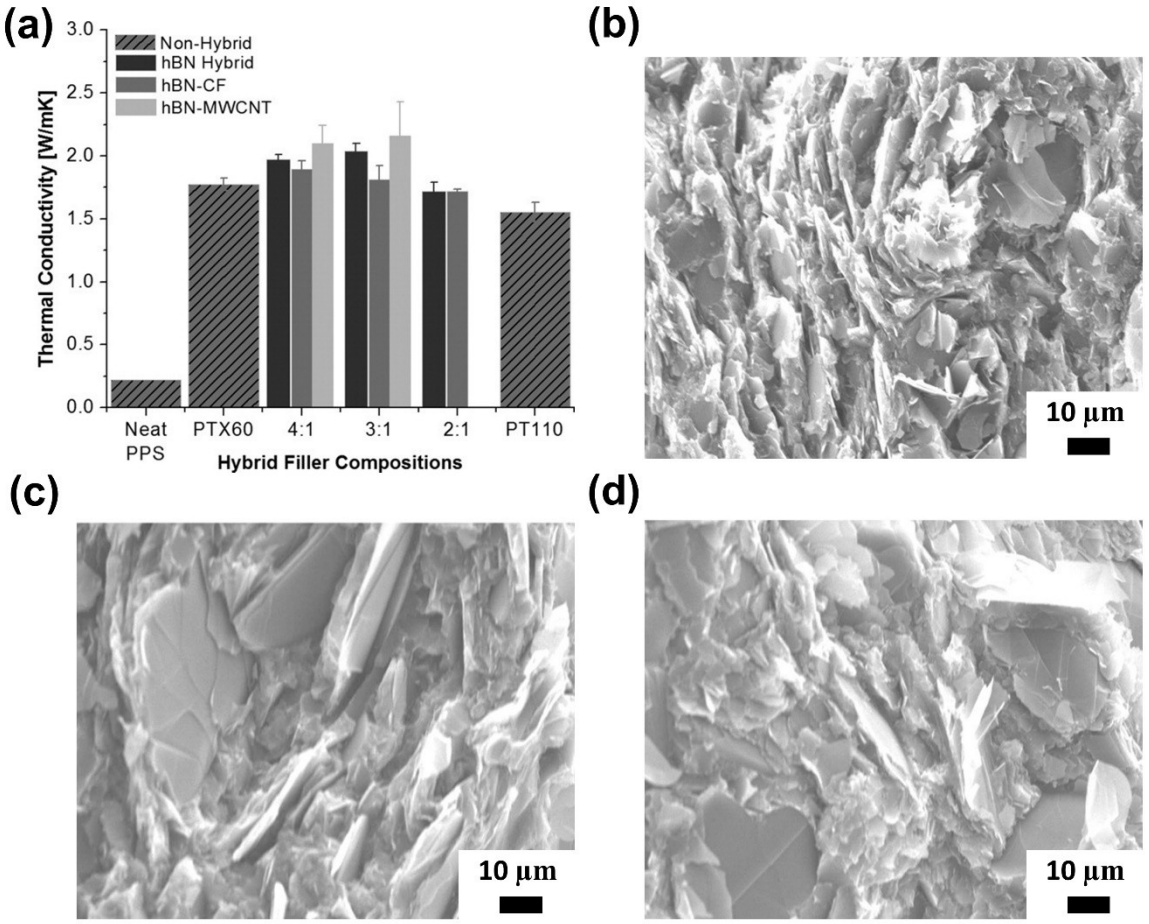

Fig. 4. (a) Thermal conductivity of the composites with different shapes and ratios of fillers and scanning electron microscopy (SEM) images of the composites with (b) PTX60, (c) PT110 and (d) 3:1 PTX60/PT110 [151]. Reprinted with permission from [151]; copyright 2012 John Wiley and Sons.

In hybrid composites, different materials can be also used as fillers. For example, Wang et al. [98] distributed different filler materials in composites, namely h-boron nitride nanosheets (h-BNNSs) and functionalized silicon carbide (f-SiC) nanowires, in a poly(vinylidene fluoride) (PVDF) matrix. The f-SiC nanowires formed bridges between the h-BNNSs, thereby forming continuous thermal conduction paths (Fig. 5a). With 20 wt% h-BNNSs and 26 wt% f-SiC nanowires, the hybrid composite showed a thermal conductivity of 1.41 W/mK, which was approximately 487.5% higher than that of pure PVDF (Fig. 5b). However, increasing the h-

BNNS content above 20 wt% degraded the thermal conductivity owing to the aggregation of h-BNNS and f-SiC nanowires (Fig. 5c, d). In another example, Choi et al. [152] fabricated a hybrid EP composite with both AlN and Al_2O_3 fillers, as shown in Fig. 6a. In addition to using different materials, they varied the sizes of the fillers, which contained 10 μm AlN and 0.5 μm Al_2O_3 (sample A), or 0.1 μm AlN with 10 μm Al_2O_3 (sample B). With a total filler content of 58.4 vol% and a large/small filler volume ratio of 7:3, they attained thermal conductivities of 3.402 and 2.842 W/mK for samples A and B, respectively (Fig. 6b, c). These values were approximately 1.8 times higher than those with single Al_2O_3 or AlN fillers, which yielded corresponding conductivities of approximately 2.2 and 1.9 W/mK, respectively. Because of the size distributions of AlN and Al_2O_3, the total surface area of fillers in sample A that contacted the polymeric matrix was smaller than that in sample B, which resulted in the higher thermal conductivity of sample A compared with that of sample B. Hong et al. [153] fabricated the EP composites with polygonal AlN and planar BN, which were bimodally distributed (Fig. 7a). They fixed the total filler content at 80 vol%, but they varied the mean particle size and volume ratio of the AlN and BN fillers. As shown in Fig. 7b, the composite with the volume ratio of 1:1 and a mean particle size ratio of 1.41 (D_{AlN} = 25.5 μm and D_{BN} = 18 μm) afforded excellent thermal conductivity of 8.0 W/mK.

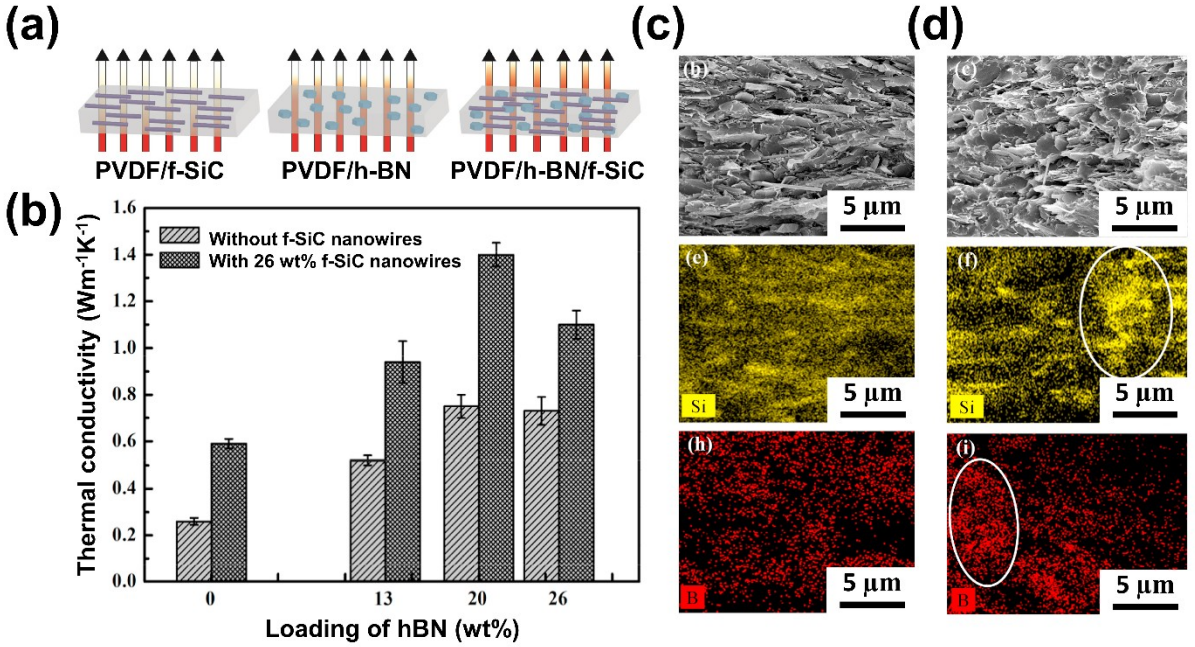

Fig. 5. (a) Schematic diagram of the thermally conductive paths through composites, (b) effect of the f-SiC nanowires on the thermal conductivity of composites with different h-BN loadings, and cross-sectional SEM images and energy dispersive X-ray spectroscopy (EDX) elemental mapping images of the PVDF/f-SiC26/h-BN with h-BN loadings of (c) 20 and (d) 26 wt% [98]. Reprinted with permission from [98]; copyright 2020 Elsevier.

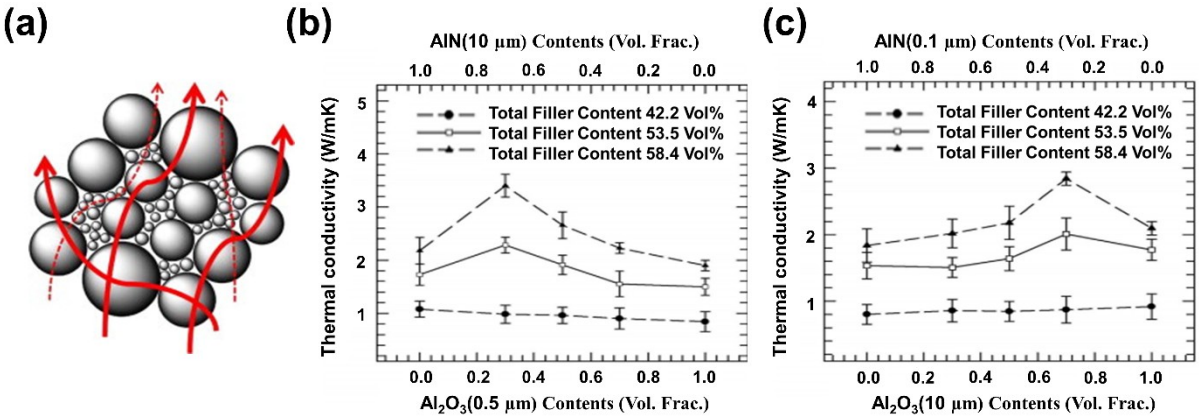

Fig. 6. (a) Schematic illustration of thermal transport in a hybrid composite with different fillers, and (b) thermal conductivity of samples (b) A and (c) B with different amounts of AlN and Al_2O_3 [152]. Reprinted with permission from [152]; copyright 2013 Elsevier.

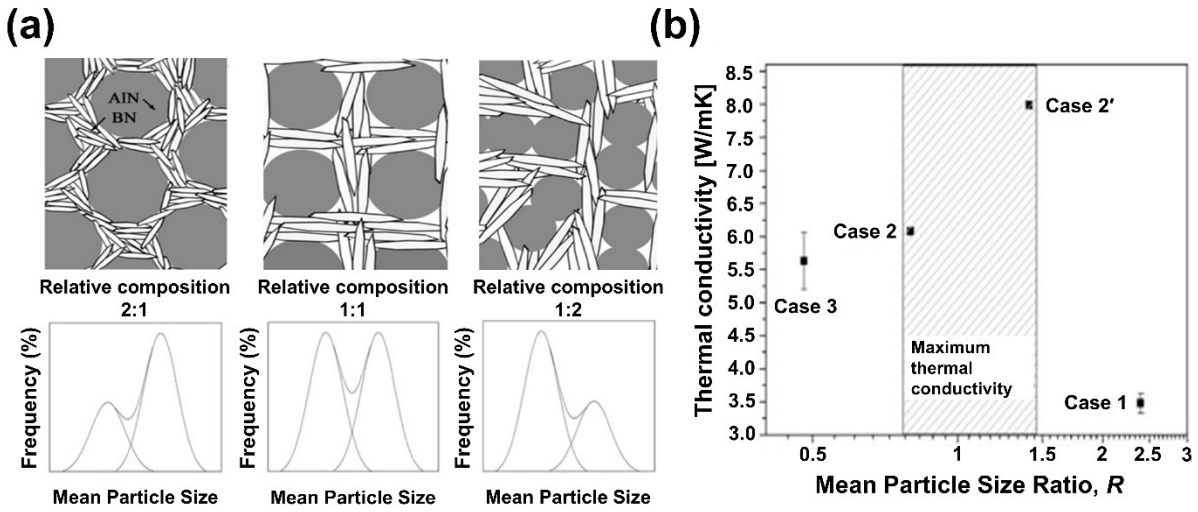

Fig. 7. (a) Schematic of the composites with large AlN and small BN at different volume ratios and (b) thermal conductivity of the composites with different size ratios [153]. Reprinted with permission from [153]; copyright 2012 Elsevier.

Metallic or carbon-based fillers are known to have a higher thermal conductivity than ceramic-based fillers. Thus, researchers have attempted to mix metallic or carbon-based fillers with ceramic fillers for high thermal conductivity. However, given that the metallic or carbon-based fillers provide electrical conductivity to the composites, their contents should be much smaller than those of ceramic fillers for thermally conductive composites with electrical insulation properties [52]. As shown in Fig. 8a, Lu et al. [126] fabricated composites by mixing modified graphene oxide (MGO) and BN in a polypropylene (PP) matrix. First, they modified BN with 3-aminopropyltriethoxysilane (APTES), and they mixed this modified BN with a silane coupling agent (SCA) and graphene oxide (GO), which electrostatically self-assembled into BN@GO composites. The BN@GO was then modified with lauramide propyl amine oxide (LAO) to form BN@MGO, which reduced the phonon scattering by enhancing the interfacial affinity between BN and PP. The thermal conductivity

and electrical resistivity of PP composites with 50 vol% BN@MGO were approximately 3.80 W/mK and $>10^9$ Ω cm, respectively (Fig. 8b). Increasing the filler contents further enhanced the thermal conductivity but decreased the electrical resistivity, which is undesirable for applications requiring electrically insulative but thermally conductive composites.

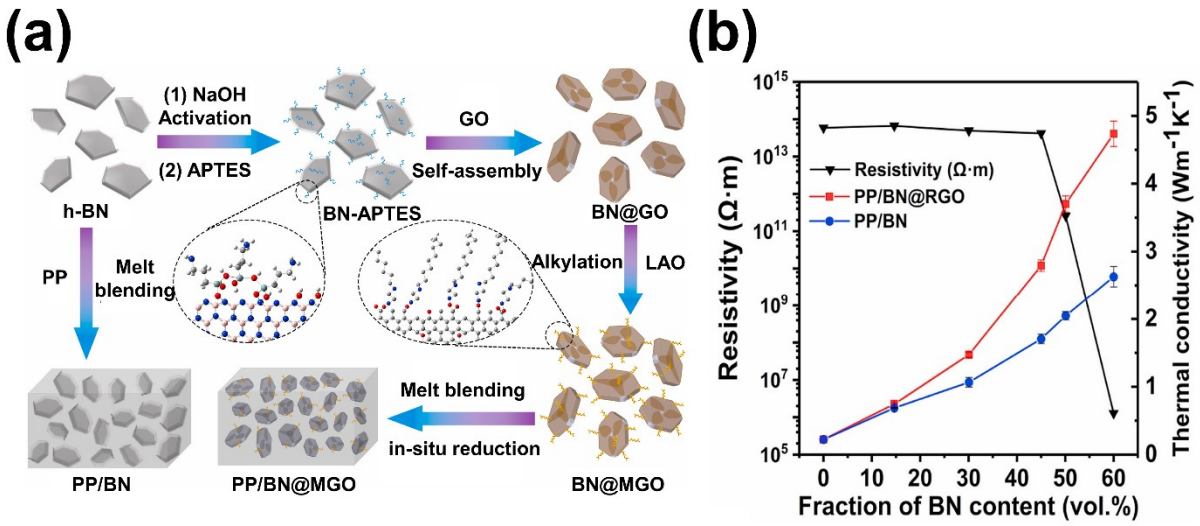

Fig. 8. (a) Schematic illustration of the formation processes for PP/BN and PP/BN@MGO composites and (b) thermal conductivity of PP/BN and PP/BN@MGO (right axis) and electrical resistivity of PP/BN@MGO (left axis) [126]. Reprinted with permission from [126]; copyright 2021 Elsevier.

2.3. Fillers with surface modification

Modifying the surface of fillers is another important strategy for enhancing the thermal conductivity of composites. The appropriate surface modification can reduce the thermal resistances at the filler–filler or filler–matrix interfaces, while enhancing the dispersion capacity of the fillers to prevent them from aggregating in the composites. Therefore, many researchers have attempted to modify the surface of fillers to attain composites with high thermal conductivity.

Cheng et al. [154] modified the surfaces of BNs with silanol groups (Si–OH), as shown in Fig. 9a, which could be covalently bonded with poly(vinyl alcohol) (PVA) using different SCAs, such as tetraethyl orthosilicate, vinyl triethoxysilane (VTES), 3-glycidoxypropyltrimethoxy silane (GPTMS), and different contents of coupling agents. In these composites, the numbers of hydrolysable Si–O–R groups and the side-chain lengths of the SCAs were important factors in controlling the thermal conductivity of the composites because the covalent bonding with the polymeric matrix decreased the interfacial thermal resistance. In addition, the side-chain length determined the disordering degree of the polymer molecular structure near the fillers; specifically, larger disordering diminished the phonon transfer, thereby reducing the thermal conductivity. In their study, as shown in Fig. 9b, the composite with BN modified with VTES exhibited the highest thermal conductivity (~1.636 W/mK), while the lowest thermal conductivity (~0.264 W/mK) was observed with the composites with GPTMS-modified fillers, even lower than that of the composite with unmodified BN (0.485 W/mK). This was because VTES, which had short side chains, yielded the largest number of Si–OH groups covalently bonded to the PVA, whereas GPTMS had the smallest number of covalent bonds with PVA and the longest side chains. Zhou et al. [155] fabricated the EP composites using AlN fillers coated with polyimide (PI), which showed a thermal conductivity of 2.03 W/mK at a filler content of 40 wt%. This value was approximately 10.6 times higher than that of the pure EP matrix and higher than those of composites with pristine AlN fillers at equal filler contents. This enhanced thermal conductivity was attributed to the PI layers on the AlN surface, which merged to form dumbbell-like structures that reduced the aggregation of AlN fillers in the EP matrix. As shown in Fig. 9c, Wang et al. [156] used soy protein isolate (SPI) to exfoliate the h-BN into BNNSs; they then sonicated the BNNSs to modify their surfaces with a hydroxyl group (-

OH) and an amino group (-NH_2). The SPI treatment caused strong bonding to the BNNSs through diverse interactions, such as hydrogen bonding, π–π conjugation, or hydrophobic interaction, thus rendering the dispersion and exfoliation of BNNSs in aqueous solution more effective. The functionalized BNNSs were mixed with CNF coated with biobased tannic acid (TA@CNF), which acted as the matrix in the composites. TA@CNF was used because hydrogen and covalent bonding between TA@CNF and the functionalized BNNSs reduced the interfacial thermal resistance. By vacuum drying the mixture at approximately 45 °C for 24 h, TA@CNF/SPI-BNNS composites were fabricated. The composites with SPI-BNNSs bridged with TA@CNF demonstrated a high thermal conductivity of 7.06 W/mK at a SPI-BNNS loading of 1.5 wt%, whereas those without SPI-BNNS showed a thermal conductivity of 1.84 W/mK (Fig. 9d).

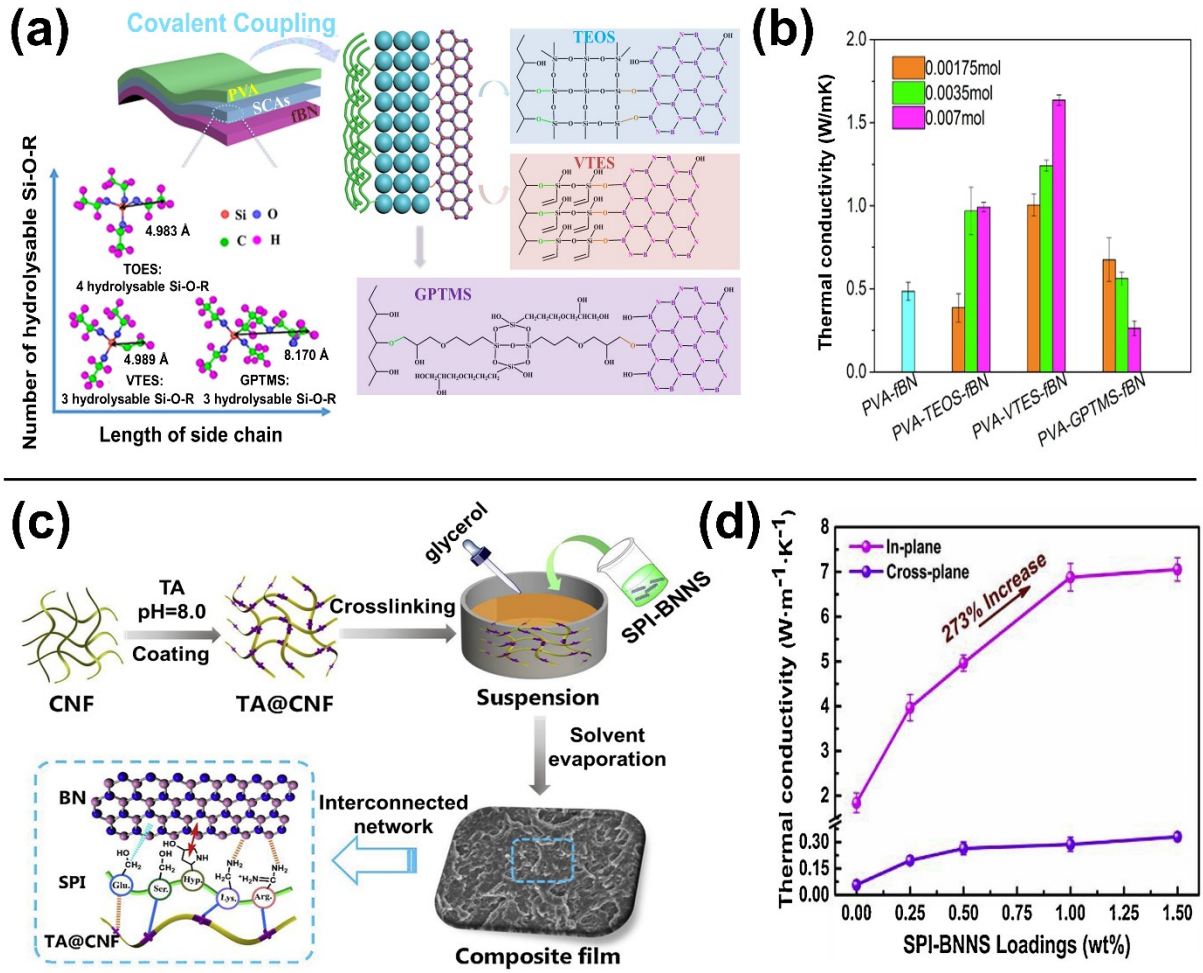

Fig. 9. (a) Schematic diagram of composites with different SCAs and (b) thermal conductivity of the composites with different SCAs types and SCA contents [154]. (c) Illustration of the preparation process for composites and the interfacial interactions of SPI-BNNS and TA@CNF and (d) thermal conductivity of the SPI-BNNS/TA@CNF composites [156]. Reprinted with permission from [154]; copyright 2020 Elsevier. Reprinted with permission from [156]; copyright 2019 Elsevier.

Although metallic and carbon fillers are not desirable for thermally conductive composites requiring electrical insulating characteristics owing to their electrical conductivity, they can be utilized by modifying their surfaces to electrically insulate them. For example, Zhao et al. [157] fabricated composites with silicon dioxide (SiO_2)-coated multiwalled carbon nanotube (MWCNT) fillers (Fig. 10a, b). They tuned the thickness of the SiO_2 from 4 to 90 nm on

MWCNTs, and the thicker SiO_2 increased the thermal conductivity while reducing the electrical conductivity (Fig. 10c, d). Specifically, the thermal conductivity and electrical resistivity of the composites with 1 wt% of the 4-nm-SiO_2-coated MWCNT fillers were ~0.28 W/mK and 4.1×10^{13} Ω cm, respectively. However, the electrical resistivity of the composite without the SiO_2 coating was lower than 10^9 Ω cm, which is unsuitable for applications requiring electrical insulation.

Meanwhile, Mao et al. [124] passivated Al particles by forming Al_2O_3 coatings, and the resulting particles were used as fillers in thermally conductive composites (Fig. 11a, b). They controlled the thickness of the Al_2O_3 coating by changing the post annealing temperature, obtaining the thickest Al_2O_3 coating by post annealing at 600 °C. The 11 nm Al_2O_3 coating resulted in a small decrease in thermal conductivity, as shown in Fig. 11c; however, it dramatically increased the electrical resistivity to be six times higher than that without the Al_2O_3 coating. The composites with these fillers at a loading of 60 wt% showed a thermal conductivity of 0.90 W/mK and an electrical resistivity of 5.5×10^{13} Ω cm (Fig. 11d). As shown in Fig. 12a, b, Yuan et al. [125] coated copper nanowires (CuNWs) with polydopamine (PDA) and used them as composite fillers, and they controlled the thickness of PDA from 0 to 100 nm. The PDA coating enhanced the thermal conductivity, where the composites filled with CuNWs coated with 25 nm of PDA exhibited a thermal conductivity of 2.87 W/mK at a filler content of 3.1 vol%, as shown in Fig. 12c, and a high electrical resistivity of 1.7×10^{14} Ω cm (Fig. 12d). However, as the thickness of the PDA increased above 25 nm, the thermal conductivity decreased, and the composites with CuNW fillers coated with 100 nm of PDA showed a thermal conductivity similar to those without PDA.

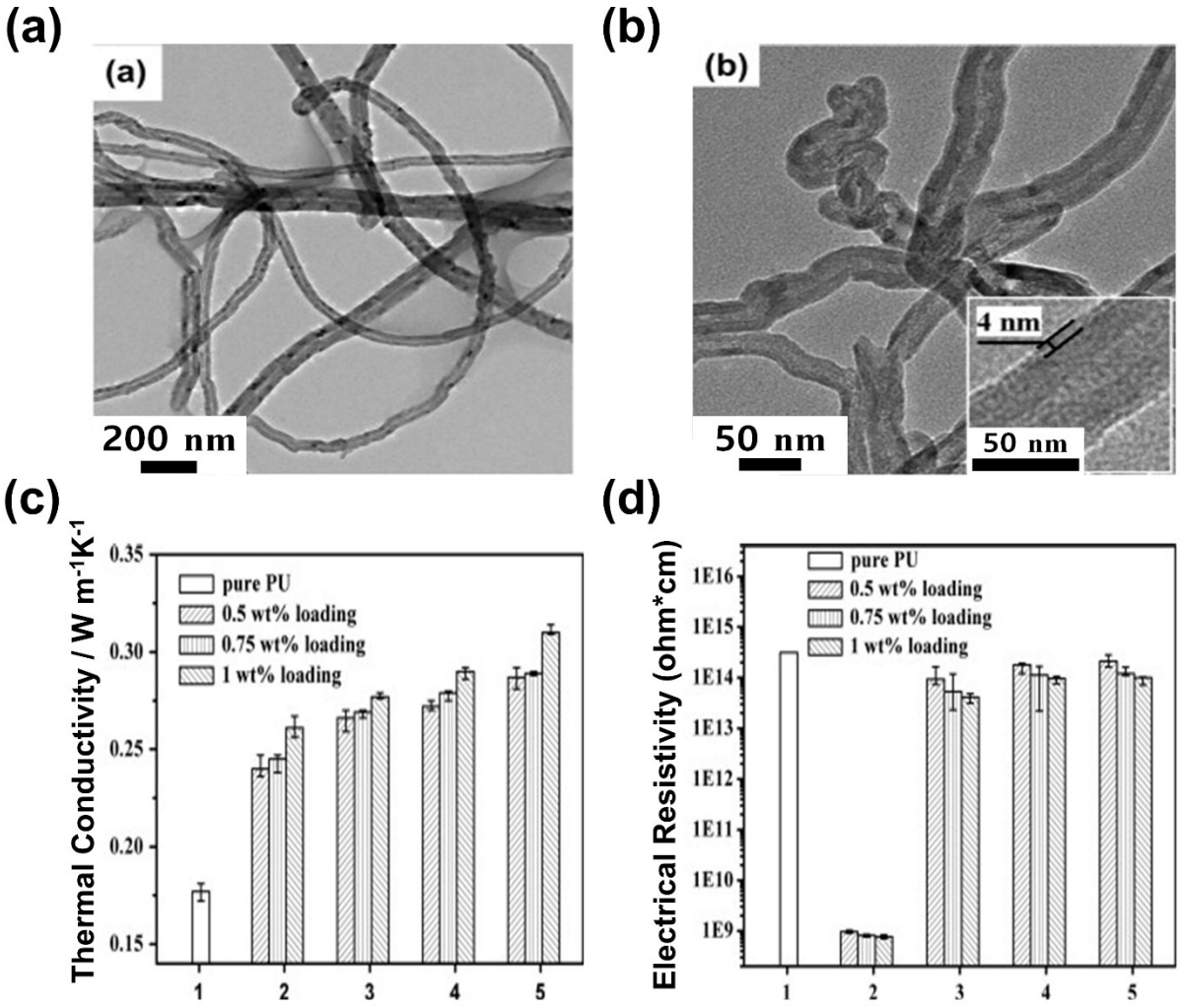

Fig. 10. Transmission electron microscopy (TEM) images of (a) pristine MWCNTs and (b) MWCNTs coated with ~4 nm of SiO_2. (c) Thermal conductivity and (d) electrical resistivity of (1) pure polyurethane (PU), (2) PU/MWCNTs, and SiO_2@MWCNTs with (3) ~4 nm, (4) 30–50 nm, and (5) 70–90 nm of SiO_2 [157]. Reprinted with permission from [157]; copyright 2014 Elsevier.

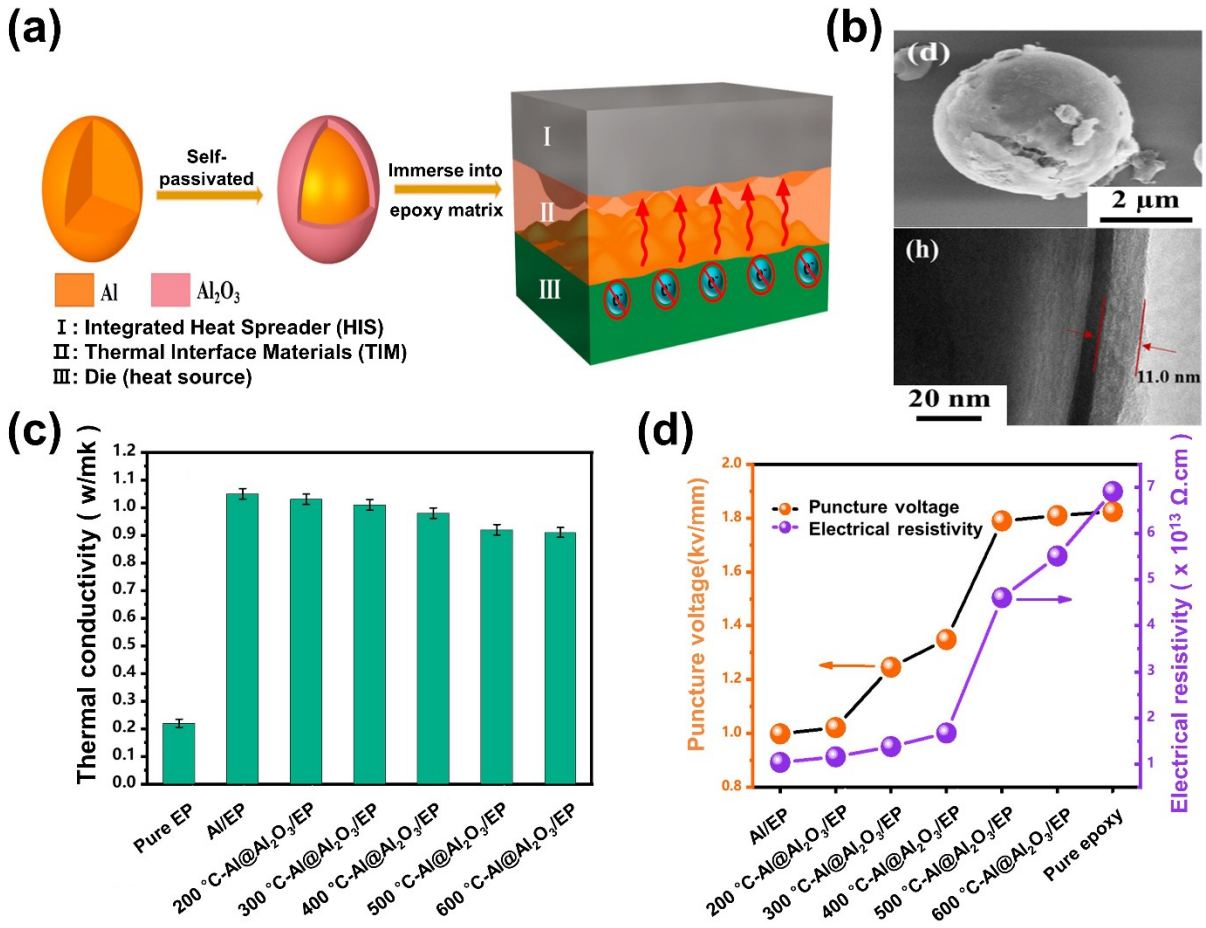

Fig. 11. (a) Schematic diagrams of the fabrication procedure, and (b) SEM and TEM images of Al@Al_2O_3 particles passivated at 600 °C. (c) Comparison of the thermal conductivity of the composites passivate at different temperatures and (d) the insulating properties of the composites [124]. Reprinted with permission from [124]; copyright 2019 Elsevier.

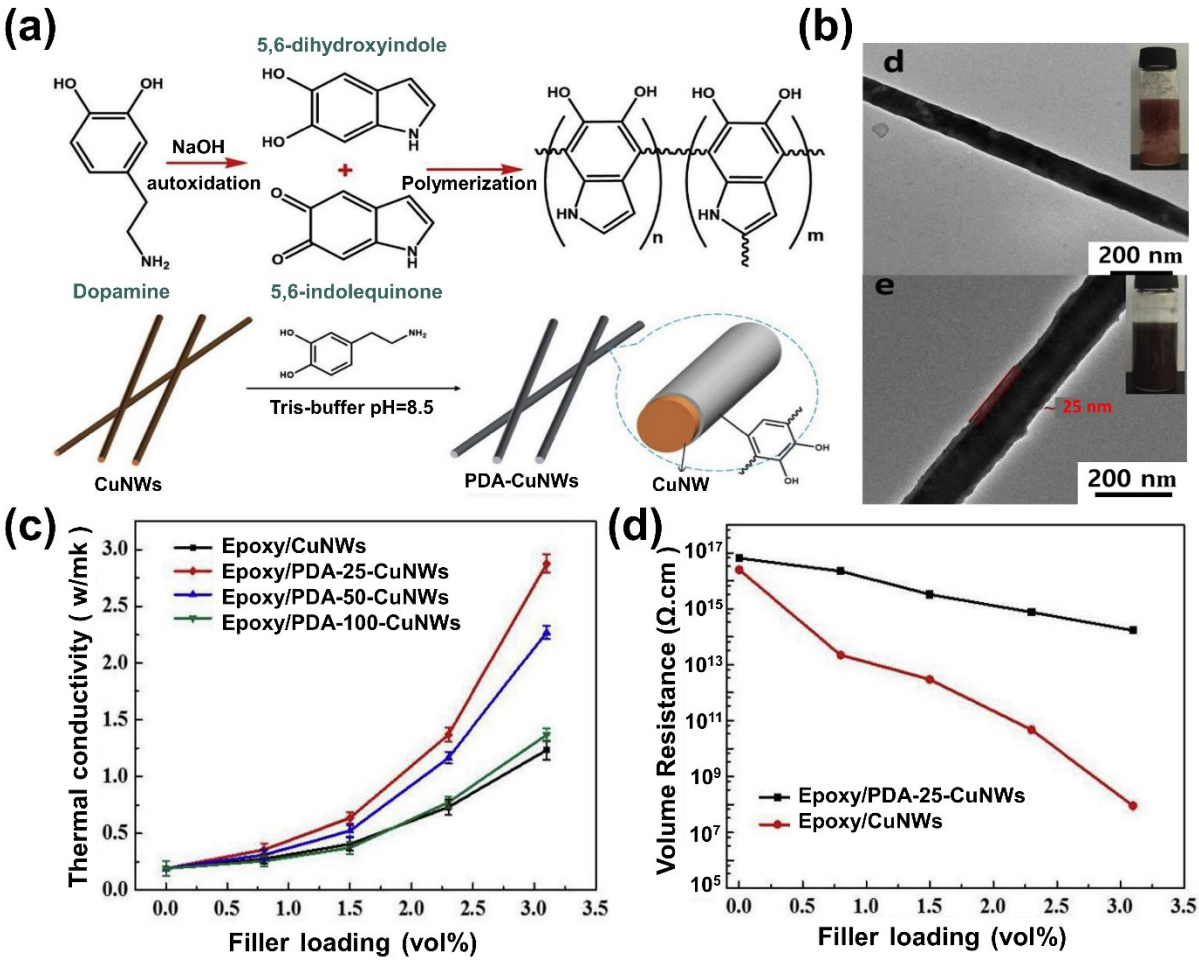

Fig. 12. (a) Preparation procedure for PDA-coated CuNWs and (b) TEM images of raw CuNWs and CuNWs coated with 25 nm of PDA; (c) thermal conductivity of the composites with CuNWs coated with different amounts of PDA as a function of the filer loading, and (d) volume resistance of the composites with raw CuNWs and with PDA-25-CuNWs [125]. Reprinted with permission from [125]; copyright 2018 Elsevier.

Overall, the surface tuning of fillers has proven advantageous in overcoming the limitations of fillers by reducing the interfacial thermal resistance and the tendency of fillers to aggregate in composites. However, surface modification may also decrease the intrinsic thermal conductivity of the fillers, thereby decreasing the total thermal conductivity of the composites. In addition, when a brittle ceramic layer is applied to the surface of the fillers, it may degrade the mechanical flexibility. Furthermore, such modifications involve an

additional synthesis process, which decreases the cost effectiveness. Therefore, to achieve high thermal conductivity without complex surface modifications, researchers have attempted to the align the fillers, as discussed in the next section.

3. Enhancement of thermal conductivity by aligning the fillers

Aligning fillers in a parallel or vertical direction is another efficient way to enhance the thermal conductivity of the composite, as it brings fillers into contact to form efficient heat dissipation paths, exploiting not only the thermal conductivity of the fillers but also the low interfacial thermal resistance of filler–filler contacts. In addition, it can prevent the aggregation of fillers by enabling uniform and effective thermal conduction using the same amount of filler composite fabrication processes without the alignment technology. Overall, the alignment of ceramic fillers has been shown to increase the thermal conductivity by 282–8707% relative to that of the composites with randomly distributed ceramic fillers.

3.1. Filler alignment in the in-plane direction

The anisotropic thermal conductivity of the composites can be enhanced using one- or two-dimensional materials such as carbon nanotubes, graphene, and BNNSs. Platelet and fiber-shaped fillers can be arranged in-plane by simple methods such as vacuum filtration or a doctor blade, both of which enhance the thermal conductivity of the composite in the parallel direction [158, 159]. Guo et al. [97] aligned nano-Al_2O_3 approximately 20 nm functionalized with APTES (f-Al_2O_3) in the in-plane direction using a vacuum filtration method (Fig. 13a). The mixed solution of f-Al_2O_3, reduced GO (rGO), and nanofibrillated cellulose (NFC) was

vacuum filtrated and dried to form composites with the f-Al_2O_3 aligned in the NFC in the horizontal direction. As shown in Fig. 13b, c, the composite with 30 wt% rGO and 5.6 wt% f-Al_2O_3 showed an in-plane thermal conductivity of 8.3 W/mK and electrical resistivity $>10^9$ Ω cm. Wang et al. [105] also used vacuum filtration to fabricate composites with horizontally aligned BNNSs in an ethylene–vinyl acetate copolymer (EVA) matrix, as shown in Fig. 13d, e. Further, the composite with 50 wt% BNNSs showed an excellent in-plane thermal conductivity of 13.2 W/mK (Fig. 13f).

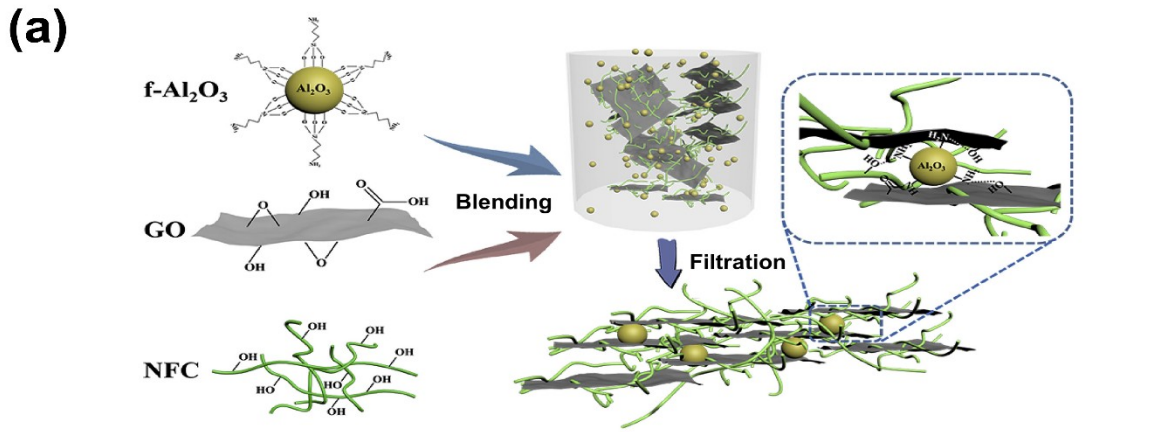
(a)
f-Al2O3
GO
NFC
Blending
Filtration

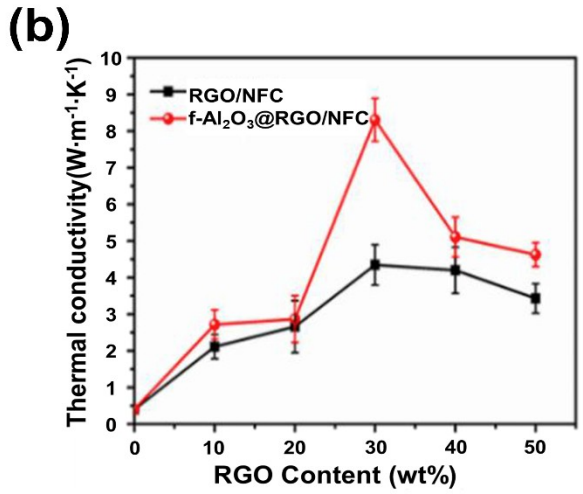
(b)
RGO/NFC
f-Al2O3@RGO/NFC
Thermal conductivity(W·m-1·K-1)
RGO Content (wt%)

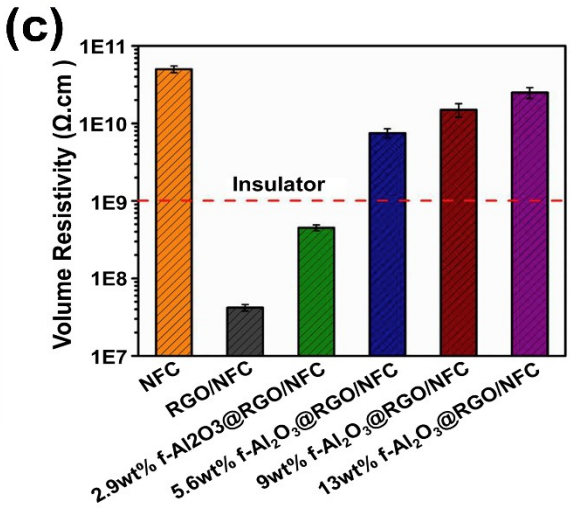
(c)
Volume Resistivity (Ω.cm)
Insulator
NFC
RGO/NFC
2.9wt% f-Al2O3@RGO/NFC
5.6wt% f-Al2O3@RGO/NFC
9wt% f-Al2O3@RGO/NFC
13wt% f-Al2O3@RGO/NFC

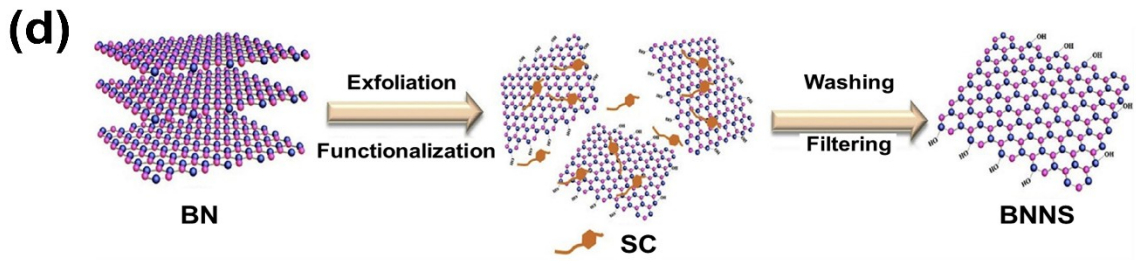
(d)
BN
Exfoliation
Functionalization
SC
Washing
Filtering
BNNS

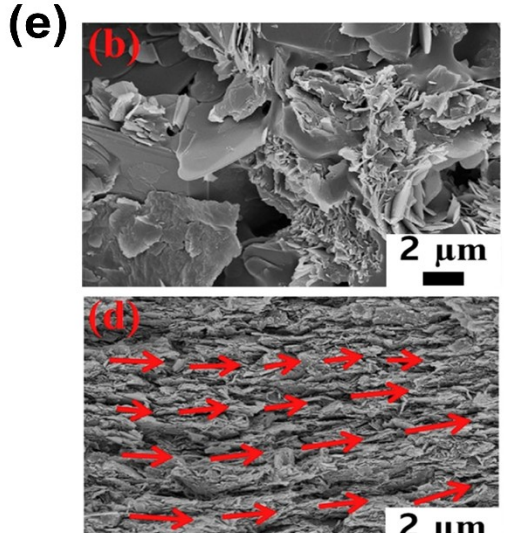
(e)
(b)
2 μm
(d)
2 μm

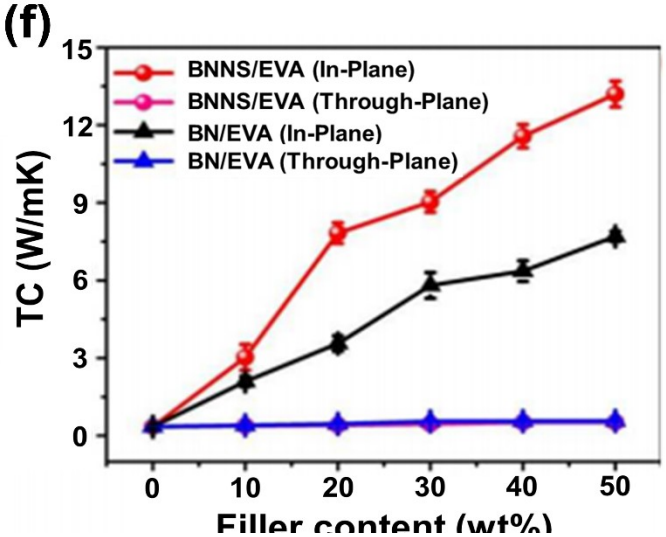
(f)
BNNS/EVA (In-Plane)
BNNS/EVA (Through-Plane)
BN/EVA (In-Plane)
BN/EVA (Through-Plane)
TC (W/mK)
Filler content (wt%)

Fig. 13. (a) Illustration of the fabrication process for f-Al_2O_3@RGO/NFC composites, (b) thermal conductivity of RGO/NFC and 5.6 wt% f-Al_2O_3@RGO/NFC composites with different RGO contents and (c) volume resistivity of pure NFC, RGO/NFC and f-Al_2O_3@RGO/NFC composites with different f-Al_2O_3 contents [97]. (d) Schematic of the process for functionalizing BNNSs, (e) cross-sectional SEM image of BN/EVA and BNNS/EVA composites with 50 wt% filler content, and (f) thermal conductivity of BNNS/EVA and BN/EVA composites with different filler contents [105]. Reprinted with permission from [97]; copyright 2019 Elsevier. Reprinted with permission from [105]; copyright 2020 Elsevier.

Meanwhile, Chen et al. [102] used a doctor blade to align BNNSs in a CNF matrix. As shown in Fig. 14a, c, d, the BNNS aligned along the direction of the shear force that formed the continuous heat dissipation paths through filler–filler contacts. The high thermal conductivity of 24.66 W/mK was observed in the in-plane direction for the composite with the aligned BNNSs at a loading of 50 wt%, which was three times higher than the conductivities of BNNS/CNF composites without shear force alignment (8.61 W/mK), as shown in Fig. 14b.

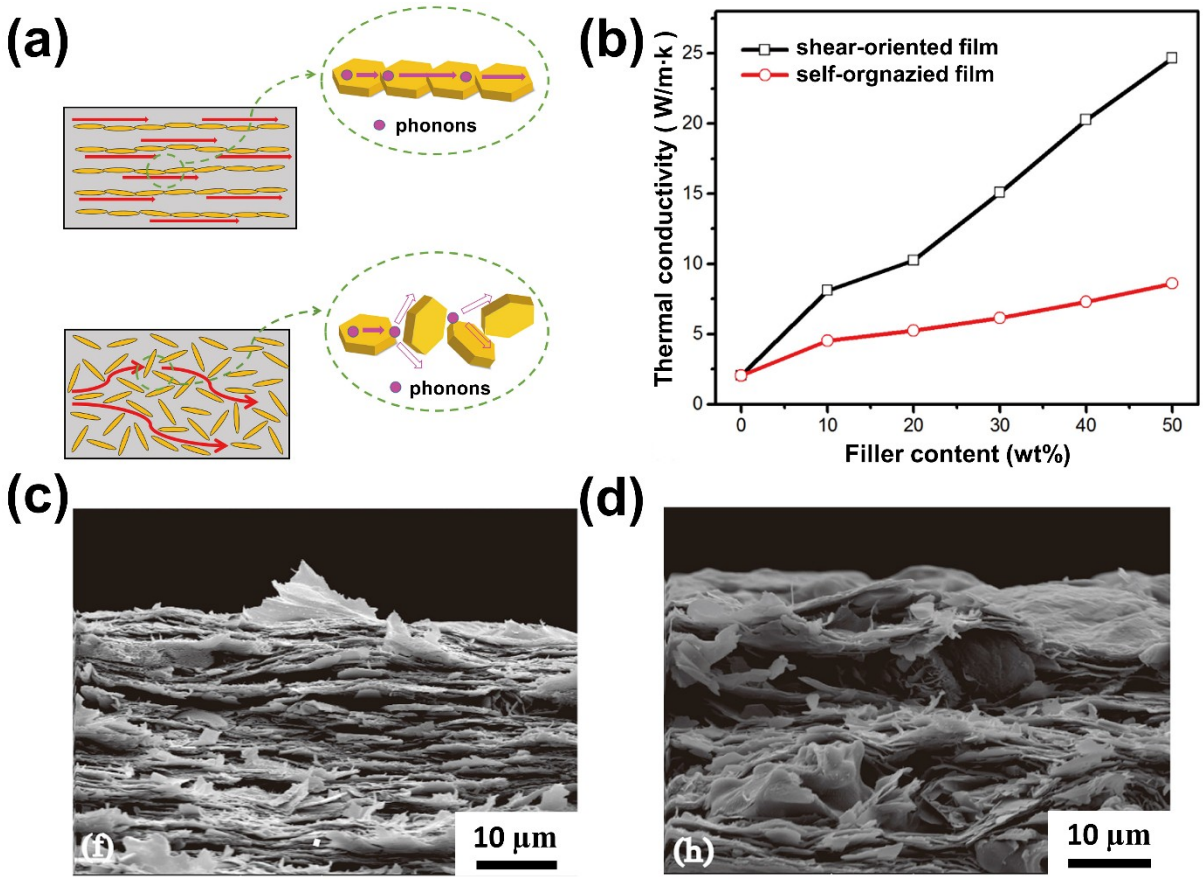

Fig. 14. (a) Schematic diagrams of thermal conduction through shear-oriented (top) and self-organized (bottom) BNNS/CNF composites, (b) thermal conductivity of shear-oriented composites and self-organized BNNS/CNF composites with different filler contents, and SEM images taken at the fractured surface of (c) shear-oriented and (d) self-organized BNNS/CNF composites [113]. Reprinted with permission from [113]; copyright 2019 Elsevier.

3.2. Filler alignment in the cross-plane direction

Although aligning the fillers in the parallel direction is simple [160, 161], TIMs with high thermal conductivity in the cross-plane direction are more desirable because they can be used to bridge a heat source and a heat sink. However, anisotropic fillers tend to lie down in-plane; thus, external stimuli, such as a temperature drop or a magnetic or electric field, are required to arrange the filler in the vertical direction, which makes the arrangement of the fillers in the

perpendicular direction more difficult than that in the in-plane direction.

For example, Jiang et al. [162] fabricated polyethylene glycol/BN framework (PBNF) composites with vertically arranged BN using unidirectional freezing, as shown in Fig. 15a. The resulting composite with 8.1 vol% PBNF showed a higher thermal conductivity in the vertical direction than the polyethylene glycol/BN without a framework (PBN) composite at the same loading, namely of 1.3 and ~0.66 W/mK, respectively. This increase was attributed to the reduction in interfacial thermal resistance and phonon scattering owing to the effective thermal conduction paths formed by the well-connected BN fillers.

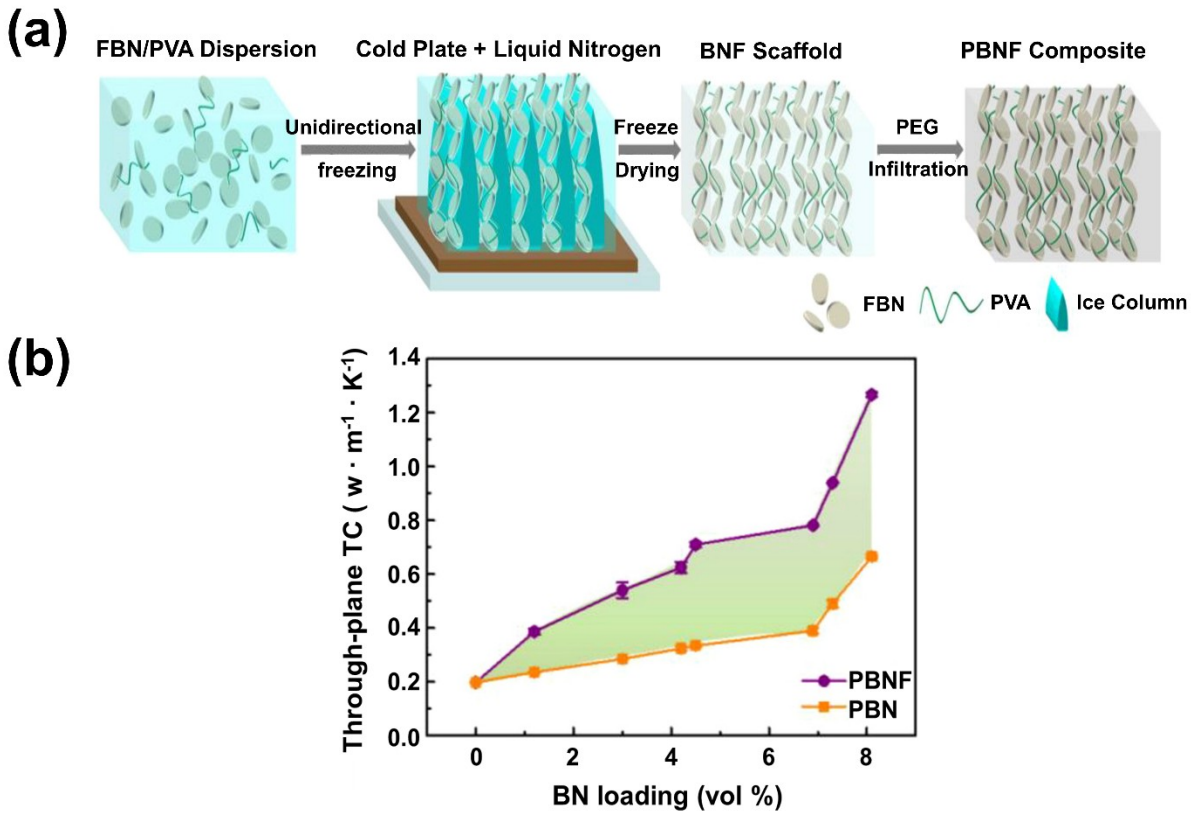

Fig. 15. (a) Schematic diagram of the preparation process for the PBNF composite and (b) comparison of the vertical thermal conductivities between the PBNF and PBN composites. Reprinted with permission from [162]; copyright 2021 American Chemical Society.

In another work, Kim et al. [114] first BNNPs with Fe_3O_4 particles (20–30 nm) through van

der Waals interactions in solution states; then, they applied an external magnetic field of 4 T to align the Fe_3O_4-decorated BNNPs in EP to form a composite (Fig. 16a). The thus-aligned BNNPs formed continuous thermal conduction paths in the direction of the magnetic field (Fig. 16b); the resulting thermal conductivity of the EP composites with a loading of 20 wt% was 1.07 W/mK in the vertical direction, whereas that of the corresponding composite with randomly distributed BNNPs was only 0.620 W/mK, as shown in Fig. 16c. Electrical field have also been used to align fillers in thermally conductive composites. As shown in Fig. 17a, Cho et al. [163] fabricated polydimethylsiloxane (PDMS) composites by aligning BNNS with an external electric field. Specifically, they applied a pulsed direct current field to a BNNS/PDMS mixture, which densely aligned the BNNS fillers along the electric field direction (Fig. 17c, d) and yielded a vertical thermal conductivity of 1.56 W/mK at a filler loading of 15 vol%, whereas the composites without filler alignment had a conductivity of only 0.4 W/mK (Fig. 17b).

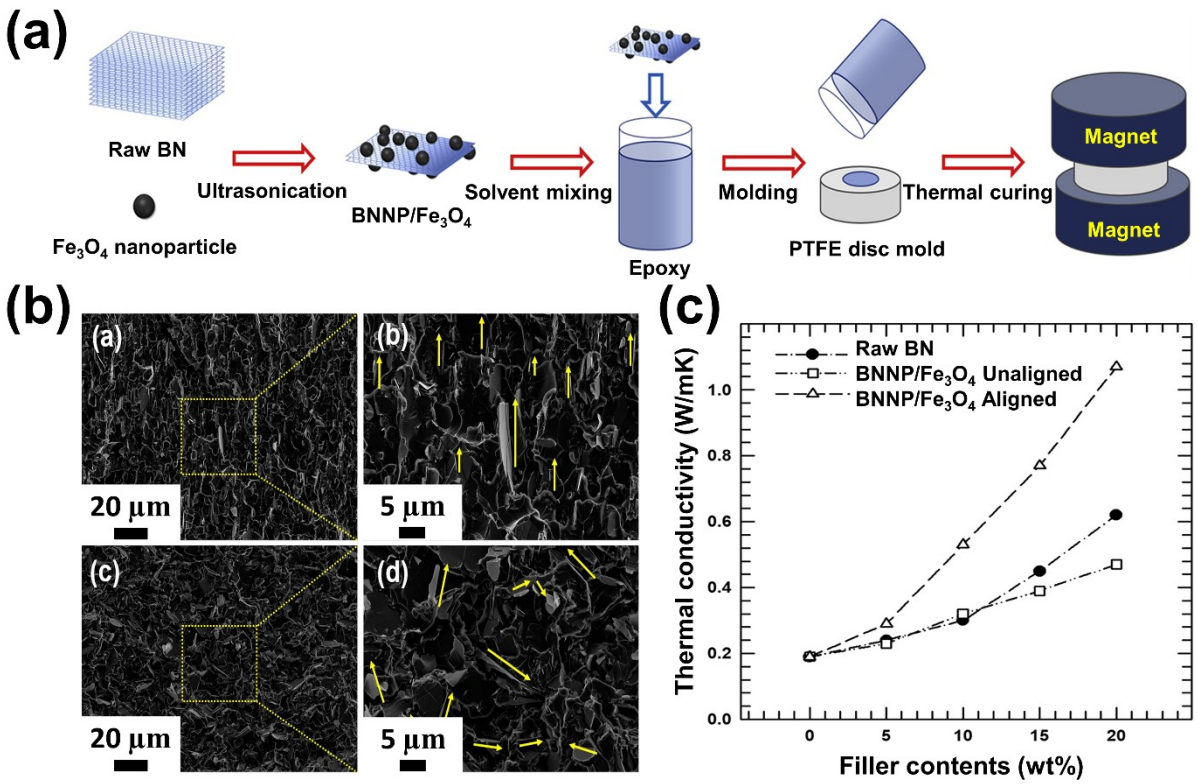

Fig. 16. (a) Schematic diagram of the fabrication process for EP composites with aligned BNNP/Fe_3O_4, (b) cross-sectional SEM images of composites with aligned and unaligned BNNP/Fe_3O_4 and (c) thermal conductivity of the composites with raw BN, unaligned BNNP/Fe_3O_4, and aligned BNNP/Fe_3O_4 [114]. Reprinted with permission from [114]; copyright 2020 Elsevier.

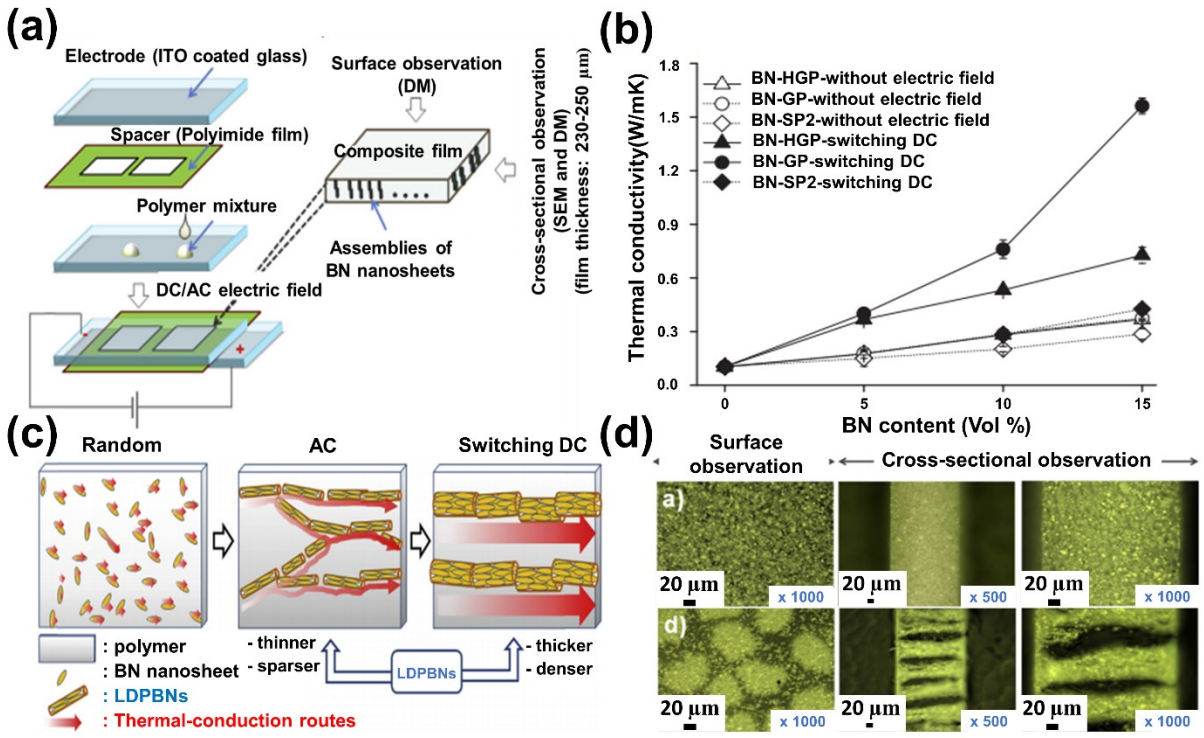

Fig. 17. (a) Schematic illustration of the experimental setups for the alignment of BNNSs using an electric field, (b) thermal conductivity of the PDMS/BNNS composites under a switching electric field, (c) schematic illustration of the process of aligning BNNSs using various types of electric fields, and (d) digital micrographs of the PDMS/BNNS composites without an electric field and with a switching electric field [163]. Reprinted with permission from [163]; copyright 2016 Elsevier.

As described thus far, the thermal conductivity of the composites has been enhanced by aligning the fillers with the aforementioned methods. However, this conductivity was enhanced only along the direction of alignment, thus introducing tremendous anisotropy into the thermal conductivity, depending on the direction. Such anisotropy is not appropriate for general-purpose thermally conductive composites because of undesirable heat localization in directions in which thermal conduction paths are not formed. Isotropic conductivity remains highly desirable for many applications, thus requiring other methods for distributing thermally conductive fillers in the matrix, as discussed in the following section.

4. 3D filler networking method

To solve the issues with the composites discussed thus far, namely the low thermal conductivity of composites with randomly distributed fillers and the anisotropic heat dissipation of composites with fillers aligned in a single direction, researchers have recently studied 3D filler networking composites [116, 118, 120, 164]. Although the composites using isotropic fillers can produce isotropic thermal conduction even in randomly distributed states, anisotropic fillers generally outperform isotropic fillers in terms of thermal conductivity. Therefore, using anisotropic fillers is preferable, but they provide unsatisfactory isotropic thermal conduction. 3D filler networking can resolve this issue by forming a continuous, 3D isotropic network from anisotropic filler backbones in the composites. Recently, 3D filler networking composites have been developed using three principal strategies: 1) construction of 3D structures with ceramic frames, which are then filled with a polymer resin to form composites, 2) formation of ceramic layers on the frames of 3D-structured polymers or metals, and 3) packing ceramic-filler-coated polymer powder to form composites. All these methods have successfully resulted in composites with ceramic fillers forming continuous thermal conduction paths in all directions, thus resolving the previously discussed limitations of thermally conductive composites by enabling multiaxial heat dissipation.

4.1. Composites with 3D-structured ceramic frames filled with polymer resin

First, 3D-structured thermally conductive composites were formed from 3D-structure ceramic frames, which were then filled with polymer resin. In such structures, the ceramic frames

form continuous thermal conduction paths, while the elasticity of the composites was provided by the polymer resin infiltrating the spaces among the ceramic frames.

Freeze-casting is one of the most extensively used methods for the formation of 3D-structured ceramic frames because of the simplicity of using an ice template. By exploiting the anisotropic solidification behavior of a solvent in a dispersed slurry, the structure of directional and porous ceramic foams can be controlled. As shown in Fig. 18a, b, Wei et al. [146] fabricated AlN honeycomb (AlN-H) structures via freeze-casting followed by EP infiltration. Tert-butyl alcohol (TBA) was used as the solvent because of its low melting point and low reactivity with AlN, which is preferable for forming honeycomb structures. The fabricated AlN-H was further treated with a SCA (KH-560) before being infiltrated with EP, thereby reducing the thermal resistance of the interface with the EP matrix. When the ceramic frame occupied 47.3 vol% of the total composite, it exhibited excellent thermal conductivity values in both horizontal and perpendicular directions to the AlN-H channels, namely 9.48 and 4.45 W/mK, respectively (Fig. 18c). In another study, Huang et al. [127] developed a bidirectional structure via freeze-casting utilizing temperature gradients in both radial and vertical directions (Fig. 19a). In these gradients, a BNNS aerogel was radially aligned as a lamellar structure, which allowed effective thermal conduction in both these directions (Fig. 19b). The composites with bidirectionally aligned BNNS at a loading of 15 vol% exhibited high thermal conductivities in the out-of-plane and in-plane directions of 4.02 and 3.87 W/mK, respectively, as shown in Fig. 19c.

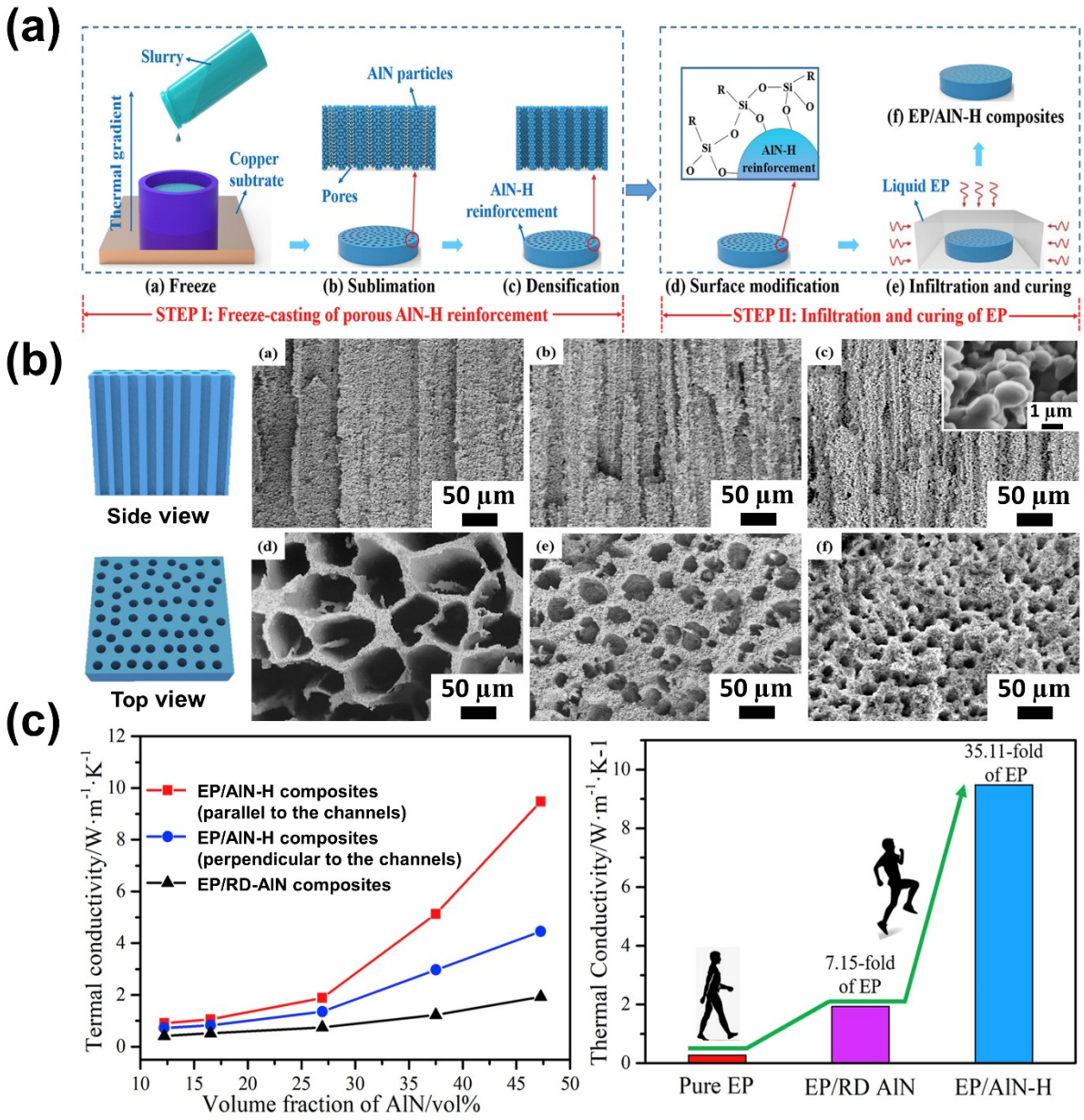

Fig. 18. (a) Schematic illustration of the fabrication procedure for EP/AlN-H composites, (b) side- and top-view SEM images of EP/AlN-H composites with different filler loadings (10, 20, and 30 vol%), and (c) thermal conductivity of pure EP, EP/RD AlN, and EP/AlN-H [146]. Reprinted with permission from [146]; copyright 2020 Elsevier.

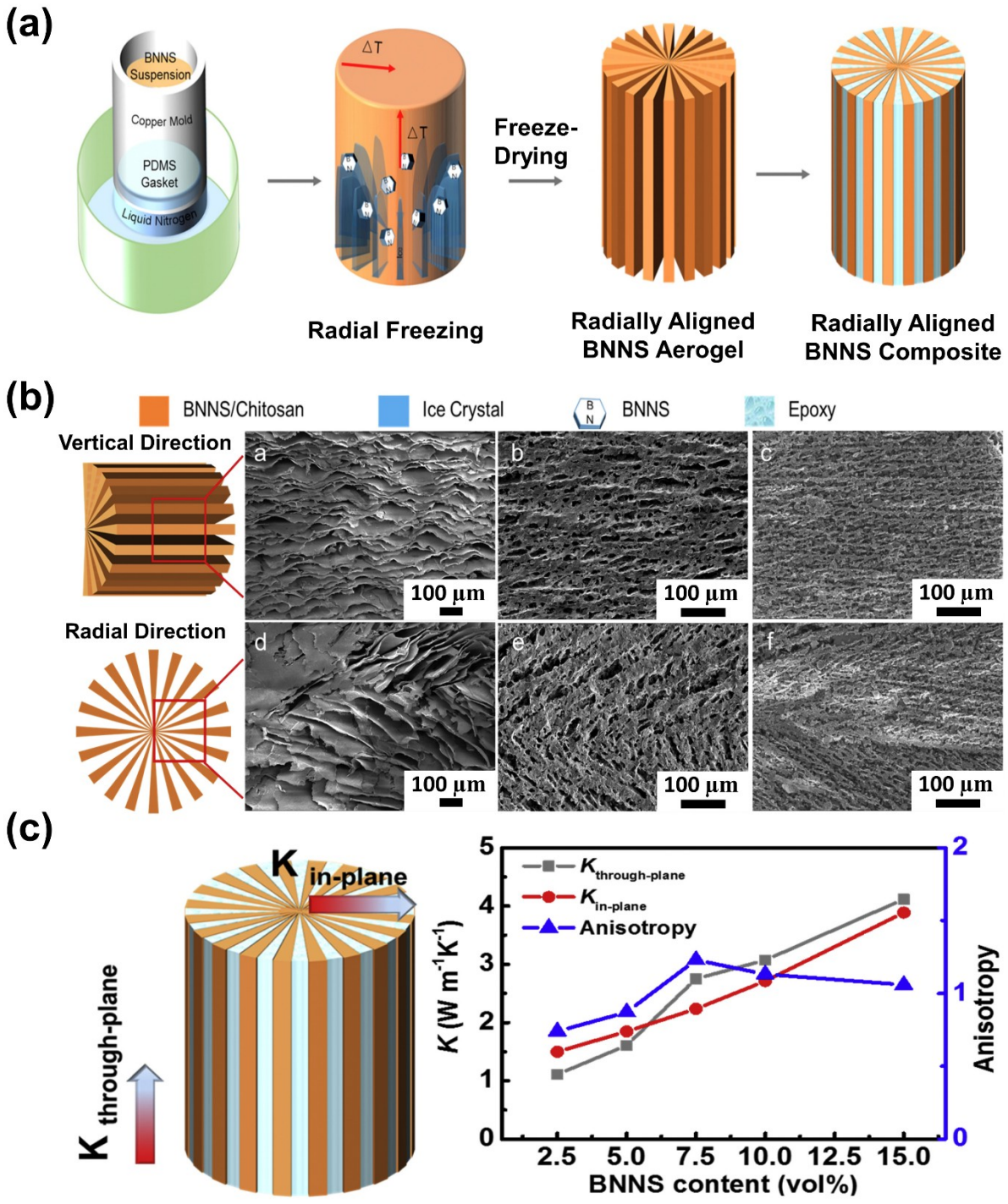

Fig. 19. (a) Schematic diagram of the process for radially aligning BNNS/EP composites through radial freeze-casting, (b) SEM images of BNNS aerogels in the vertical and radial directions with different BNNS loadings (2.5, 5, and 10 vol%), and (c) thermal conductivity of the BNNS/EP composites with different BNNS contents [127]. Reprinted with permission from [127]; copyright 2020 Elsevier.

Another way to fabricate thermally conductive composites with 3D-structured ceramic frames is freeze-drying (also known as lyophilization), wherein ice crystals form in the ceramic structure at low temperatures and pressures. These crystals are then removed by sublimation, thereby forming 3D-structured ceramic frames. As shown in Fig. 20a, Chen et al. [122] fabricated thermally conductive composites with 3D-structured BNNS and CNF frames using freeze-drying. First, CNF and BNNSs were mixed with urea and epichlorohydrin as a cross-linking agent to form 3D-C-BNNS hydrogels. Subsequent freeze-drying converted the 3D-C-BNNS hydrogel into an aerogel structure. By filling the vacant spaces in the aerogel with EP resin, they fabricated thermally conductive composites with 3D-structured BNNS/CNF frames (Fig. 20b), which exhibited a high thermal conductivity of 3.13 W/mK as well as electrical resistivity > 10^{15} Ω cm at a BNNS loading of 9.6 vol% (Fig. 20c). Wang et al. [57] also used freeze-drying to develop thermally conductive composites from BNNS functionalized with $_{D}$-glucose, which was mixed with poly(amic acid) (PAA) and then freeze-dried to form the aerogel structure of the fillers. The functionalization of $_{D}$-glucose formed hydroxyl groups on the surfaces of BNNSs, which improved their dispersibility in water and formed hydrogen bonds with PAA. The aerogels were then cross-linked in a tube furnace while purging with nitrogen at a maximum temperature of 300 °C for 2 h, which formed polyimide composites with 3D-structured BNNS frames (Fig. 20d, e). The thus-fabricated thermally conductive composites showed thermal conductivities of 6.7 W/mK (out-of-plane) and 2.2 W/mK (in-plane) at a functionalized BNNS content of 50 wt%, as shown in Fig. 20f.

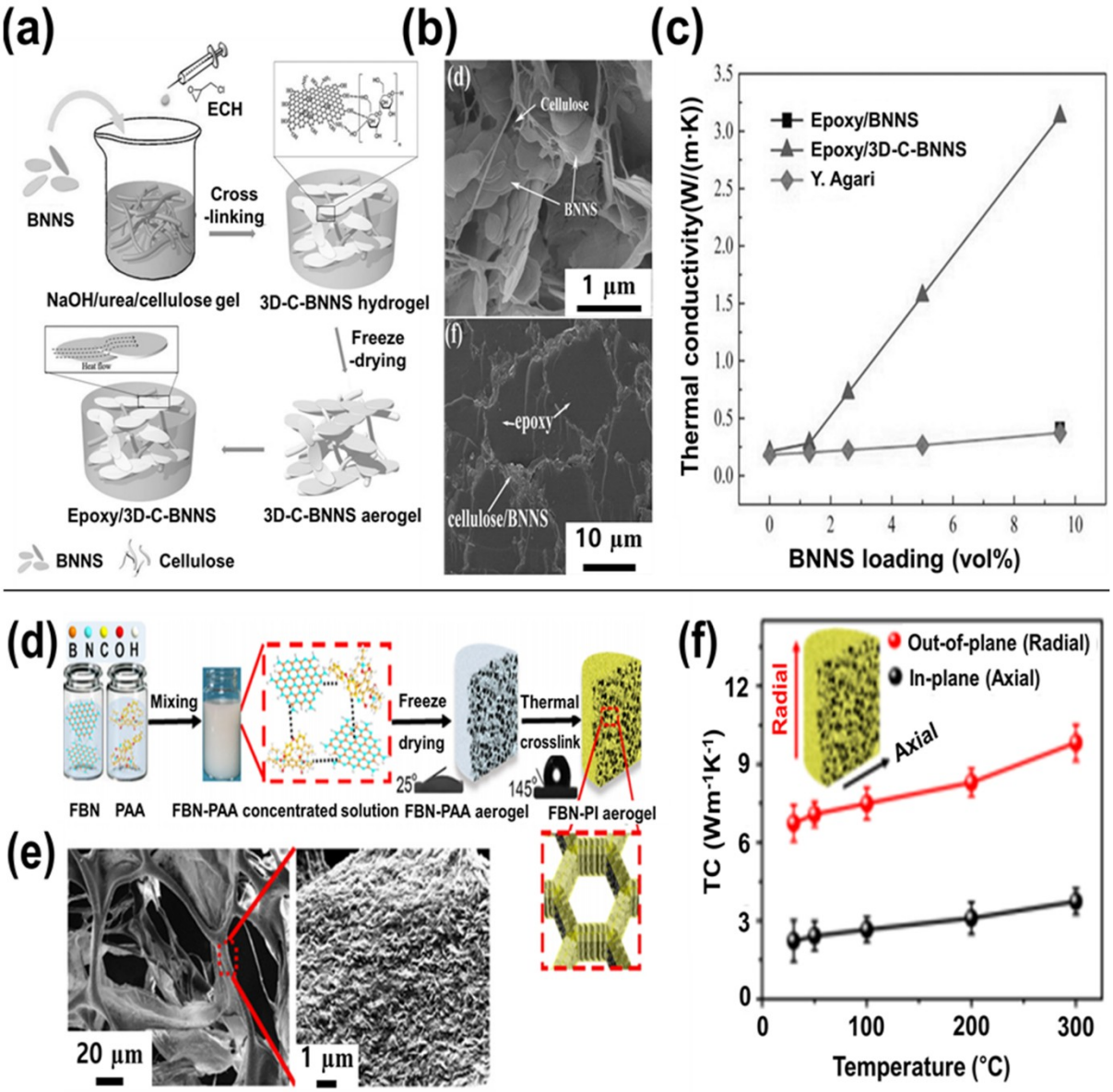

Fig. 20. (a) Schematic illustration of the fabrication procedure for EP/3D-C-BNNS composites, (b) SEM images of the 3D-C-BNNS aerogel and the fractured surface of EP/3D-C-BNNS composite, and (c) thermal conductivity of the EP/3D-C-BNNS composites [122]. (d) Schematic illustration of the fabrication procedure, (e) SEM images, and (f) thermal conductivity of the FBN-PI aerogel [57]. Reprinted with permission from [122]; copyright 2016 John Wiley and Sons. Reprinted with permission from [57]; copyright 2019 American Chemical Society.

The 3D-structured ceramic frames have also been fabricated with the use of foaming agents.

In these methods, the fillers are mixed with the foaming agents and then processed at high temperatures or pressures to form 3D-structured ceramic frames. The foaming agent is completely decomposed under conditions specified for the agent. The polymeric resins fill the spaces in the 3D-structured ceramic frames, thus forming 3D-structured, thermally conductive composites. As shown in Fig. 21a, b, Xu et al. [165] used NH_4HCO_3 as a foaming agent to fabricate the EP composites with 3D-structured BN frames. Specifically, they mixed BN fillers with NH_4HCO_3 followed by pressing at 300 MPa and heating at 80 °C for 12 h to form 3D-structured BN frames. By removing NH_4HCO_3 in a NH_3 and CO_2 gas, they successfully synthesized 3D-structured BN foams (BNFs). They then fabricated thermally conductive composites by immersing the BNFs in the EP resin with a subsequent thermal curing process, thereby yielding BN composites with an excellent thermal conductivity of 6.11 W/mK at a BN content of 59.43 vol% (Fig. 21c). In another study, Tian et al. [121] used sodium dodecyl sulfate (SDS) mixed with gelatin as a foaming agent, wherein SDS was the main foaming agent, while gelatin maintained the structural integrity of resulting 3D-structured BN frames (Fig. 22a). With a similar method to that used by Xu et al. [165], the EP resin was poured into the 3D-structured BNFs and thermally cured to form thermally conductive composites (Fig. 22b). As shown in Fig. 22c, the composites with a BN content of 24.4 wt% exhibited high thermal conductivities of 5.19 and 3.48 W/mK in the in-plane and out-of-plane directions, respectively. As shown in Fig. 23a, c, Xiao et al. [166] fabricated 3D-structured Al_2O_3 frames with albumen powder as the foaming agent and sintering at a maximum temperature of 1550 °C for 2 h, which the decomposed foaming agent was. The resulting foams were then infiltrated with EP resin and thermally cured, thereby forming thermally conductive composites with 3D-structured Al_2O_3 frames and affording an excellent thermal conductivity of 2.58 W/mK with an Al_2O_3 content of 23.32 vol% (Fig. 23b).

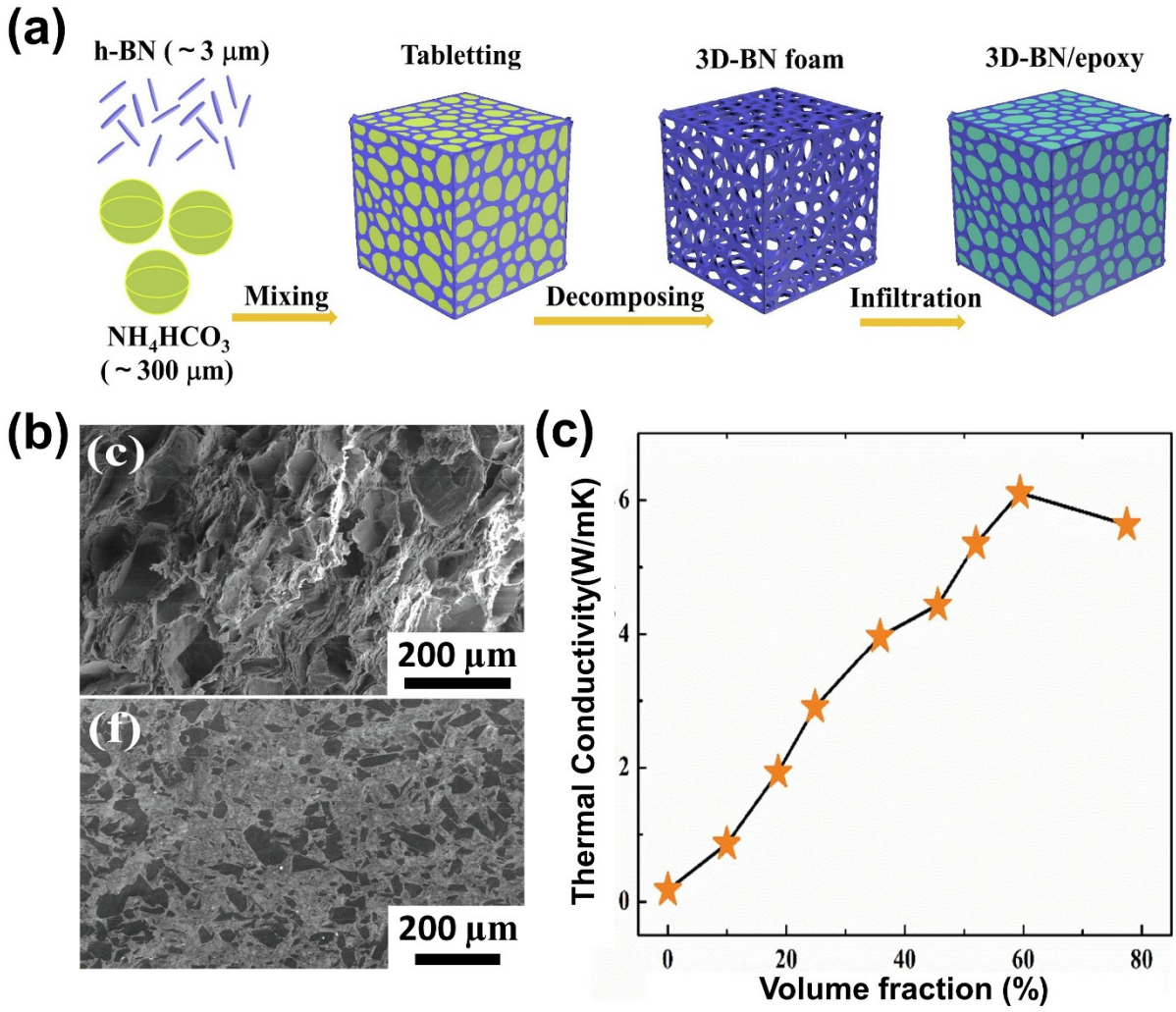

Fig. 21. (a) Schematic illustration of the fabrication process for 3D-BN/EP composites, (b) cross-sectional SEM image of 3D-BNF and top-view image of a polished surface of the 3D-BN/EP composite, and (c) thermal conductivity of 3D-BN EP composites with different BN volume fractions [165]. Reprinted with permission from [165]; copyright 2020 Elsevier.

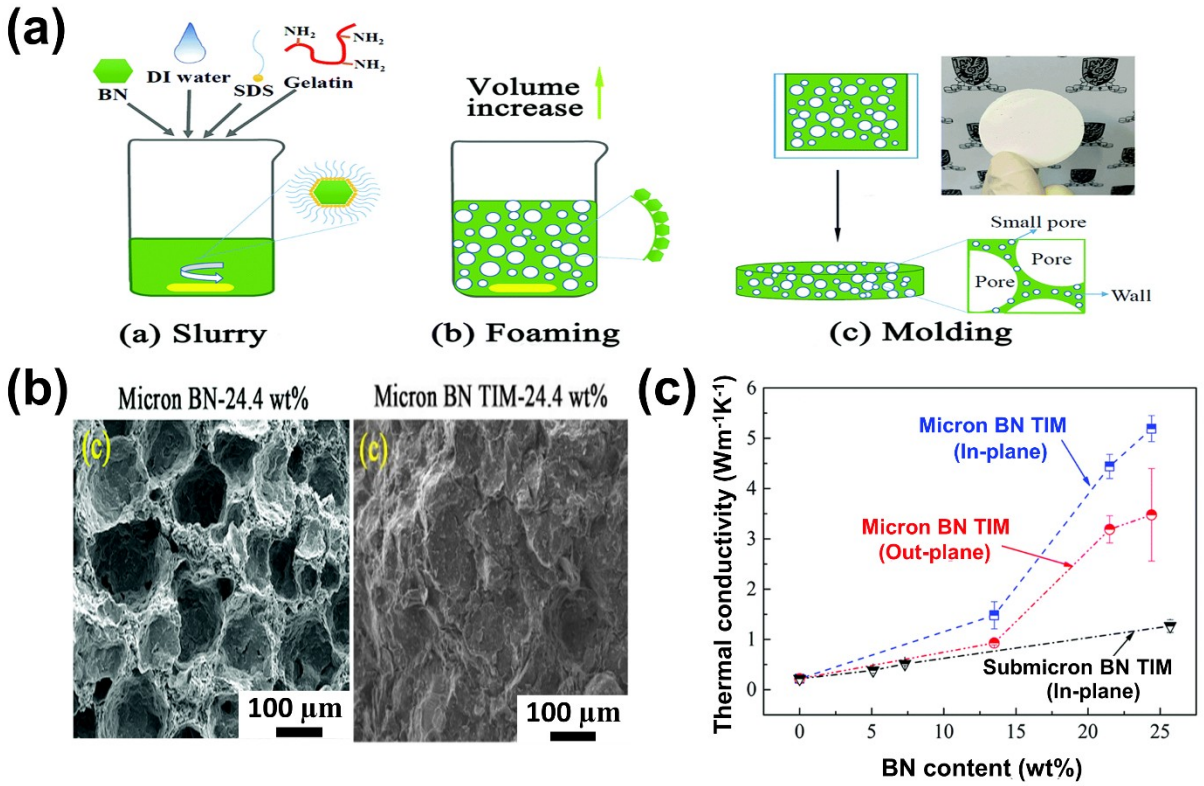

Fig. 22. (a) Schematic illustration of the fabrication process for porous BNF, (b) SEM images of microstructures of the porous BNF and BN/EP composites, and (c) thermal conductivity of the 3D BN/EP composites with different BN contents [121]. Reprinted with permission from [121]; copyright 2018 Royal Society of Chemistry.

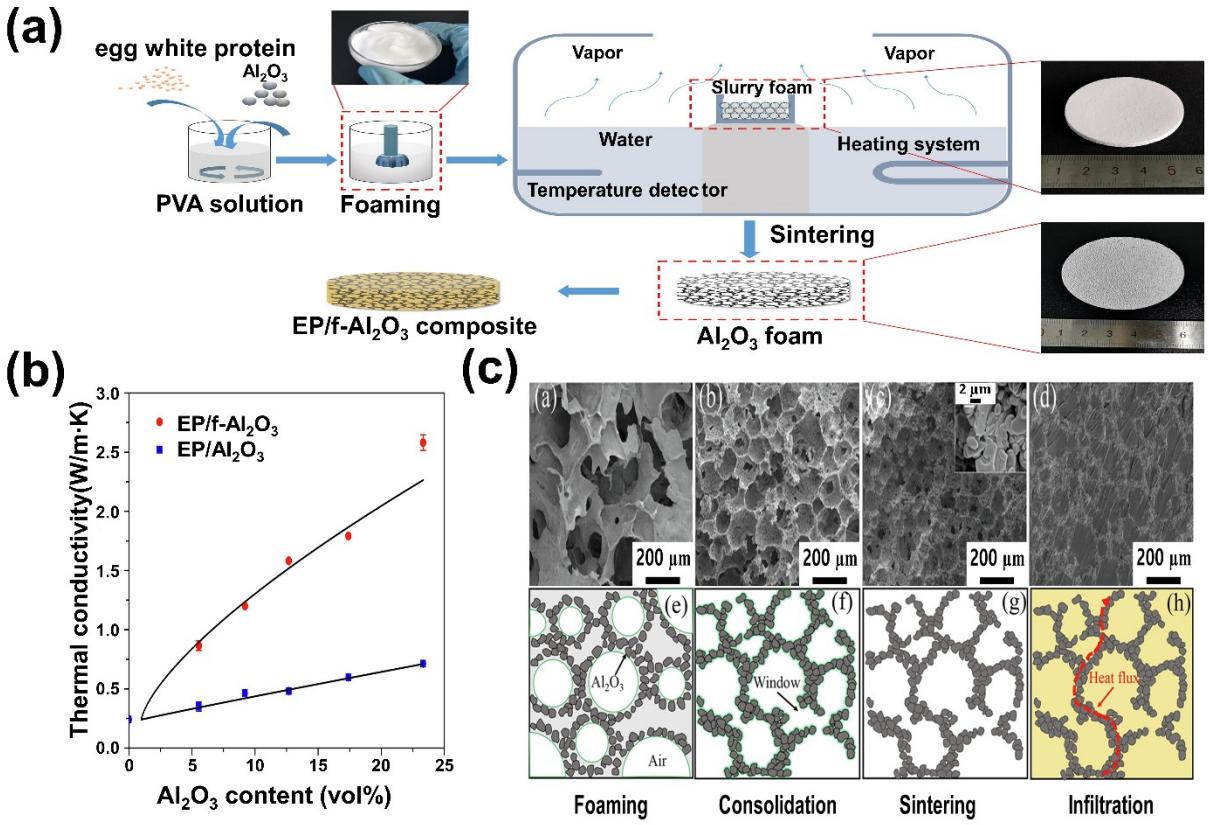

Fig. 23. (a) Schematic illustration of the preparation process for 3D Al_2O_3/EP composites, (b) thermal conductivity 3D Al_2O_3/EP composites and Al_2O_3/EP composites with different Al_2O_3 contents, and (c) SEM images and schematic diagrams of the thermally conductive network during the fabrication of the 3D Al_2O_3/EP composite [166]. Reprinted with permission from [166]; copyright 2019 Elsevier.

Salt templates have also been used to fabricate 3D-structured ceramic frames for composites, wherein the recrystallization of NaCl mixed with ceramic fillers forms foam cores, which are then removed with water, thus forming 3D-structured ceramic frames. As shown in Fig. 24a, b, Xiao et al. [167] fabricated thermally conductive composites with 3D-structured frames of hollow BN microbeads (BNMBs) using salt templates. First, they mixed BNs with NaCl in a PVA solution; then, the NaCl coupled with BN recrystallized under magnetic stirring at 90 °C for 1 h. After removing the NaCl cores with cold water, hollow BNMBs were left behind,

which were then infiltrated with EP resin to form composites (Fig. 24c). The thermally conductive composites exhibited excellent in-plane and out-of-plane thermal conductivities of 17.61 and 5.08 W/mK, respectively, with 65.6 vol% BNMBs having average diameters of approximately 35 μm (Fig. 24d). Chen et al. [168] also used the salt template process to fabricate 3D-structured, thermally conductive composites. They mixed BN, PVDF, and NaCl and fabricated 3D-structured BN/PVDF frames using a salt template process similar to that described above, including the recrystallization and removal of NaCl (Fig. 25a). The fabricated 3D-structured BN/PVDF frames were converted into BN/carbon structures by defluorinating PVDF with a solution of NaOH and tetra-n-butylammonium bromide. The defluorination process enhanced the thermal conductivity by matching the phonon spectra at the filler–polymer interface in a manner similar to that for BN, thereby reducing phonon scattering (Fig. 25b). The thermal conductivities of the composites with and without the defluorination process were 1.47 and 1.2 W/mK at a BN loading of 21 wt%, respectively, as shown in Fig. 25c, d.

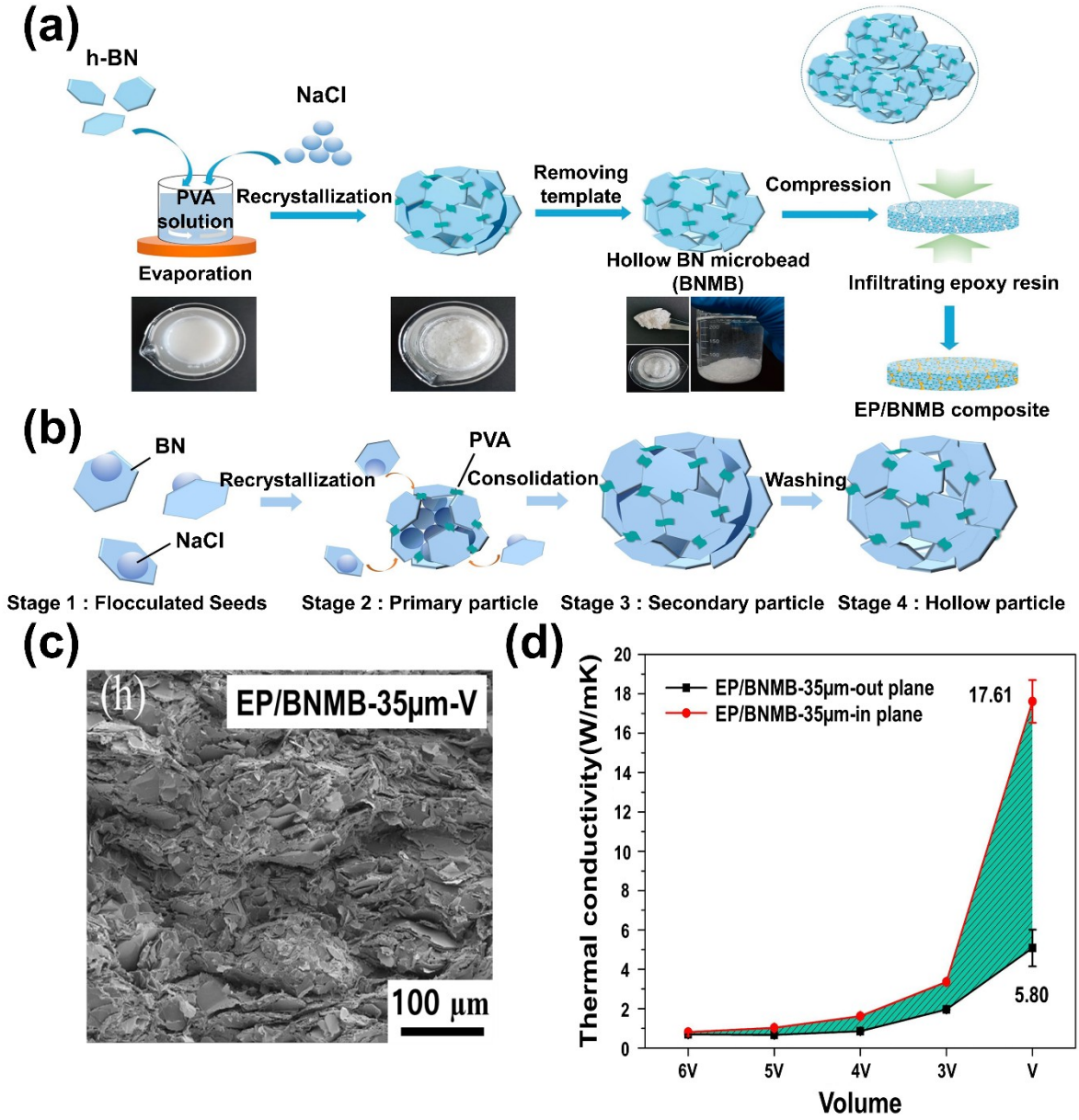

Fig. 24. (a) Schematic illustrations of the fabrication procedure for EP/BNMB composites and (b) the formation mechanism of hollow BNMBs, (c) cross-sectional SEM image of the EP/BNMB-35 μm composite and (d) thermal conductivity of EP/BNMB-35 μm composites under different pressures [167]. Reprinted with permission from [167]; copyright 2019 Elsevier.

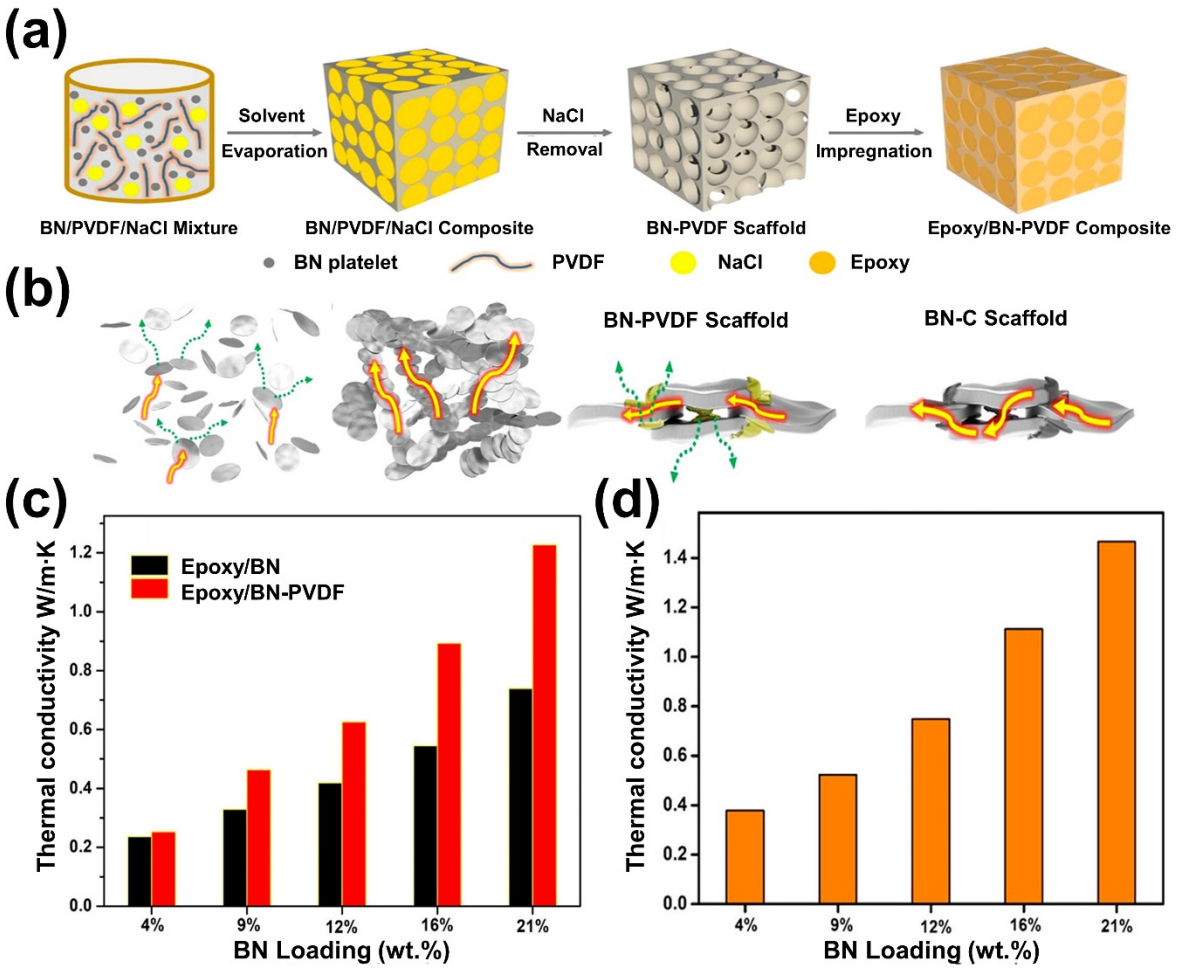

Fig. 25. (a) Schematic illustrations of the preparation process for EP/BN-PVDF composites and (b) thermal conduction mechanism of the composites with and without BN-PVDF and BN-C scaffolds; thermal conductivity of the (c) EP/BN-PVDF and (d) EP/BN-C composites [168]. Reprinted with permission from [168]; copyright 2020 American Chemical Society.

4.2. Methods utilizing a 3D-structured matrix

Forming ceramic layers on the 3D-structured matrix is another way to construct thermally conductive composites with continuous thermal conduction paths. In this method, chemical vapor deposition (CVD) has been used extensively to form a thin ceramic layer on the 3D-structured matrix.

Fang et al. [169] used Ni foams were as templates, which they coated with BN using CVD (Fig. 26a). By selectively etching away the Ni, they first fabricated BNFs, which they then infiltrated with BNNSs mixed in PDMS to form 3D-structured, thermally conductive composites wherein the BNNSs provided additional thermal conduction paths by bridging the BN frames (Fig. 26b). As shown in Fig. 26c, the fabricated composites demonstrated a thermal conductivity of 0.56 W/mK at 10.4 wt% of BNF and BNNSs. Meanwhile, Xue et al. [170] used 3D carbon-nanorod-based foams (3D-Cs) as templates and formed BN on this frame using an in situ carbothermal reduction CVD process, as shown in Fig. 26d. The final form of the BN was determined by the CVD reaction time. The BN initially formed nanorods (3D-R-BNs), which were transformed into BN nanosheets (3D-NS-BN) in a reaction with an excess of B_2O_2 and N_2. After dipping the 3D-BNFs into the poly(methyl methacrylate) (PMMA) solution, 3D-structured thermally conductive composites with continuous 3D-BN frames were fabricated. The composite with rod-shaped 3D-R-BN at filler contents of 51 wt % exhibited excellent thermally conductive values of 10.31 and 9.48 W/mK in the out-of-plane and in-plane directions, respectively, while those with nanosheet-based 3D-NS-BN were 6.75 and 6.14 W/mK, even at a higher loading of 56 wt% (Fig. 26f). This difference was due to the excessive reaction executed to form 3D-NS-BN, which changed the continually aligned BN nanorods in the initial 3D-R-BN morphology into hollow-structured BN nanosheets, thereby hindering heat flow (Fig. 26e). Vu et al. [171] fabricated 3D-rGO foams through freeze-drying and in situ carbothermal reduction and used them as templates for the formation of SiC layers through CVD, as shown in Fig 26g, h. Thermally conductive composites were then fabricated by infiltrating EP resin into the 3D-SiC foams, followed by thermal curing at 120 °C for 4 h and then at 160 °C for another 4 h. The fabricated composites had an excellent thermal conductivity of 10.26 W/mK at a SiC content of

approximately 6.5 vol% (Fig. 26i).

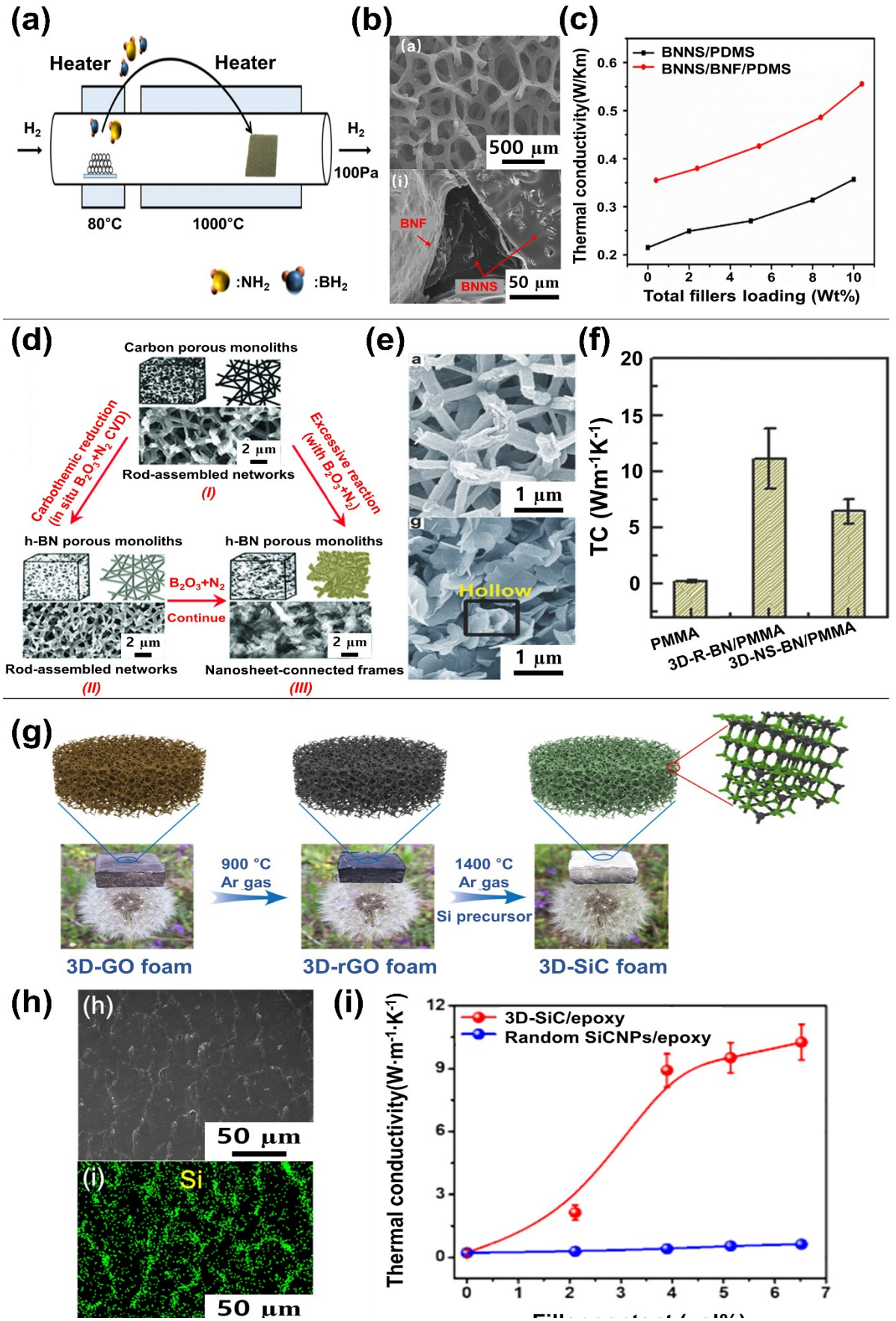
(a)
Heater
Heater
H2
H2
100Pa
80°C
1000°C
:NH2
:BH2
(b)
(a)
500 μm
(i)
BNF
BNNS
50 μm
(c)
BNNS/PDMS
BNNS/BNF/PDMS
Thermal conductivity(W/Km)
Total fillers loading (Wt%)
(d)
Carbon porous monoliths
2 μm
Rod-assembled networks
(I)
Carbothemic reduction (in situ B2O3+N2 CVD)
Excessive reaction (with B2O3+N2)
h-BN porous monoliths
h-BN porous monoliths
B2O3+N2
Continue
2 μm
2 μm
Rod-assembled networks
Nanosheet-connected frames
(II)
(III)
(e)
a
1 μm
g
Hollow
1 μm
(f)
TC (Wm-1K-1)
PMMA
3D-R-BN/PMMA
3D-NS-BN/PMMA
(g)
900 °C
Ar gas
1400 °C
Ar gas
Si precursor
3D-GO foam
3D-rGO foam
3D-SiC foam
(h)
(h)
50 μm
(i)
Si
50 μm
(i)
3D-SiC/epoxy
Random SiCNPs/epoxy
Thermal conductivity(W·m-1·K-1)

Fig. 26. (a) Schematic illustration of the fabrication of BNF, (b) SEM images of BNF and the BNNS/BNF/PDMS composite, and (c) thermal conductivity of BNNS/BNF/PDMS composites with different filler contents [169]. (d) Schematic fabrication procedure for 3D-R-BN and 3D-NS-BN frames, (e) SEM images of 3D-R-BN and 3D-NS-BN frames, and (f) thermal conductivity of pure PMMA, 3D-R-BN/PMMA, and 3D-NS-BN/PMMA composites [170]. (g) Schematic illustration of the fabrication process for 3D-SiC foam, (h) SEM image of 3D-SiC/EP composite and EDX mapping of Si in the composite, and (i) thermal conductivity of 3D-SiC/EP and random SiC/EP composites with different filler contents [171]. Reprinted with permission from [169]; copyright 2017 Elsevier. Reprinted with permission from [170]; copyright 2018 John Wiley and Sons. Reprinted with permission from [171]; copyright 2020 Elsevier.

The aforementioned methods eliminated the templates used to form 3D-structured ceramic foams by etching or substitution methods. However, other methods have exploited 3D templates without removing them, which is more convenient given that there no removal process involving toxic chemical etching is required. Avoiding such removal processes is definitely preferable for industrial use. For example, Lee et al. [172] fabricated thermally conductive composites by simply impregnating an EP/BN mixture through Cu foam. In the resulting composites, the 3D-structured Cu frames and aggregated BN worked as thermal conductive paths, yielding a high thermal conductivity of 2.017 W/mK. In addition, the EP resin filling and covering the Cu/BN frames afforded a volume resistivity of 1.21×10^{13} Ω cm, which is sufficient for applications requiring electrical insulation. As shown in Fig. 27a, Wang et al. [173] functionalized a melamine foam (MF) template with polyethyleneimine (PEI) to positively charge the MF surface. Subsequently, BNNSs with negatively charged surfaces were successfully coated onto the MF/PEI frames (Fig. 27b). Then, they infiltrated EP resin into the frame using vacuum infiltration to form thermally conductive composites, which showed a thermal conductivity of 0.6 W/mK at a BNNS loading of approximately 1.1

vol%, as shown in Fig. 27c. This conductivity was relatively low owing to the low BNNS contents, but this value may be significantly enhanced by increasing the filler contents.

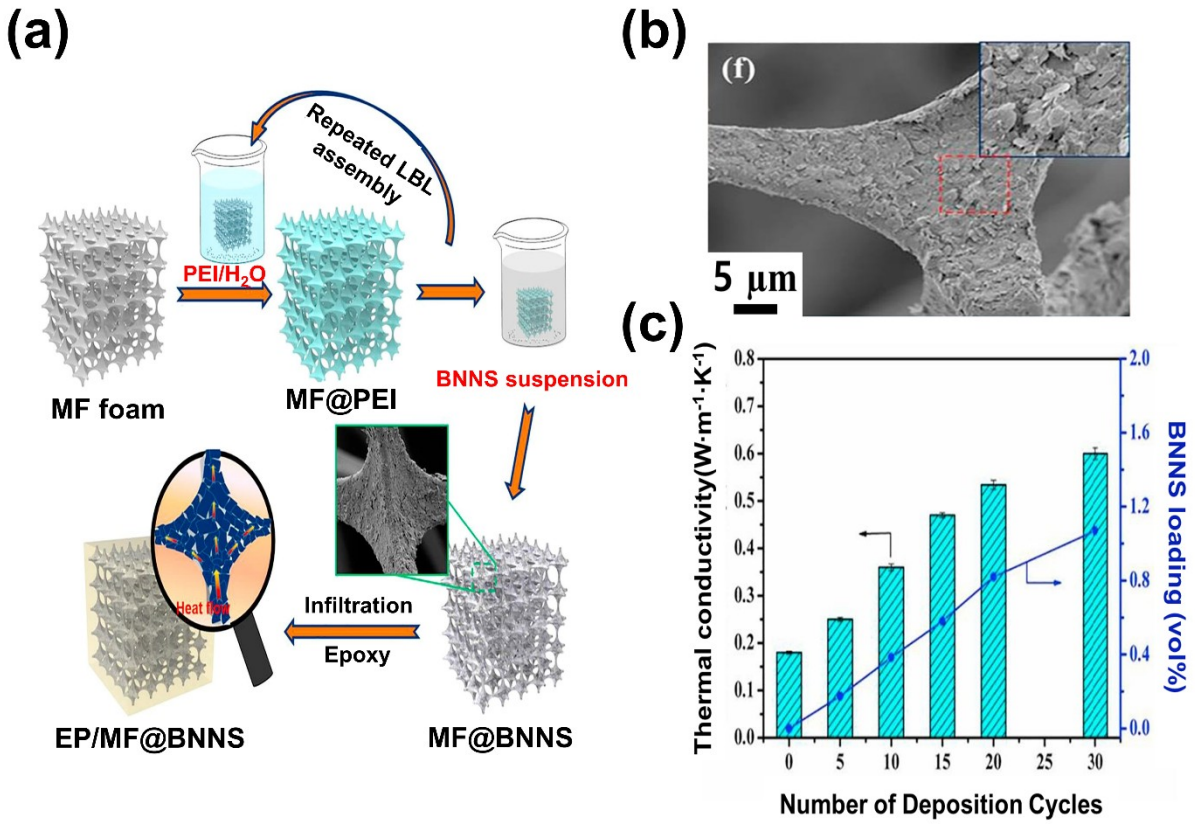

Fig. 27. (a) Schematic diagram of the fabrication procedure for EP/MF@BNNS composites, (b) SEM image of MF@BNNS frame, and (c) thermal conductivity of EP/MF@BNNS composites with various deposition cycles and BNNS contents [173]. Reprinted with permission from [173]; copyright 2018 Elsevier.

4.3. In situ fabrication of thermally conductive composites

In the in situ fabrication methods, composites are fabricated by heating and pressing ceramic-filler-coated polymer particles. These methods are highly attractive because of the availability of simple and scalable processes. Cao et al. [174] fabricated BNNS-covered PI microspheres, which they used to construct 3D-structured PI/BNNS composites simply by hot pressing for

20 min at a high temperature of 230 °C and pressure of 20 MPa (Fig. 28a). The BNNSs attached to the surface of the PI through van der Waals interactions in the isopropyl alcohol solution. At high temperatures near the glass-transition temperature of PI, the PI microspheres were merged, which resulted in the continuous connection of BNNSs in the composites (Fig. 28b). As shown in Fig. 28c, the fabricated composite exhibited a high thermal conductivity of 4.25 W/mK at a BNNS content of 12.4 vol%. Jiang et al. [175] also used an in situ process to fabricate thermally conductive composites from PPS and BN. As shown in Fig. 29a, they positively charged the surfaces of BN flakes using APTES, and they modified PPS with sulfonic acid to give it negatively charged surfaces. They then mixed these charged components into PEI along with glutaraldehyde, which acted as a cross-linking and supporting agent to strongly bond the PPS and BN. Finally, by applying a high temperature of 280 °C and a pressure of 10 MPa for 15 min, they formed thermally conductive composites with 3D-structured BN frames (Fig. 29b). The fabricated composite with 40 vol% BN demonstrated a high thermal conductivity of 4.15 W/mK (Fig. 29c).

Li et al. [176] fabricated the thermally conductive composite with PP granules, PP fiber (PF), and h-BN, which they mixed with an adhesive vinyl acetate-ethylene copolymer emulsion (VAE707), during which the h-BNs covered the surface of the PP granules and PF. Subsequently, they hot pressed the mixture at 190 °C for 15 min at 20 MPa, thus forming the thermally conductive composites with 3D structured BN frames. During the hot-pressing process, the PF wrapped with BN formed continuous heat dissipation paths that increased the thermal conductivity (Fig. 30a). As shown in Fig. 30b, with a BN content of 40 wt% and a PF content of 6 wt%, the composites showed a high thermal conductivity equal to 3.85 W/mK, while that of a composite without PF but with equal BN contents was only 1.12 W/mK. As shown in Fig. 31a, b, Yuan et al. [119] also used an in situ method to fabricate 3D structured

composites with PDA-coated GO and polystyrene (PS). The GO was coated with PDA to improve its electrical insulation properties and was then mixed with PS microspheres via ultrasonication and mechanical stirring. After drying, they heated the mixture at 60 °C to remove water and form π–π bonds between the PS and GO-PDA. Hot pressing was then performed at 150 °C for 10 min at 600 MPa to form thermally conductive composites with 3D-structured GO-PDA frames. With 0.96 vol% GO-PDA, the thermal conductivities of the composites were 4.13 and 4.56 W/mK in the in-plane and out-of-plane directions, respectively, while the volume resistance was > 10^{14} Ω cm, as shown in Fig. 31c, d.

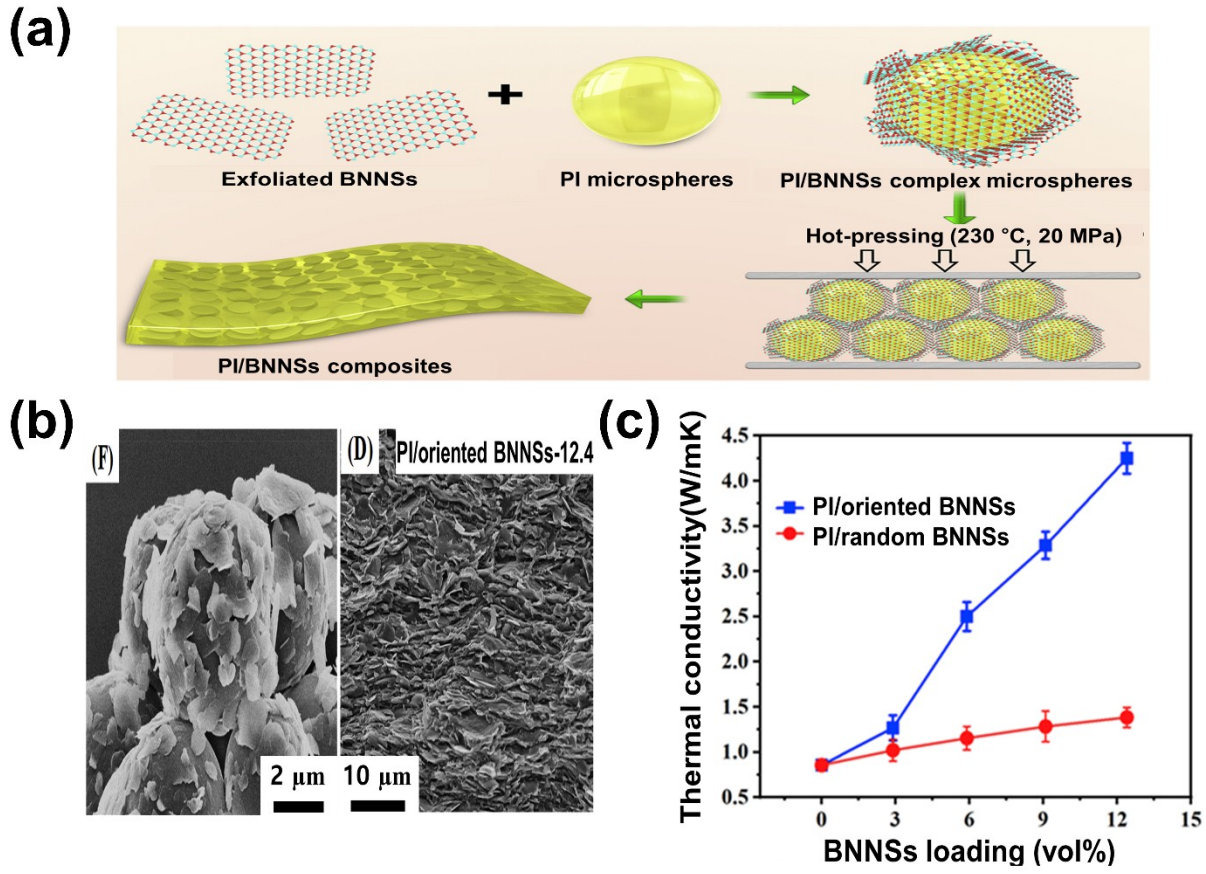

Fig. 28. (a) Schematic illustration of the formation process for PI/oriented BNNSs composites, (b) SEM images of BNNS-coated PI microspheres and the PI/oriented BNNS composite, and (c) thermal conductivity of the composite with oriented BNNSs and random BNNSs at different BNNSs contents [174]. Reprinted with permission from [174]; copyright 2020 Elsevier.

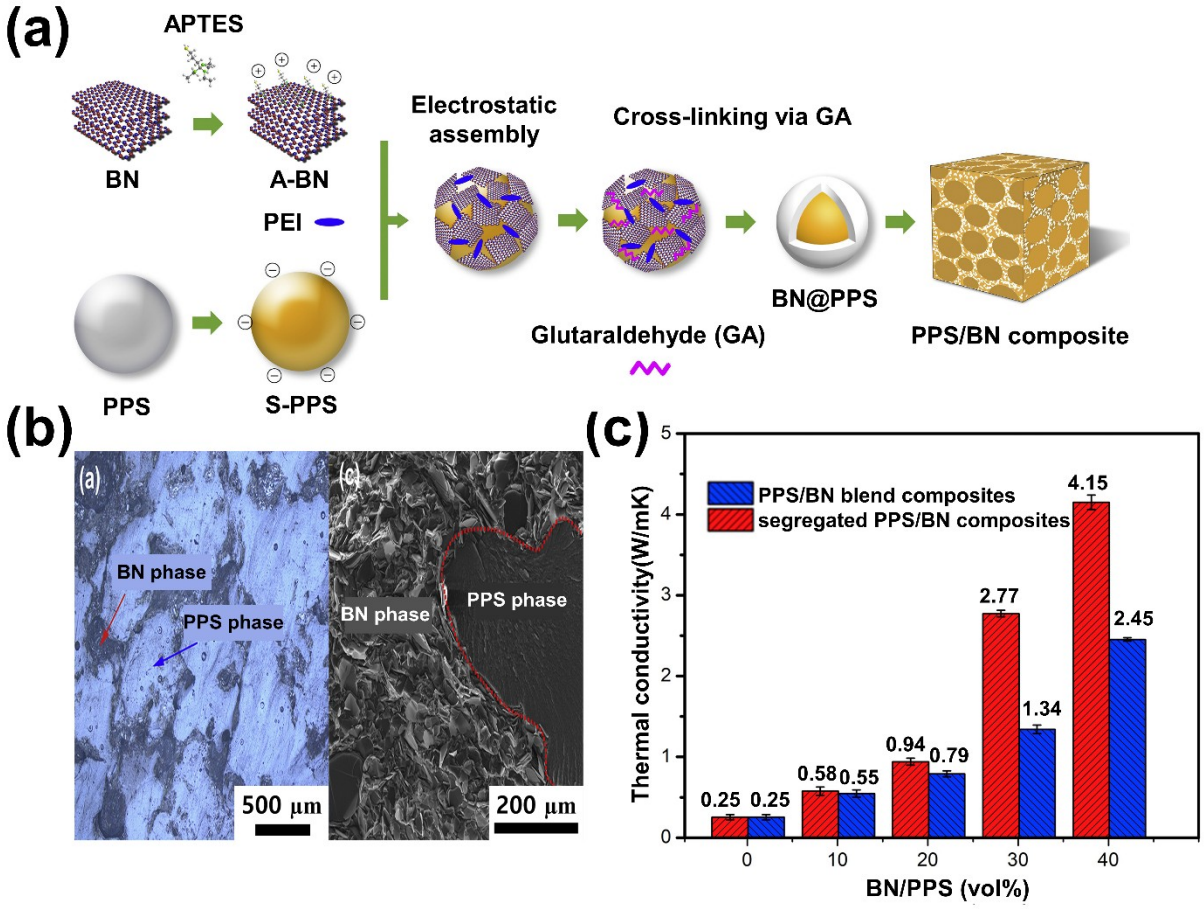

Fig. 29. (a) Schematic illustration of the preparation procedure for BN@PPS and PPS/BN composites, (b) optical microscopy and SEM images of the segregated structure of the PPS/BN composite with 30 vol% BN, and (c) thermal conductivity of the segregated and blended PPS/BN composites with different filler contents [175]. Reprinted with permission from [175]; copyright 2017 Elsevier.

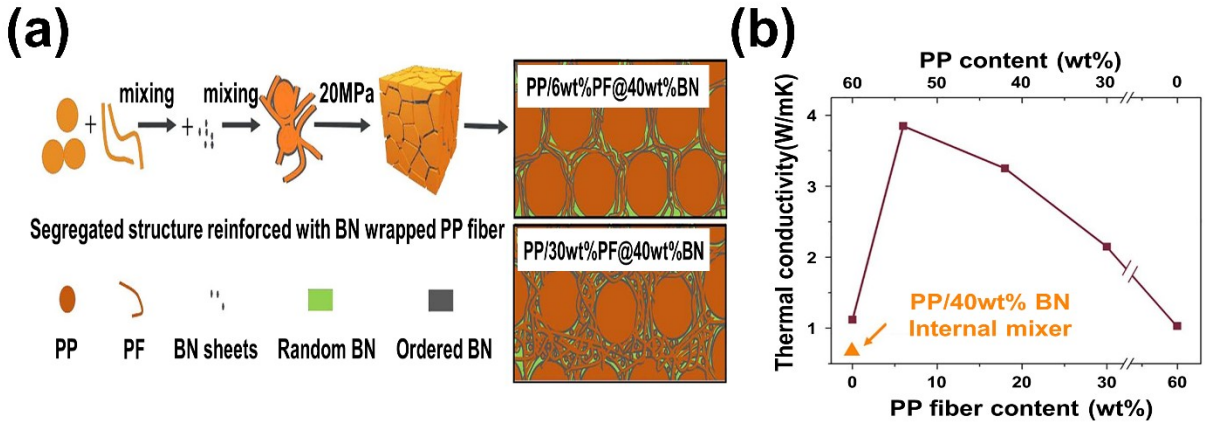

Fig. 30. (a) Schematic illustration of the fabrication process for segregated PP/PF@BN and colored SEM

images of PP/6 wt% PF@40 wt% BN and (b) thermal conductivity of the PP/PF@40 wt% BN composite with different contents of PP and PF [176]. Reprinted with permission from [176]; copyright 2020 Elsevier.

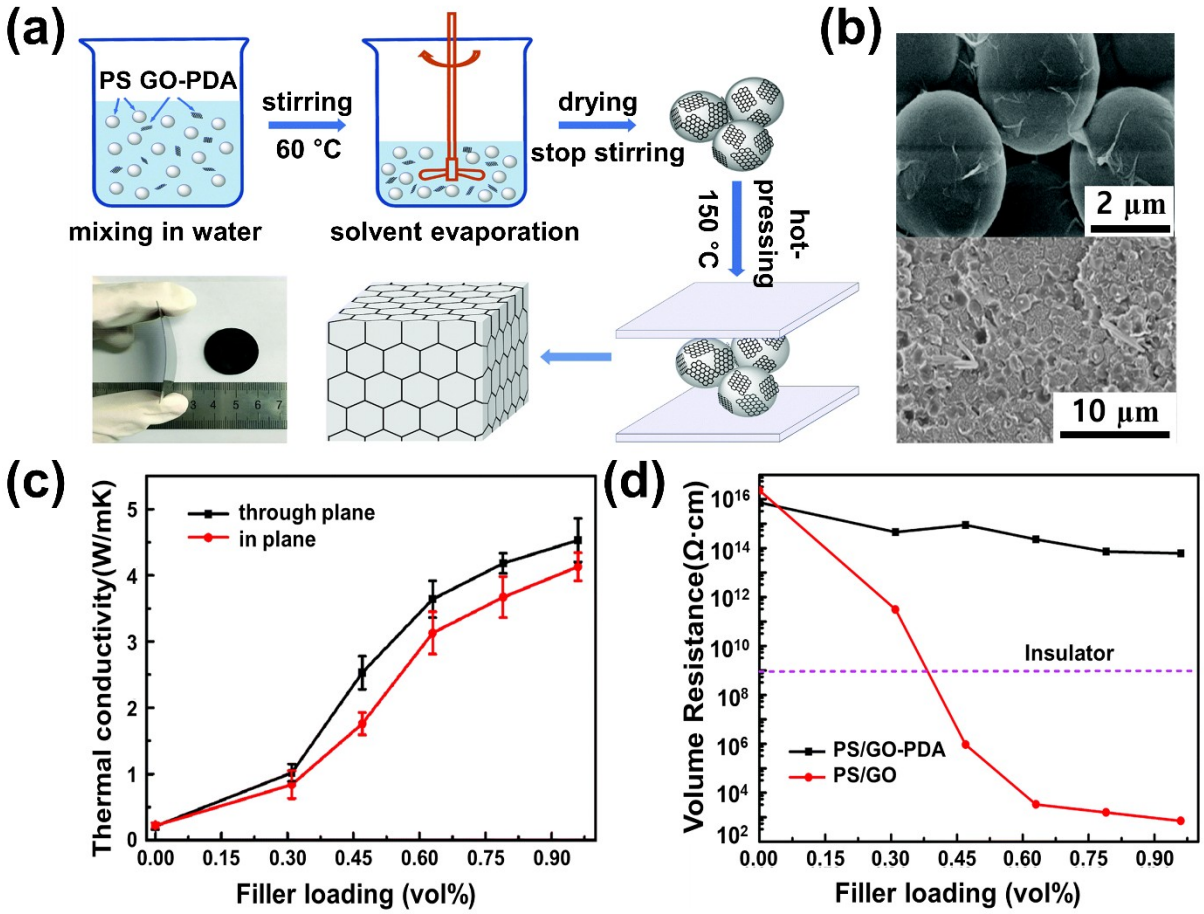

Fig. 31. (a) Schematic diagram of the formation process for PS/GO-PDA composites, (b) SEM images of PS/GO-PDA microspheres and the fractured surface of the PS/GO-PDA composite, (c) in-plane and through-plane thermal conductivity of PS/GO-PDA composites with different filler contents, and (d) volume resistance of the PS/GO and PS/GO-PDA composites with different filler contents [119]. Reprinted with permission from [119]; copyright 2019 Royal Society of Chemistry.

5. Summary

As technological trends move toward flexibility, lighter weight, miniaturization, and high integration density, the importance of thermal management in electronic devices continues to

increase as the tremendous heat generated by these devices can potentially cause devices to malfunction. Thus, composites with high thermal conductivity are often applied to electronic devices to efficiently release this heat energy. The electrical resistivity of such composites is also important because many devices require electrical insulation to prevent electrical current from flowing unexpectedly through the wrong conducting components.

The performance of thermally conductive composites is largely determined by the type of fillers and the arrangement of these fillers in the composites. Ceramic fillers with high thermal conductivity and excellent electrical insulation properties are some of the most promising components for the thermally conductive composites. Three methods are mainly used to fabricate thermally conductive composites with ceramic fillers, namely 1) random dispersion, 2) anisotropic alignment, and 3) 3D structuring of ceramic fillers. Randomly dispersing fillers results in isotropic thermal conduction, which is preferable for most of the application areas, but high filler loading content is required to achieve the target thermal conductivity, which is disadvantageous in terms of cost effectiveness. Anisotropic alignment of ceramic fillers is an alternative way to increase the thermal conductivity, and it requires a lower filler content than random dispersion. This method enhances thermal conductivity by forming continuous thermal conduction paths through continually arranged ceramic fillers, thereby reducing the interfacial thermal resistance. However, anisotropic composites are useful only in specific applications requiring thermal conduction in a single directional. Meanwhile, 3D-structured ceramic filler composites are regarded as the most promising materials for isotropic thermal conductivity with low filler contents. An isotropic 3D network of ceramic fillers in the composites, high thermal conductivity can be produced through the entire composite volume, while providing excellent electrical insulation properties.

This review aimed to provide readers with an in-depth understanding of ceramic-filler-based thermally conductive composites, especially those constructed by 3D-structured filler networking. This review also discussed the properties of various types of ceramic fillers used for thermally conductive composites. It then summarized different scientific strategies for enhancing the thermal conductivity of the composites, especially 3D-filler network composites. The sections were categorized mainly based on the arrangement of the ceramic filler within the composites, including 1) random dispersion, 2) anisotropic alignment, and 3) the 3D structuring of ceramic fillers. All the reviewed articles are summarized in Table 2.

1) Random dispersion of ceramic fillers in composites: The easiest and most cost-effective methods for fabricating thermally conductive composites involve the random dispersion of fillers in the composite; however, large amounts of the fillers are required to achieve sufficient thermal conductivity. In addition, high filler loadings increase the viscosity of the composite mixture and consequently degrade the mechanical performance of the final composites. Furthermore, the random dispersion method can cause the fillers to agglomerate, which reduces the thermal conductivity owing to the increased thermal resistance through the matrix. Therefore, researchers have attempted various ways to enhance the thermal conductivity, such as multiple types of fillers in hybrid composites or surface modifying the fillers, but the resulting thermal conductivity has remained lower than that of aligned composites.

2) Anisotropic alignment of ceramic fillers: Some research groups have aligned fillers in the polymer matrix by applying an external force through vacuum filtration, a doctor blade, or a magnetic or electric field, among others. The fillers form continuous thermal conduction paths in the direction of the alignment, which dramatically increased the thermal conductivity

of the composite along that direction. Moreover, because alignment can prevent the fillers from locally agglomerating, the composites show higher thermal conductivity than those of the composites fabricated with randomly dispersed fillers, even with an equal amount of fillers. However, the anisotropic enhancement of thermal conductivity still limits the total thermal conduction performance of the composites, as the thermal conductivity perpendicular to the filler alignment is much lower than that in parallel with the alignment direction. This anisotropic thermal conduction is thus unsuitable for applications requiring uniaxial heat dissipation properties, such as underfill composites for the packaging of electronic devices; thus, a method for improving the isotropic thermal conduction is urgently required.

3) 3D-structuring of ceramic fillers: To resolve the aforementioned limitations of composites with randomly dispersed and anisotropically aligned fillers, composites with 3D structured filler networking have been studied intensively. 3D-structured ceramic filler frames are fabricated by various methods, such as freeze-casting, foaming agent, CVD, and hot pressing. The advantages and disadvantages of these filler alignment methods are summarized in Table 3. The interconnected fillers in 3D structures form continuous, 3D structured, thermally conductive paths that enhance the thermal conductivity by decreasing the interfacial thermal resistance between fillers without causing filler aggregation. In addition, composites with 3D-structured ceramic filler frames show high uniaxial thermal conductivity at a lower filler contents than those with a random filler dispersion. Nonetheless, these 3D composites still have several limitations that need to be resolved. First, there is still room for improvement in the thermal conductivity. Although the filler–filler interfacial thermal resistance is low, the interfacial thermal resistance between fillers and polymer should also be decreased to enhance thermal conductivity. Surface modifying the fillers may be an option for reducing the interfacial thermal resistance between two materials by increasing the reactivity of the

functionalized fillers with the polymer matrix. However, such surface modification might deteriorate the mechanical properties of the composites. In addition, excessive surface tuning might decrease the intrinsic thermal conductivity of the fillers. Therefore, the relation between the surface modification and the thermal and mechanical properties of the composites should be studied in further detail. Finally, the methods for fabricating 3D-structured ceramic filler frames are complicated, and they increase production time and decrease cost-efficiency. Therefore, for industrial-scale production, new methods or materials must be developed to achieve the facile, cost-efficient production of the 3D networking composites, which will accelerate the use of these composites in industry.

Acknowledgement

We gratefully acknowledge financial support from the National Research Foundation (NRF) of Korea, which is funded by the Ministry of Science, Information and Communications Technology (Grant Nos. 2021R1F1A1054886, NRF-2019K1A3A1A47000624 and 2019K1A3A1A25000230).

Table 2. Summary of the thermal conductivities of the composites.

Method	Filler		Matrix	Filler contents	Thermal conductivity (W/mK)	η (%)	Remarks	Ref.
Random dispersion method	Al_2O_3		EP	80 wt%	1.37	~6.2	Without modification	[132]
	SiC		EP	20 vol%	~0.8	N/A	Without modification	[137]
	AlN		Polyetherimide	57.4 vol%	1.21	~7.04	Without modification	[141]
	BNNSs		EP	30 wt%	~ 0.624	~10.53	Without modification	[43]
	Micro-sized h-BN /Nano-sized h-BN		PMIA	30 wt%	0.94	~10.29	APTES-modified h-BN	[150]
	Spherical h-BN /Platelet h-BN		PPS	33.3 vol%	2.04	~24.84	APTES-modified h-BN	[151]
	h-BNNS/f-SiC		PVDF	46 wt%	1.41	~10.60	APTES-functionalized SiC	[98]
	Al_2O_3 /AlN	Sample A	EP	58.4 vol%	3.402	~27.41	AlN (10 μm) and Al_2O_3 (0.5 μm)	[152]
		Sample B			2.842	~22.62	AlN (0.1 μm) and Al_2O_3 (10 μm)	
	AlN/BN		EP	80 vol%	8.0	N/A	APTES-modified AlN and BN	[153]
	BN@MGO		PP	50 vol%	~3.80	~29.67	APTES-modified BN and LAO-modified GO	[126]
	BN		PVA	33 wt%	1.636	N/A	Using VTES SCAs	[154]

	AlN@PI	EP	40 wt%	2.03	~22.88	PI-coated AlN	[155]
	SPI-BNNSs	TA@CNF	1.5 wt%	7.06	~189.13	SPI-functionalized BNNSs	[156]
	SiO_2@MWCNTs	PU	1 wt%	~0.28	~58.19	SiO_2-coated MWCNTs	[157]
	Al@Al_2O_3	EP	60 wt%	~0.90	~5.152	Al_2O_3-coated Al	[124]
	CuNW@PDA	EP	3.1 vol%	2.87	~430.6	PDA-coated CuNWs	[125]
Anisotropic alignment method	RGO@f-Al_2O_3	NFC	30 wt% of RGO, 5.6 wt% of f-Al_2O_3	8.3 (∥)	~55.48	APTES-modified Al_2O_3 /Vacuum filtration	[97]
	BNNSs	EVA	50 wt%	13.2 (∥)	~73.43	Sodium-cholate-functionalized BNNS /Vacuum filtration	[105]
	BNNSs	CNF	50 wt%	24.66 (∥)	~22.18	Doctor blade	[113]
	BNNSs	Polyethylene glycol	8.1 vol%	1.3 (⊥)	~67.9	Unidirectional freezing	[162]
	BNNPs	EP	20 wt%	1.07 (⊥)	~23.16	Fe_3O_4-coated BNNsP /Magnetic field	[114]
	BNNSs	PDMS	15 vol%	1.56 (⊥)	~97.33	Electrical field	[163]
3D-structuring method: 1) 3D-structured ceramic frame	AlN	EP	47.3 vol%	4.45 (∥), 9.48 (⊥)	~32.73 (∥), ~72.12 (⊥)	KH-560-modified AlN-H /Freeze-casting	[146]
	BNNSs	EP	15 vol%	3.87 (∥), 4.02 (⊥)	~136.7 (∥), ~142.2 (⊥)	Freeze-casting	[127]
	CNF-BNNSs	EP	9.6 vol% of BNNS	3.13	N/A	Freeze-drying	[122]

	BNNSs	PI aerogel	50 wt%	2.2 (∥), 6.7 (⊥)	~56.67 (∥), ~105.2 (⊥)	D-glucose-functionalized BNNSs /Freeze-drying	[57]
	BN	EP	59.43 vol%	6.11	~55.43	Foaming agents	[165]
	BN	EP	24.4 wt%	5.19 (∥), 3.48 (⊥)	N/A	Foaming agents	[121]
	Al_2O_3	EP	23.32 vol%	2.58	~41.81	Foaming agents	[166]
	BNMBs	EP	65.6 vol%	17.61 (∥), 5.08 (⊥)	~132.7 (∥), ~37.20 (⊥)	Salt template	[167]
	BN	EP	21 wt%	1.47	~36.41	Salt template	[168]
3D-structuring method: 2) utilizing a 3D-structured matrix	BNF/BNNS	PDMS	10.4 wt%	0.56	~16.03	CVD	[169]
	BN nanorods	PMMA	51 wt%	9.48 (∥), 10.31 (⊥)	~82.53 (∥), ~89.93 (⊥)	CVD	[170]
	BN nanosheets		56 wt%	6.14 (∥), 6.75 (⊥)	~48.0 (∥), ~53.00 (⊥)		
	SiC	EP	~6.5 vol%	10.26	~849.8	CVD	[171]
	BN (Cu base)	EP	25 wt% of BN	2.017	N/A	Vacuum impregnation	[172]
	BNNS (MF base)	EP	~1.1 vol% of BNNS	0.60	~217.3	L-B-L assembly	[173]
3D-structuring method: 3) in situ fabrication	BNNSs	PI	12.4 vol%	4.25	~32.26	Hot pressing	[174]
	BN	PPS	40 vol%	4.15	~39.00	APTES-modified BN /Hot pressing	[175]
	BN	PP	40 wt%	3.85	~37.60	Hot pressing	[176]
	GO	PS	0.96 vol%	4.13 (∥), 4.56 (⊥)	~2286 (∥), ~2535 (⊥)	PDA-coated GO /Hot pressing	[119]

* η (%): Thermal conductivity enhancement efficiency; $\eta = \frac{K_c - K_m}{f\,K_m} \times 100$, where K_c and K_m are the thermal conductivities of the composite and pure polymer matrix, respectively, and f represents the volume or weight fraction (%) of fillers.

Table 3. Advantages and disadvantages of each method.

Method		Advantage	Disadvantage
Randomly Dispersion		· Simplest · Short time process · Low cost process	· Necessity of high filler loading · Insufficient thermal conductivity
Anisotropic Alignment	Vacuum filtration	· High thermal conductivity in parallel direction · Simple · Densely packed filler alignment	· Anisotropic enhancement of thermal conductivity · Long time process · Difficult for mass production
	Doctor blade	· High thermal conductivity in parallel direction · Simple · Short time process · Easy for mass production	· Anisotropic enhancement of thermal conductivity
	Unidirectional freezing	· High thermal conductivity in vertical direction	· Anisotropic enhancement of thermal conductivity · Long time process · Difficult for mass production
	Magnetic field	· High thermal conductivity in vertical direction	· Anisotropic enhancement of thermal conductivity · Additional magnetic materials coating step · Long time process · Difficult for mass production
	Electrical field	· High thermal conductivity in vertical direction	· Anisotropic enhancement of thermal conductivity · Long time process · Difficult for mass production
3D Structuring	Freeze casting	· Isotropic enhancement of thermal conductivity	· Long time process · Difficult for mass production

	Freeze drying	· Isotropic enhancement of thermal conductivity	· Long time process · Difficult for mass production
	Foaming agent	· Isotropic enhancement of thermal conductivity · Simple	-
	Salt template	· Isotropic enhancement of thermal conductivity · Simple	-
	CVD	· Isotropic enhancement of thermal conductivity · High purity and quality of fillers	· High cost process · High temperature process · Necessity of catalyst etching process · Difficult for mass production
	Layer-by-Layer assembly	· Isotropic enhancement of thermal conductivity · Simple	-
	Hot pressing	· Isotropic enhancement of thermal conductivity	· Suitable for thermoplastic polymer

References

[1] Zhang F, Feng Y, Feng W. Three-dimensional interconnected networks for thermally conductive polymer composites: Design, preparation, properties, and mechanisms. Materials Science and Engineering: R: Reports. 2020;142.

[2] Chen H, Ginzburg VV, Yang J, Yang Y, Liu W, Huang Y, et al. Thermal conductivity of polymer-based composites: Fundamentals and applications. Progress in Polymer Science. 2016;59:41-85.

[3] Vu MC, Bach Q-V, Nguyen DD, Tran TS, Goodarzi M. 3D interconnected structure of poly(methyl methacrylate) microbeads coated with copper nanoparticles for highly thermal conductive epoxy composites. Composites Part B: Engineering. 2019;175.

[4] Wu K, Zhang Y, Gong F, Liu D, Lei C, Fu Q. Highly thermo-conductive but electrically insulating filament via a volume-confinement self-assembled strategy for thermoelectric wearables. Chemical Engineering Journal. 2020.

[5] Choudhari VG, Dhoble DAS, Sathe TM. A review on effect of heat generation and various thermal management systems for lithium ion battery used for electric vehicle. Journal of Energy Storage. 2020;32.

[6] Kim J, Oh J, Lee H. Review on battery thermal management system for electric vehicles. Applied Thermal Engineering. 2019;149:192-212.

[7] Wang Z, Meng G, Wang L, Tian L, Chen S, Wu G, et al. Simultaneously enhanced dielectric properties and through-plane thermal conductivity of epoxy composites with alumina and boron nitride nanosheets. Sci Rep. 2021;11(1):2495.

[8] Kim K, Ahn K, Ju H, Kim J. Improvement of Insulating and Thermal Properties of SiO_2-Coated Copper Nanowire Composites. Industrial & Engineering Chemistry Research. 2016;55(10):2713-20.

[9] Huang L, Lv X, Tang Y, Ge G, Zhang P, Li Y. Effect of Alumina Nanowires on the Thermal Conductivity and Electrical Performance of Epoxy Composites. Polymers (Basel). 2020;12(9).

[10] Anithambigai P, Shanmugan S, Mutharasu D, Zahner T, Lacey D. Study on thermal performance of high power LED employing aluminum filled epoxy composite as thermal interface material. Microelectronics Journal. 2014;45(12):1726-33.

[11] Fang S, Wang W, Liang J, Liang Z, Qin Y, Lv J. Heat dissipation analysis of bendable AlGaInP micro-LED arrays. AIP Advances. 2017;7(1).

[12] Ben Hamida MB, Almeshaal MA, Hajlaoui K, Rothan YA. A three-dimensional thermal management study for cooling a square Light Edding Diode. Case Studies in Thermal Engineering. 2021;27:101223.

[13] Hamidnia M, Luo Y, Wang XD. Application of micro/nano technology for thermal management of high power LED packaging – A review. Applied Thermal Engineering. 2018;145:637-51.

[14] Cho E-C, Huang J-H, Li C-P, Chang-Jian C-W, Lee K-C, Hsiao Y-S, et al. Graphene-based thermoplastic composites and their application for LED thermal management. Carbon. 2016;102:66-73.

[15] Luo X, Hu R, Liu S, Wang K. Heat and fluid flow in high-power LED packaging and applications. Progress in Energy and Combustion Science. 2016;56:1-32.

[16] Xiao C, He H, Li J, Cao S, Zhu W. An effective and efficient numerical method for thermal management in 3D stacked integrated circuits. Applied Thermal Engineering. 2017;121:200-9.

[17] Tavakkoli F, Ebrahimi S, Wang S, Vafai K. Analysis of critical thermal issues in 3D integrated circuits. International Journal of Heat and Mass Transfer. 2016;97:337-52.

[18] Cheng H-C, Huang T-C, Hwang P-W, Chen W-H. Heat dissipation assessment of through silicon via (TSV)-based 3D IC packaging for CMOS image sensing. Microelectronics Reliability. 2016;59:84-94.

[19] Ren Z, Yu Z, Kim JC, Lee J. Hotspot Management by Holey Silicon-Metal Composites for 1 kW/cm^2 and Beyond. 2019 18th IEEE Intersociety Conference on Thermal and Thermomechanical Phenomena in Electronic Systems (ITherm): IEEE; 2019. p. 1253-9.

[20] Luo J, Wu Y, Sun Y, Wang G, Liu Y, Zhao X, et al. Preparation and Characterization of High Thermal Conductivity and Low CTE Polyimide Composite Reinforced with Diamond Nanoparticles/SiC Whiskers for 3D IC Interposer RDL Dielectric. Applied Sciences. 2019;9(9).

[21] Tu KN. Reliability challenges in 3D IC packaging technology. Microelectronics Reliability. 2011;51(3):517-23.

[22] Song R, Zhao X, Wang Z, Fu H, Han K, Qian W, et al. Sandwiched Graphene Clad Laminate: A Binder-Free Flexible Printed Circuit Board for 5G Antenna Application. Advanced Engineering Materials. 2020;22(10).

[23] Bowrothu R, Kim H-I, Smith CS, Arnold DP, Yoon Y-K. 35-GHz Barium Hexaferrite/PDMS Composite-Based Millimeter-Wave Circulators for 5G Applications. IEEE Transactions on Microwave Theory and Techniques. 2020;68(12):5065-71.
[24] Shi H, Liu X, Lou Y. Materials and micro drilling of high frequency and high speed printed circuit board: a review. The International Journal of Advanced Manufacturing Technology. 2018;100(1-4):827-41.
[25] Ge M, Li Q, Zhang J, Zhao C, Lu C, Yin Z, et al. Enhancing thermal conductivity of the insulating layer of high-frequency copper clad laminates via incorporating surface modified spherical hBN fillers. Journal of Materials Science: Materials in Electronics. 2020;31(5):4214-23.
[26] Yuan W, Yang X, Zhang G, Li X. A thermal conductive composite phase change material with enhanced volume resistivity by introducing silicon carbide for battery thermal management. Applied Thermal Engineering. 2018;144:551-7.
[27] Smith J, Singh R, Hinterberger M, Mochizuki M. Battery thermal management system for electric vehicle using heat pipes. International Journal of Thermal Sciences. 2018;134:517-29.
[28] Chen Y, Luo W, Wang J, Huang J. Enhanced Thermal Conductivity and Durability of a Paraffin Wax Nanocomposite Based on Carbon-Coated Aluminum Nanoparticles. The Journal of Physical Chemistry C. 2017;121(23):12603-9.
[29] Huang R, Xie J, Wu X, Zhang G, Yang X. Preparation of Composite Cooling Boards Composed of Thermal Conductive Silica Gel and Phase Change Materials for Battery Thermal Management. Energy & Fuels. 2021;35(16):13466-73.
[30] Malik M, Dincer I, Rosen MA. Review on use of phase change materials in battery thermal management for electric and hybrid electric vehicles. International Journal of Energy Research. 2016;40(8):1011-31.
[31] Luo W, Zhou L, Fu K, Yang Z, Wan J, Manno M, et al. A Thermally Conductive Separator for Stable Li Metal Anodes. Nano Lett. 2015;15(9):6149-54.
[32] Zuo LL, Ma Q, Li SC, Lin BC, Fan M, Meng QH, et al. Highly Thermal Conductive Separator with In-Built Phosphorus Stabilizer for Superior Ni-Rich Cathode Based Lithium Metal Batteries. Advanced Energy Materials. 2020;11(3).
[33] Huang X. Separator technologies for lithium-ion batteries. Journal of Solid State Electrochemistry. 2010;15(4):649-62.
[34] Yang Y, Huang X, Cao Z, Chen G. Thermally conductive separator with hierarchical nano/microstructures for improving thermal management of batteries. Nano Energy. 2016;22:301-9.
[35] Hauge HH, Presser V, Burheim O. In-situ and ex-situ measurements of thermal conductivity of supercapacitors. Energy. 2014;78:373-83.
[36] Zhang Y, Hao N, Lin X, Nie S. Emerging challenges in the thermal management of cellulose nanofibril-based supercapacitors, lithium-ion batteries and solar cells: A review. Carbohydr Polym. 2020;234:115888.
[37] Sun T, Peavey JL, David Shelby M, Ferguson S, O'Connor BT. Heat shrink formation of a corrugated thin film thermoelectric generator. Energy Conversion and Management. 2015;103:674-80.
[38] Selvam C, Manikandan S, Krishna NV, Lamba R, Kaushik SC, Mahian O. Enhanced thermal performance of a thermoelectric generator with phase change materials. International Communications in Heat and Mass Transfer. 2020;114.
[39] Kim D, Kim C, Park J, Kim TY. Highly enhanced thermoelectric energy harvesting from a high-temperature heat source by boosting thermal interface conduction. Energy Conversion and Management. 2019;183:360-8.
[40] Bilotti E, Fenwick O, Schroeder BC, Baxendale M, Taroni-Junior P, Degousée T, et al. 6.14 Organic Thermoelectric Composites Materials. In: Beaumont PWR, Zweben CH, editors. Comprehensive Composite Materials II. Oxford: Elsevier; 2018. p. 408-30.
[41] Zhang G, Song M, Li Z, Zhao P, Gu Z, Wang H, et al. A novel heat dissipation material for high-brightness light-emitting-diode devices. Materials Chemistry and Physics. 2013;139(2-3):741-6.
[42] Moore AL, Shi L. Emerging challenges and materials for thermal management of electronics. Materials Today. 2014;17(4):163-74.
[43] Lin Z, McNamara A, Liu Y, Moon K-s, Wong C-P. Exfoliated hexagonal boron nitride-based polymer nanocomposite with enhanced thermal conductivity for electronic encapsulation. Composites Science and Technology. 2014;90:123-8.
[44] Lin Z, Yao Y, Mcnamara A, Moon K, Wong CP. Single/few-layer boron nitride-based nanocomposites for high thermal conductivity underfills. 2012 IEEE 62nd Electronic Components and Technology Conference2012. p. 1437-41.
[45] Li G, He Y, Zhu P, Zhao T, Sun R, Lu D, et al. Tailored surface chemistry of SiO_2 particles with improved rheological, thermal-mechanical and adhesive properties of epoxy based composites for underfill

applications. Polymer. 2018;156:111-20.
[46] Hao H, Hui D, Lau D. Material advancement in technological development for the 5G wireless communications. Nanotechnology Reviews. 2020;9(1):683-99.
[47] Wu B, Mao X, Xu Y, Li R, Wu N, Tang X. Improved dielectric and thermal properties of core-shell structured SiO_2/polyolefin polymer composites for high-frequency copper clad laminates. Applied Surface Science. 2021;544:148911.
[48] Ge M, Zhang J, Zhao C, Lu C, Du G. Effect of hexagonal boron nitride on the thermal and dielectric properties of polyphenylene ether resin for high-frequency copper clad laminates. Materials & Design. 2019;182:108028.
[49] Hao M, Li J, Park S, Moura S, Dames C. Efficient thermal management of Li-ion batteries with a passive interfacial thermal regulator based on a shape memory alloy. Nature Energy. 2018;3(10):899-906.
[50] Rajadurai MDS, Ananth S. Battery Thermal Management in Electrical Vehicle. International Journal of Innovative Science, Engineering & Technology. 2020;7(2).
[51] Liu Z, Jiang Y, Hu Q, Guo S, Yu L, Li Q, et al. Safer Lithium-Ion Batteries from the Separator Aspect: Development and Future Perspectives. ENERGY & ENVIRONMENTAL MATERIALS. 2021;4(3):336-62.
[52] Yin X, Wang L, Kim Y, Ding N, Kong J, Safanama D, et al. Thermal Conductive 2D Boron Nitride for High-Performance All-Solid-State Lithium-Sulfur Batteries. Adv Sci (Weinh). 2020;7(19):2001303.
[53] Zhang Y, Zhang C, Feng Y, Zhang T, Chen Q, Chi Q, et al. Excellent energy storage performance and thermal property of polymer-based composite induced by multifunctional one-dimensional nanofibers oriented in-plane direction. Nano Energy. 2019;56:138-50.
[54] Chi Q, Gao Z, Zhang T, Zhang C, Zhang Y, Chen Q, et al. Excellent Energy Storage Properties with High-Temperature Stability in Sandwich-Structured Polyimide-Based Composite Films. ACS Sustainable Chemistry & Engineering. 2018;7(1):748-57.
[55] Karthick K, Joy GC, Suresh S, Dhanuskodi R. Impact of Thermal Interface Materials for Thermoelectric Generator Systems. Journal of Electronic Materials. 2018;47(10):5763-72.
[56] Wu K, Zhang Y, Gong F, Liu D, Lei C, Fu Q. Highly thermo-conductive but electrically insulating filament via a volume-confinement self-assembled strategy for thermoelectric wearables. Chemical Engineering Journal. 2021;421.
[57] Wang J, Liu D, Li Q, Chen C, Chen Z, Song P, et al. Lightweight, Superelastic Yet Thermoconductive Boron Nitride Nanocomposite Aerogel for Thermal Energy Regulation. ACS Nano. 2019;13(7):7860-70.
[58] Zhang Y, Heo Y-J, Son Y-R, In I, An K-H, Kim B-J, et al. Recent advanced thermal interfacial materials: A review of conducting mechanisms and parameters of carbon materials. Carbon. 2019;142:445-60.
[59] Zhou Y, Wu S, Long Y, Zhu P, Wu F, Liu F, et al. Recent Advances in Thermal Interface Materials. ES Materials & Manufacturing. 2020;7:4-24.
[60] Razeeb KM, Dalton E, Cross GLW, Robinson AJ. Present and future thermal interface materials for electronic devices. International Materials Reviews. 2017;63(1):1-21.
[61] Li J, Yin J, Liu X, Zhao H, Li Y, Zhu C, et al. Locally connected nano-micro two-dimensional fillers in nanocomposites for advanced thermal management. Composites Part A: Applied Science and Manufacturing. 2020;128.
[62] Cai X, Dong X, Lv W, Ji C, Jiang Z, Zhang X, et al. Synergistic enhancement of thermal conductivity for low dielectric constant boron nitride–polytetrafluoroethylene composites by adding small content of graphene nanosheets. Composites Communications. 2020;17:163-9.
[63] Wu Y, Ye K, Liu Z, Wang B, Yan C, Wang Z, et al. Cotton Candy-Templated Fabrication of Three-Dimensional Ceramic Pathway within Polymer Composite for Enhanced Thermal Conductivity. ACS Appl Mater Interfaces. 2019;11(47):44700-7.
[64] Hu M, Feng J, Ng KM. Thermally conductive PP/AlN composites with a 3-D segregated structure. Composites Science and Technology. 2015;110:26-34.
[65] Yim Y-J, Park S-J. Effect of silver-plated expanded graphite addition on thermal and electrical conductivities of epoxy composites in the presence of graphite and copper. Composites Part A: Applied Science and Manufacturing. 2019;123:253-9.
[66] Shen Z, Feng J. Highly Thermally Conductive Composite Films Based on Nanofibrillated Cellulose in Situ Coated with a Small Amount of Silver Nanoparticles. ACS Appl Mater Interfaces. 2018;10(28):24193-200.
[67] Zhang Z, Li W, Wang X, Liu W, Chen K, Gan W. Low effective content of reduced graphene oxide/silver nanowire hybrids in epoxy composites with enhanced conductive properties. Journal of Materials Science: Materials in Electronics. 2019;30(8):7384-92.
[68] Zhang L, Yin J, Yu W, Wang M, Xie H. Great Thermal Conductivity Enhancement of Silicone Composite with Ultra-Long Copper Nanowires. Nanoscale Res Lett. 2017;12(1):462.

[69] Yang X, Fan S, Li Y, Guo Y, Li Y, Ruan K, et al. Synchronously improved electromagnetic interference shielding and thermal conductivity for epoxy nanocomposites by constructing 3D copper nanowires/thermally annealed graphene aerogel framework. Composites Part A: Applied Science and Manufacturing. 2020;128.
[70] Barani Z, Mohammadzadeh A, Geremew A, Huang C-Y, Coleman D, Mangolini L, et al. Thermal Properties of the Binary-Filler Hybrid Composites with Graphene and Copper Nanoparticles. Advanced Functional Materials. 2020;30(8):1904008.
[71] Meng F, Huang F, Guo Y, Chen J, Chen X, Hui D, et al. In situ intercalation polymerization approach to polyamide-6/graphite nanoflakes for enhanced thermal conductivity. Composites Part B: Engineering. 2017;117:165-73.
[72] Zhang Y, Choi JR, Park S-J. Interlayer polymerization in amine-terminated macromolecular chain-grafted expanded graphite for fabricating highly thermal conductive and physically strong thermoset composites for thermal management applications. Composites Part A: Applied Science and Manufacturing. 2018;109:498-506.
[73] Liu Z, Chen Y, Li Y, Dai W, Yan Q, Alam FE, et al. Graphene foam-embedded epoxy composites with significant thermal conductivity enhancement. Nanoscale. 2019;11(38):17600-6.
[74] Song S, Zhang Y. Carbon nanotube/reduced graphene oxide hybrid for simultaneously enhancing the thermal conductivity and mechanical properties of styrene -butadiene rubber. Carbon. 2017;123:158-67.
[75] Che J, Wu K, Lin Y, Wang K, Fu Q. Largely improved thermal conductivity of HDPE/expanded graphite/carbon nanotubes ternary composites via filler network-network synergy. Composites Part A: Applied Science and Manufacturing. 2017;99:32-40.
[76] Wang J, Zhang X, Liu Y, Xu C, Zhang H, Wu D, et al. Preparation of flexible and elastic thermal conductive nanocomposites via ultrasonic-assisted forced infiltration. Composites Science and Technology. 2021;202.
[77] Lee Sanchez WA, Huang CY, Chen JX, Soong YC, Chan YN, Chiou KC, et al. Enhanced Thermal Conductivity of Epoxy Composites Filled with Al_2O_3/Boron Nitride Hybrids for Underfill Encapsulation Materials. Polymers (Basel). 2021;13(1).
[78] Chen C, Xue Y, Li X, Wen Y, Liu J, Xue Z, et al. High-performance epoxy/binary spherical alumina composite as underfill material for electronic packaging. Composites Part A: Applied Science and Manufacturing. 2019;118:67-74.
[79] Ge M, Zhang J, Zhao C, Lu C, Du G. Effect of hexagonal boron nitride on the thermal and dielectric properties of polyphenylene ether resin for high-frequency copper clad laminates. Materials & Design. 2019;182.
[80] Zhang W, Lu C, Ge M, Bu F, Zhang J. Surface modified and gradation-mixed Al_2O_3 as an effective filler for the polyphenylene oxide (PPO) insulative layer in copper clad laminates. Journal of Materials Science: Materials in Electronics. 2020;31(23):21602-16.
[81] Sargolzaeiaval Y, Padmanabhan Ramesh V, Neumann TV, Misra V, Vashaee D, Dickey MD, et al. Flexible thermoelectric generators for body heat harvesting – Enhanced device performance using high thermal conductivity elastomer encapsulation on liquid metal interconnects. Applied Energy. 2020;262.
[82] Wu K, Yu L, Lei C, Huang J, Liu D, Liu Y, et al. Green Production of Regenerated Cellulose/Boron Nitride Nanosheet Textiles for Static and Dynamic Personal Cooling. ACS Appl Mater Interfaces. 2019;11(43):40685-93.
[83] Gao T, Yang Z, Chen C, Li Y, Fu K, Dai J, et al. Three-Dimensional Printed Thermal Regulation Textiles. ACS Nano. 2017;11(11):11513-20.
[84] Kim HS, Jang J-u, Lee H, Kim SY, Kim SH, Kim J, et al. Thermal Management in Polymer Composites: A Review of Physical and Structural Parameters. Advanced Engineering Materials. 2018;20(10).
[85] Burger N, Laachachi A, Ferriol M, Lutz M, Toniazzo V, Ruch D. Review of thermal conductivity in composites: Mechanisms, parameters and theory. Progress in Polymer Science. 2016;61:1-28.
[86] Kargar F, Barani Z, Salgado R, Debnath B, Lewis JS, Aytan E, et al. Thermal Percolation Threshold and Thermal Properties of Composites with High Loading of Graphene and Boron Nitride Fillers. ACS Appl Mater Interfaces. 2018;10(43):37555-65.
[87] Pak SY, Kim HM, Kim SY, Youn JR. Synergistic improvement of thermal conductivity of thermoplastic composites with mixed boron nitride and multi-walled carbon nanotube fillers. Carbon. 2012;50(13):4830-8.
[88] Tarani E, Terzopoulou Z, Bikiaris DN, Kyratsi T, Chrissafis K, Vourlias G. Thermal conductivity and degradation behavior of HDPE/graphene nanocomposites. Journal of Thermal Analysis and Calorimetry. 2017;129(3):1715-26.
[89] Karuppanan S, Afrooza IE, Binti Megat Yusoff PSM, Ahmad F, Muhsan AS, Abdul Karim ZA, et al. A

Numerical Analysis for Predicting the Thermal Conductivity of Carbon Nanotube Reinforced Copper-Matrix Nanocomposites. MATEC Web of Conferences. 2014;13.
[90] Pei Q-X, Sha Z-D, Zhang Y-W. A theoretical analysis of the thermal conductivity of hydrogenated graphene. Carbon. 2011;49(14):4752-9.
[91] Ruan K, Shi X, Guo Y, Gu J. Interfacial thermal resistance in thermally conductive polymer composites: A review. Composites Communications. 2020;22.
[92] Ouyang Y, Ding F, Bai L, Li X, Hou G, Fan J, et al. Design of network Al_2O_3 spheres for significantly enhanced thermal conductivity of polymer composites. Composites Part A: Applied Science and Manufacturing. 2020;128.
[93] An D, Duan X, Cheng S, Zhang Z, Yang B, Lian Q, et al. Enhanced thermal conductivity of natural rubber based thermal interfacial materials by constructing covalent bonds and three-dimensional networks. Composites Part A: Applied Science and Manufacturing. 2020;135.
[94] Liu B, Li Y, Fei T, Han S, Xia C, Shan Z, et al. Highly thermally conductive polystyrene/polypropylene/boron nitride composites with 3D segregated structure prepared by solution-mixing and hot-pressing method. Chemical Engineering Journal. 2020;385.
[95] Fu C, Li Q, Lu J, Mateti S, Cai Q, Zeng X, et al. Improving thermal conductivity of polymer composites by reducing interfacial thermal resistance between boron nitride nanotubes. Composites Science and Technology. 2018;165:322-30.
[96] Hong H, Kim JU, Kim TI. Effective Assembly of Nano-Ceramic Materials for High and Anisotropic Thermal Conductivity in a Polymer Composite. Polymers (Basel). 2017;9(9).
[97] Guo S, Zheng R, Jiang J, Yu J, Dai K, Yan C. Enhanced thermal conductivity and retained electrical insulation of heat spreader by incorporating alumina-deposited graphene filler in nano-fibrillated cellulose. Composites Part B: Engineering. 2019;178.
[98] Wang B, Yin X, Peng D, Zhang Y, Wu W, Gu X, et al. Highly thermally conductive PVDF-based ternary dielectric composites via engineering hybrid filler networks. Composites Part B: Engineering. 2020;191:107978.
[99] Ren L, Zeng X, Sun R, Xu J-B, Wong C-P. Spray-assisted assembled spherical boron nitride as fillers for polymers with enhanced thermally conductivity. Chemical Engineering Journal. 2019;370:166-75.
[100] Kim K, Ju H, Kim J. Vertical particle alignment of boron nitride and silicon carbide binary filler system for thermal conductivity enhancement. Composites Science and Technology. 2016;123:99-105.
[101] Zhou W-Y, Qi S-H, Zhao H-Z, Liu N-L. Thermally conductive silicone rubber reinforced with boron nitride particle. Polymer Composites. 2007;28(1):23-8.
[102] Tessema A, Zhao D, Moll J, Xu S, Yang R, Li C, et al. Effect of filler loading, geometry, dispersion and temperature on thermal conductivity of polymer nanocomposites. Polymer Testing. 2017;57:101-6.
[103] Hong H, Jung YH, Lee JS, Jeong C, Kim JU, Lee S, et al. Anisotropic Thermal Conductive Composite by the Guided Assembly of Boron Nitride Nanosheets for Flexible and Stretchable Electronics. Advanced Functional Materials. 2019;29(37).
[104] Zhang K, Tao P, Zhang Y, Liao X, Nie S. Highly thermal conductivity of CNF/AlN hybrid films for thermal management of flexible energy storage devices. Carbohydr Polym. 2019;213:228-35.
[105] Wang Z-G, Liu W, Liu Y-H, Ren Y, Li Y-P, Zhou L, et al. Highly thermal conductive, anisotropically heat-transferred, mechanically flexible composite film by assembly of boron nitride nanosheets for thermal management. Composites Part B: Engineering. 2020;180.
[106] Yang D, Wei Q, Yu L, Ni Y, Zhang L. Natural rubber composites with enhanced thermal conductivity fabricated via modification of boron nitride by covalent and non-covalent interactions. Composites Science and Technology. 2021;202.
[107] Zhang K, Lu Y, Hao N, Nie S. Enhanced thermal conductivity of cellulose nanofibril/aluminum nitride hybrid films by surface modification of aluminum nitride. Cellulose. 2019;26(16):8669-83.
[108] Kuang Z, Chen Y, Lu Y, Liu L, Hu S, Wen S, et al. Fabrication of highly oriented hexagonal boron nitride nanosheet/elastomer nanocomposites with high thermal conductivity. Small. 2015;11(14):1655-9.
[109] Xie B-H, Huang X, Zhang G-J. High thermal conductive polyvinyl alcohol composites with hexagonal boron nitride microplatelets as fillers. Composites Science and Technology. 2013;85:98-103.
[110] Zhu H, Li Y, Fang Z, Xu J, Cao F, Wan J, et al. Highly Thermally Conductive Papers with Percolative Layered Boron Nitride Nanosheets. ACS Nano. 2014;8(4):3606-13.
[111] Xue Y, Li X, Wang H, Zhao F, Zhang D, Chen Y. Improvement in thermal conductivity of through-plane aligned boron nitride/silicone rubber composites. Materials & Design. 2019;165.
[112] Kim K, Kim J. Magnetic aligned AlN/epoxy composite for thermal conductivity enhancement at low filler content. Composites Part B: Engineering. 2016;93:67-74.

[113] Chen L, Xiao C, Tang Y, Zhang X, Zheng K, Tian X. Preparation and properties of boron nitride nanosheets/cellulose nanofiber shear-oriented films with high thermal conductivity. Ceramics International. 2019;45(10):12965-74.
[114] Kim Y, Kim J. Fabrication of Fe_3O_4 coated boron nitride nanoplatelets by liquid-phase exfoliation for thermally enhanced epoxy composites via magnetic alignment. Composites Science and Technology. 2020;188.
[115] Chen L, Hou X, Song N, Shi L, Ding P. Cellulose/graphene bioplastic for thermal management: Enhanced isotropic thermally conductive property by three-dimensional interconnected graphene aerogel. Composites Part A: Applied Science and Manufacturing. 2018;107:189-96.
[116] Su Z, Wang H, He J, Guo Y, Qu Q, Tian X. Fabrication of Thermal Conductivity Enhanced Polymer Composites by Constructing an Oriented Three-Dimensional Staggered Interconnected Network of Boron Nitride Platelets and Carbon Nanotubes. ACS Appl Mater Interfaces. 2018;10(42):36342-51.
[117] Bo Z, Zhu H, Ying C, Yang H, Wu S, Kong J, et al. Tree-inspired radially aligned, bimodal graphene frameworks for highly efficient and isotropic thermal transport. Nanoscale. 2019;11(44):21249-58.
[118] Li J, Li F, Zhao X, Zhang W, Li S, Lu Y, et al. Jelly-Inspired Construction of the Three-Dimensional Interconnected BN Network for Lightweight, Thermally Conductive, and Electrically Insulating Rubber Composites. ACS Applied Electronic Materials. 2020;2(6):1661-9.
[119] Yuan H, Wang Y, Li T, Wang Y, Ma P, Zhang H, et al. Fabrication of thermally conductive and electrically insulating polymer composites with isotropic thermal conductivity by constructing a three-dimensional interconnected network. Nanoscale. 2019;11(23):11360-8.
[120] Ashton TS, Moore AL. Foam-like hierarchical hexagonal boron nitride as a non-traditional thermal conductivity enhancer for polymer-based composite materials. International Journal of Heat and Mass Transfer. 2017;115:273-81.
[121] Tian Z, Sun J, Wang S, Zeng X, Zhou S, Bai S, et al. A thermal interface material based on foam-templated three-dimensional hierarchical porous boron nitride. Journal of Materials Chemistry A. 2018;6(36):17540-7.
[122] Chen J, Huang X, Zhu Y, Jiang P. Cellulose Nanofiber Supported 3D Interconnected BN Nanosheets for Epoxy Nanocomposites with Ultrahigh Thermal Management Capability. Advanced Functional Materials. 2017;27(5).
[123] Mateti S, Yang K, Liu X, Huang S, Wang J, Li LH, et al. Bulk Hexagonal Boron Nitride with a Quasi-Isotropic Thermal Conductivity. Advanced Functional Materials. 2018;28(28).
[124] Mao D, Chen J, Ren L, Zhang K, Yuen MMF, Zeng X, et al. Spherical core-shell $Al@Al_2O_3$ filled epoxy resin composites as high-performance thermal interface materials. Composites Part A: Applied Science and Manufacturing. 2019;123:260-9.
[125] Yuan H, Wang Y, Li T, Ma P, Zhang S, Du M, et al. Highly thermal conductive and electrically insulating polymer composites based on polydopamine-coated copper nanowire. Composites Science and Technology. 2018;164:153-9.
[126] Lu Y, Cao J, Ren S, Gao W, Chen H, Chen S, et al. Boron nitride self-assembly cladding structure promoting thermal property and dimensional stability of polymer composites. Composites Science and Technology. 2021;201.
[127] Huang T, Li Y, Chen M, Wu L. Bi-directional high thermal conductive epoxy composites with radially aligned boron nitride nanosheets lamellae. Composites Science and Technology. 2020;198:108322.
[128] Permal A, Devarajan M, Hung HL, Zahner T, Lacey D, Ibrahim K. Thermal and mechanical properties of epoxy composite filled with binary particle system of polygonal aluminum oxide and boron nitride platelets. Journal of Materials Science. 2016;51(16):7415-26.
[129] Hu Y, Du G, Chen N. A novel approach for Al_2O_3/epoxy composites with high strength and thermal conductivity. Composites Science and Technology. 2016;124:36-43.
[130] Ruan M, Yang D, Guo W, Zhang L, Li S, Shang Y, et al. Improved dielectric properties, mechanical properties, and thermal conductivity properties of polymer composites via controlling interfacial compatibility with bio-inspired method. Applied Surface Science. 2018;439:186-95.
[131] Yang H, Luan W, Tu S-T. Corrosion Behavior and Thermal Conductivity of Plasma Sprayed AlN/Al_2O_3 Coating. MATERIALS TRANSACTIONS. 2006;47(7):1649-53.
[132] Yan R, Su F, Zhang L, Li C. Highly enhanced thermal conductivity of epoxy composites by constructing dense thermal conductive network with combination of alumina and carbon nanotubes. Composites Part A: Applied Science and Manufacturing. 2019;125.
[133] Shen D, Zhan Z, Liu Z, Cao Y, Zhou L, Liu Y, et al. Enhanced thermal conductivity of epoxy composites filled with silicon carbide nanowires. Sci Rep. 2017;7(1):2606.

[134] Nhuapeng W, Thamjaree W, Kumfu S, Singjai P, Tunkasiri T. Fabrication and mechanical properties of silicon carbide nanowires/epoxy resin composites. Current Applied Physics. 2008;8(3-4):295-9.
[135] Zhou T, Wang X, Cheng P, Wang T, Xiong D, Wang X. Improving the thermal conductivity of epoxy resin by the addition of a mixture of graphite nanoplatelets and silicon carbide microparticles. Express Polymer Letters. 2013;7(7):585-94.
[136] Fan J, Xu S. Aluminum oxide particles/silicon carbide whiskers' synergistic effect on thermal conductivity of high-density polyethylene composites. Iranian Polymer Journal. 2018;27(5):339-47.
[137] Yang K, Gu M. Enhanced thermal conductivity of epoxy nanocomposites filled with hybrid filler system of triethylenetetramine-functionalized multi-walled carbon nanotube/silane-modified nano-sized silicon carbide. Composites Part A: Applied Science and Manufacturing. 2010;41(2):215-21.
[138] Ohashi M, Kawakami S, Yokogawa Y, Lai G-C. Spherical Aluminum Nitride Fillers for Heat-Conducting Plastic Packages. Journal of the American Ceramic Society. 2005;88(9):2615-8.
[139] Xie S-H, Zhu B-K, Li J-B, Wei X-Z, Xu Z-K. Preparation and properties of polyimide/aluminum nitride composites. Polymer Testing. 2004;23(7):797-801.
[140] Yu H, Li L, Kido T, Xi G, Xu G, Guo F. Thermal and insulating properties of epoxy/aluminum nitride composites used for thermal interface material. Journal of Applied Polymer Science. 2012;124(1):669-77.
[141] Wu S-Y, Huang Y-L, Ma C-CM, Yuen S-M, Teng C-C, Yang S-Y. Mechanical, thermal and electrical properties of aluminum nitride/polyetherimide composites. Composites Part A: Applied Science and Manufacturing. 2011;42(11):1573-83.
[142] Hu L-H, Wang Y-K, Wang S-C. Aluminum nitride surface functionalized by polymer derived silicon oxycarbonitride ceramic for anti-hydrolysis. Journal of Alloys and Compounds. 2019;772:828-33.
[143] Wang X, Qiang D, Hosier I, Zhu Y, Chen G, Andritsch T. Effect of water on the breakdown and dielectric response of polypropylene/nano-aluminium nitride composites. Journal of Materials Science. 2020;55(21):8900-16.
[144] Martínez Molina RA, Bedolla Becerril JE, Aguilar Reyes EA, Aguilar RAP, Arreola Fernandez C. Fabrication and characterization of aluminum nitride sponges using a mixture of two porous formation methods. MRS Advances. 2019;4(54):2977-87.
[145] Dai S, Zhang T, Mo S, Cai Y, Yuan W, Ma T, et al. Study on Preparation, Thermal Conductivity, and Electrical Insulation Properties of Epoxy/AlN. IEEE Transactions on Applied Superconductivity. 2019;29(2):1-6.
[146] Wei Z, Xie W, Ge B, Zhang Z, Yang W, Xia H, et al. Enhanced thermal conductivity of epoxy composites by constructing aluminum nitride honeycomb reinforcements. Composites Science and Technology. 2020;199:108304.
[147] Yu C, Zhang J, Tian W, Fan X, Yao Y. Polymer composites based on hexagonal boron nitride and their application in thermally conductive composites. RSC Advances. 2018;8(39):21948-67.
[148] Kim K, Ju H, Kim J. Filler orientation of boron nitride composite via external electric field for thermal conductivity enhancement. Ceramics International. 2016;42(7):8657-63.
[149] Yung KC, Liem H. Enhanced thermal conductivity of boron nitride epoxy-matrix composite through multi-modal particle size mixing. Journal of Applied Polymer Science. 2007;106(6):3587-91.
[150] Duan G, Wang Y, Yu J, Zhu J, Hu Z. Improved thermal conductivity and dielectric properties of flexible PMIA composites with modified micro- and nano-sized hexagonal boron nitride. Frontiers of Materials Science. 2019;13(1):64-76.
[151] Leung SN, Khan MO, Chan E, Naguib HE, Dawson F, Adinkrah V, et al. Synergistic effects of hybrid fillers on the development of thermally conductive polyphenylene sulfide composites. Journal of Applied Polymer Science. 2013;127(5):3293-301.
[152] Choi S, Kim J. Thermal conductivity of epoxy composites with a binary-particle system of aluminum oxide and aluminum nitride fillers. Composites Part B: Engineering. 2013;51:140-7.
[153] Hong J-P, Yoon S-W, Hwang T, Oh J-S, Hong S-C, Lee Y, et al. High thermal conductivity epoxy composites with bimodal distribution of aluminum nitride and boron nitride fillers. Thermochimica Acta. 2012;537:70-5.
[154] Cheng H, Zhao K, Gong Y, Wang X, Wang R, Wang F, et al. Covalent coupling regulated thermal conductivity of poly(vinyl alcohol)/boron nitride composite film based on silane molecular structure. Composites Part A: Applied Science and Manufacturing. 2020;137.
[155] Zhou Y, Yao Y, Chen CY, Moon K, Wang H, Wong CP. The use of polyimide-modified aluminum nitride fillers in AlN@PI/epoxy composites with enhanced thermal conductivity for electronic encapsulation. Sci Rep. 2014;4:4779.
[156] Wang Z, Wen Y, Zhao S, Zhang W, Ji Y, Zhang S, et al. Soy protein as a sustainable surfactant to

functionalize boron nitride nanosheets and its application for preparing thermally conductive biobased composites. Industrial Crops and Products. 2019;137:239-47.
[157] Zhao J, Du F, Cui W, Zhu P, Zhou X, Xie X. Effect of silica coating thickness on the thermal conductivity of polyurethane/SiO_2 coated multiwalled carbon nanotube composites. Composites Part A: Applied Science and Manufacturing. 2014;58:1-6.
[158] Niu H, Ren Y, Guo H, Małycha K, Orzechowski K, Bai S-L. Recent progress on thermally conductive and electrical insulating rubber composites: Design, processing and applications. Composites Communications. 2020;22:100430.
[159] Xue Y, Li X, Wang H, Zhao F, Zhang D, Chen Y. Improvement in thermal conductivity of through-plane aligned boron nitride/silicone rubber composites. Materials & Design. 2019;165:107580.
[160] Song N, Hou X, Chen L, Cui S, Shi L, Ding P. A Green Plastic Constructed from Cellulose and Functionalized Graphene with High Thermal Conductivity. ACS Appl Mater Interfaces. 2017;9(21):17914-22.
[161] Feng C-P, Yang L-Y, Yang J, Bai L, Bao R-Y, Liu Z-Y, et al. Recent advances in polymer-based thermal interface materials for thermal management: A mini-review. Composites Communications. 2020;22.
[162] Jiang F, Song N, Ouyang R, Ding P. Wall Density-Controlled Thermal Conductive and Mechanical Properties of Three-Dimensional Vertically Aligned Boron Nitride Network-Based Polymeric Composites. ACS Appl Mater Interfaces. 2021;13(6):7556-66.
[163] Cho H-B, Nakayama T, Suematsu H, Suzuki T, Jiang W, Niihara K, et al. Insulating polymer nanocomposites with high-thermal-conduction routes via linear densely packed boron nitride nanosheets. Composites Science and Technology. 2016;129:205-13.
[164] Hao L-C, Li Z-X, Sun F, Ding K, Zhou X-N, Song Z-X, et al. High-performance epoxy composites reinforced with three-dimensional Al_2O_3 ceramic framework. Composites Part A: Applied Science and Manufacturing. 2019;127.
[165] Xu X, Hu R, Chen M, Dong J, Xiao B, Wang Q, et al. 3D boron nitride foam filled epoxy composites with significantly enhanced thermal conductivity by a facial and scalable approach. Chemical Engineering Journal. 2020;397.
[166] Xiao C, Chen L, Tang Y, Zhang X, Zheng K, Tian X. Three dimensional porous alumina network for polymer composites with enhanced thermal conductivity. Composites Part A: Applied Science and Manufacturing. 2019;124.
[167] Xiao C, Tang Y, Chen L, Zhang X, Zheng K, Tian X. Preparation of highly thermally conductive epoxy resin composites via hollow boron nitride microbeads with segregated structure. Composites Part A: Applied Science and Manufacturing. 2019;121:330-40.
[168] Chen X, Lim JSK, Yan W, Guo F, Liang YN, Chen H, et al. Salt Template Assisted BN Scaffold Fabrication toward Highly Thermally Conductive Epoxy Composites. ACS Appl Mater Interfaces. 2020;12(14):16987-96.
[169] Fang H, Bai S-L, Wong CP. Thermal, mechanical and dielectric properties of flexible BN foam and BN nanosheets reinforced polymer composites for electronic packaging application. Composites Part A: Applied Science and Manufacturing. 2017;100:71-80.
[170] Xue Y, Zhou X, Zhan T, Jiang B, Guo Q, Fu X, et al. Densely Interconnected Porous BN Frameworks for Multifunctional and Isotropically Thermoconductive Polymer Composites. Advanced Functional Materials. 2018;28(29).
[171] Vu MC, Thieu NAT, Choi WK, Islam MA, Kim S-R. Ultralight covalently interconnected silicon carbide aerofoam for high performance thermally conductive epoxy composites. Composites Part A: Applied Science and Manufacturing. 2020;138.
[172] Lee S, Kim J. Thermally conductive 3D binetwork structured aggregated boron nitride/Cu-foam/polymer composites. Synthetic Metals. 2020;270.
[173] Wang X, Wu P. Melamine foam-supported 3D interconnected boron nitride nanosheets network encapsulated in epoxy to achieve significant thermal conductivity enhancement at an ultralow filler loading. Chemical Engineering Journal. 2018;348:723-31.
[174] Cao L, Wang J, Dong J, Zhao X, Li H-B, Zhang Q. Preparation of highly thermally conductive and electrically insulating PI/BNNSs nanocomposites by hot-pressing self-assembled PI/BNNSs microspheres. Composites Part B: Engineering. 2020;188.
[175] Jiang Y, Liu Y, Min P, Sui G. BN@PPS core-shell structure particles and their 3D segregated architecture composites with high thermal conductivities. Composites Science and Technology. 2017;144:63-9.
[176] Li X, Li C, Zhang X, Jiang Y, Xia L, Wang J, et al. Simultaneously enhanced thermal conductivity and mechanical properties of PP/BN composites via constructing reinforced segregated structure with a trace

amount of BN wrapped PP fiber. Chemical Engineering Journal. 2020;390.

Figure and Table Captions

Fig. 1. Schematic diagrams of heat flow in devices (a) without and (b) with TIMs.

Fig. 2. Schematic diagrams of heat flow in (a) a pure polymer and thermally conductive composites with (b)

randomly dispersed fillers, (c) anisotropically aligned fillers, and (d) 3D networking fillers.

Fig. 3. Overview of thermally conductive composites [34, 40, 77, 97, 105, 124-127]. Reprinted with permission from [34]; copyright 2016 Elsevier. Reprinted with permission from [40]; copyright 2018 Elsevier. Reprinted with permission from [77]; copyright 2021 MDPI. Reprinted with permission from [97]; copyright 2019 Elsevier. Reprinted with permission from [105]; copyright 2020 Elsevier. Reprinted with permission from [124]; copyright 2019 Elsevier. Reprinted with permission from [125]; copyright 2018 Elsevier. Reprinted with permission from [126]; copyright 2021 Elsevier. Reprinted with permission from [127]; copyright 2020 Elsevier.

Fig. 4. (a) Thermal conductivity of the composites with different shapes and ratios of fillers and scanning electron microscopy (SEM) images of the composites with (b) PTX60, (c) PT110 and (d) 3:1 PTX60/PT110 [151]. Reprinted with permission from [151]; copyright 2012 John Wiley and Sons.

Fig. 5. (a) Schematic diagram of the thermally conductive paths through composites, (b) effect of the f-SiC nanowires on the thermal conductivity of composites with different h-BN loadings, and cross-sectional SEM images and energy dispersive X-ray spectroscopy (EDX) elemental mapping images of the PVDF/f-SiC26/h-BN with h-BN loadings of (c) 20 and (d) 26 wt% [98]. Reprinted with permission from [98]; copyright 2020 Elsevier.

Fig. 6. (a) Schematic illustration of thermal transport in a hybrid composite with different fillers, and (b) thermal conductivity of samples (b) A and (c) B with different amounts of AlN and Al_2O_3 [152]. Reprinted with permission from [152]; copyright 2013 Elsevier.

Fig. 7. (a) Schematic of the composites with large AlN and small BN at different volume ratios and (b) thermal conductivity of the composites with different size ratios [153]. Reprinted with permission from [153]; copyright 2012 Elsevier.

Fig. 8. (a) Schematic illustration of the formation processes for PP/BN and PP/BN@MGO composites and (b) thermal conductivity of PP/BN and PP/BN@MGO (right axis) and electrical resistivity of PP/BN@MGO (left axis) [126]. Reprinted with permission from [126]; copyright 2021 Elsevier.

Fig. 9. (a) Schematic diagram of composites with different SCAs and (b) thermal conductivity of the composites

with different SCAs types and SCA contents [154]. (c) Illustration of the preparation process for composites and the interfacial interactions of SPI-BNNS and TA@CNF and (d) thermal conductivity of the SPI-BNNS/TA@CNF composites [156]. Reprinted with permission from [154]; copyright 2020 Elsevier. Reprinted with permission from [156]; copyright 2019 Elsevier.

Fig. 10. Transmission electron microscopy (TEM) images of (a) pristine MWCNTs and (b) MWCNTs coated with ~4 nm of SiO_2. (c) Thermal conductivity and (d) electrical resistivity of (1) pure polyurethane (PU), (2) PU/MWCNTs, and SiO_2@MWCNTs with (3) ~4 nm, (4) 30–50 nm, and (5) 70–90 nm of SiO_2 [157]. Reprinted with permission from [157]; copyright 2014 Elsevier.

Fig. 11. (a) Schematic diagrams of the fabrication procedure, and (b) SEM and TEM images of Al@Al_2O_3 particles passivated at 600 °C. (c) Comparison of the thermal conductivity of the composites passivate at different temperatures and (d) the insulating properties of the composites [124]. Reprinted with permission from [124]; copyright 2019 Elsevier.

Fig. 12. (a) Preparation procedure for PDA-coated CuNWs and (b) TEM images of raw CuNWs and CuNWs coated with 25 nm of PDA; (c) thermal conductivity of the composites with CuNWs coated with different amounts of PDA as a function of the filer loading, and (d) volume resistance of the composites with raw CuNWs and CuNWs coated with 25 nm of PDA [125]. Reprinted with permission from [125]; copyright 2018 Elsevier.

Fig. 13. (a) Illustration of the fabrication process for f-Al_2O_3@RGO/NFC composites, (b) thermal conductivity of RGO/NFC and 5.6 wt% f-Al_2O_3@RGO/NFC composites with different RGO contents and (c) volume resistivity of pure NFC, RGO/NFC and f-Al_2O_3@RGO/NFC composites with different f-Al_2O_3 contents [97]. (d) Schematic of the process for functionalizing BNNSs, (e) cross-sectional SEM image of BN/EVA and BNNS/EVA composites with 50 wt% filler content, and (f) thermal conductivity of BNNS/EVA and BN/EVA composites with different filler contents [105]. Reprinted with permission from [97]; copyright 2019 Elsevier. Reprinted with permission from [105]; copyright 2020 Elsevier.

Fig. 14. (a) Schematic diagrams of thermal conduction through shear-oriented (top) and self-organized (bottom) BNNS/CNF composites, (b) thermal conductivity of shear-oriented composites and self-organized BNNS/CNF composites with different filler contents, and SEM images taken at the fractured surface of (c) shear-oriented and (d) self-organized BNNS/CNF composites [113]. Reprinted with permission from [113]; copyright 2019

Elsevier.

Fig. 15. (a) Schematic diagram of the preparation process for the PBNF composite and (b) comparison of the vertical thermal conductivities between the PBNF and PBN composites. Reprinted with permission from [162]; copyright 2021 American Chemical Society.

Fig. 16. (a) Schematic diagram of the fabrication process for EP composites with aligned BNNP/Fe_3O_4, (b) cross-sectional SEM images of composites with aligned and unaligned BNNP/Fe_3O_4 and (c) thermal conductivity of the composites with raw BN, unaligned BNNP/Fe_3O_4, and aligned BNNP/Fe_3O_4 [114]. Reprinted with permission from [114]; copyright 2020 Elsevier.

Fig. 17. (a) Schematic illustration of the experimental setups for the alignment of BNNSs using an electric field, (b) thermal conductivity of the PDMS/BNNS composites under a switching electric field, (c) schematic illustration of the process of aligning BNNSs using various types of electric fields, and (d) digital micrographs of the PDMS/BNNS composites without an electric field and with a switching electric field [163]. Reprinted with permission from [163]; copyright 2016 Elsevier.

Fig. 18. (a) Schematic illustration of the fabrication procedure for EP/AlN-H composites, (b) side- and top-view SEM images of EP/AlN-H composites with different filler loadings (10, 20, and 30 vol%), and (c) thermal conductivity of pure EP, EP/RD AlN, and EP/AlN-H [146]. Reprinted with permission from [146]; copyright 2020 Elsevier.

Fig. 19. (a) Schematic diagram of the process for radially aligning BNNS/EP composites through radial freeze-casting, (b) SEM images of BNNS aerogels in the vertical and radial directions with different BNNS loadings (2.5, 5, and 10 vol%), and (c) thermal conductivity of the BNNS/EP composites with different BNNS contents [127]. Reprinted with permission from [127]; copyright 2020 Elsevier.

Fig. 20. (a) Schematic illustration of the fabrication procedure for EP/3D-C-BNNS composites, (b) SEM images of the 3D-C-BNNS aerogel and the fractured surface of EP/3D-C-BNNS composite, and (c) thermal conductivity of the EP/3D-C-BNNS composites [122]. (d) Schematic illustration of the fabrication procedure, (e) SEM images, and (f) thermal conductivity of the FBN-PI aerogel [57]. Reprinted with permission from [122]; copyright 2016 John Wiley and Sons. Reprinted with permission from [57]; copyright 2019 American

Chemical Society.

Fig. 21. (a) Schematic illustration of the fabrication process for 3D-BN/EP composites, (b) cross-sectional SEM image of 3D-BNF and top-view image of a polished surface of the 3D-BN/EP composite, and (c) thermal conductivity of 3D-BN EP composites with different BN volume fractions [165]. Reprinted with permission from [165]; copyright 2020 Elsevier.

Fig. 22. (a) Schematic illustration of the fabrication process for porous BNF, (b) SEM images of microstructures of the porous BNF and BN/EP composites, and (c) thermal conductivity of the 3D BN/EP composites with different BN contents [121]. Reprinted with permission from [121]; copyright 2018 Royal Society of Chemistry.

Fig. 23. (a) Schematic illustration of the preparation process for 3D Al_2O_3/EP composites, (b) thermal conductivity 3D Al_2O_3/EP composites and Al_2O_3/EP composites with different Al_2O_3 contents, and (c) SEM images and schematic diagrams of the thermally conductive network during the fabrication of the 3D Al_2O_3/EP composite [166]. Reprinted with permission from [166]; copyright 2019 Elsevier.

Fig. 24. (a) Schematic illustrations of the fabrication procedure for EP/BNMB composites and (b) the formation mechanism of hollow BNMBs, (c) cross-sectional SEM image of the EP/BNMB-35 μm composite and (d) thermal conductivity of EP/BNMB-35 μm composites under different pressures [167]. Reprinted with permission from [167]; copyright 2019 Elsevier.

Fig. 25. (a) Schematic illustrations of the preparation process for EP/BN-PVDF composites and (b) thermal conduction mechanism of the composites with and without BN-PVDF and BN-C scaffolds; thermal conductivity of the (c) EP/BN-PVDF and (d) EP/BN-C composites [168]. Reprinted with permission from [168]; copyright 2020 American Chemical Society.

Fig. 26. (a) Schematic illustration of the fabrication of BNF, (b) SEM images of BNF and the BNNS/BNF/PDMS composite, and (c) thermal conductivity of BNNS/BNF/PDMS composites with different filler contents [169]. (d) Schematic fabrication procedure for 3D-R-BN and 3D-NS-BN frames, (e) SEM images of 3D-R-BN and 3D-NS-BN frames, and (f) thermal conductivity of pure PMMA, 3D-R-BN/PMMA, and 3D-NS-BN/PMMA composites [170]. (g) Schematic illustration of the fabrication process for 3D-SiC foam, (h) SEM image of 3D-SiC/EP composite and EDX mapping of Si in the composite, and (i) thermal conductivity of 3D-SiC/EP and random SiC/EP composites with different filler contents [171]. Reprinted with permission from

[169]; copyright 2017 Elsevier. Reprinted with permission from [170]; copyright 2018 John Wiley and Sons. Reprinted with permission from [171]; copyright 2020 Elsevier.

Fig. 27. (a) Schematic diagram of the fabrication procedure for EP/MF@BNNS composites, (b) SEM image of MF@BNNS frame, and (c) thermal conductivity of EP/MF@BNNS composites with various deposition cycles and BNNS contents [173]. Reprinted with permission from [173]; copyright 2018 Elsevier.

Fig. 28. (a) Schematic illustration of the formation process for PI/oriented BNNSs composites, (b) SEM images of BNNS-coated PI microspheres and the PI/oriented BNNS composite, and (c) thermal conductivity of the composite with oriented BNNSs and random BNNSs at different BNNSs contents [174]. Reprinted with permission from [174]; copyright 2020 Elsevier.

Fig. 29. (a) Schematic illustration of the preparation procedure for BN@PPS and PPS/BN composites, (b) optical microscopy and SEM images of the segregated structure of the PPS/BN composite with 30 vol% BN, and (c) thermal conductivity of the segregated and blended PPS/BN composites with different filler contents [175]. Reprinted with permission from [175]; copyright 2017 Elsevier.

Fig. 30. (a) Schematic illustration of the fabrication process for segregated PP/PF@BN and colored SEM images of PP/6 wt% PF@40 wt% BN and (b) thermal conductivity of the PP/PF@40 wt% BN composite with different contents of PP and PF [176]. Reprinted with permission from [176]; copyright 2020 Elsevier.

Fig. 31. (a) Schematic diagram of the formation process for PS/GO-PDA composites, (b) SEM images of PS/GO-PDA microspheres and the fractured surface of the PS/GO-PDA composite, (c) in-plane and through-plane thermal conductivity of PS/GO-PDA composites with different filler contents, and (d) volume resistance of the PS/GO and PS/GO-PDA composites with different filler contents [119]. Reprinted with permission from [119]; copyright 2019 Royal Society of Chemistry.

Table 1. Thermal and electrical conductivities and other properties of various fillers

Table 2. Summary of the thermal conductivities of the composites.

Table 3. Advantages and disadvantages of each method